UNIVERSITY OF OKLAHOMA

GRADUATE COLLEGE

DESIGN OF CONTINUITY CONNECTIONS FOR PRECAST, PRETENSIONED GIRDERS USING ULTRA-HIGH PERFORMANCE CONCRETE

A THESIS

SUBMITTED TO THE GRADUATE FACULTY

in partial fulfillment of the requirements for the

Degree of

MASTER OF SCIENCE

By

ZACHARY GAGE TIRY
Norman, Oklahoma
2023

Downloaded from SHAREOK. Persistent Handle URL: https://hdl.handle.net/11244/337578

DESIGN OF CONTINUITY CONNECTIONS FOR PRECAST, PRETENSIONED GIRDERS USING ULTRA-HIGH PERFORMANCE CONCRETE

A THESIS APPROVED FOR THE
SCHOOL OF CIVIL ENGINEERING AND ENVIRONMENTAL SCIENCE

BY THE COMMITTEE CONSISTING OF

Dr. Royce Floyd, Chair

Dr. Jeffery Volz

Dr. Philip Scott Harvey Jr.

© Copyright by ZACHARY GAGE TIRY 2023

All Rights Reserved.

Acknowledgments

I would like to thank my advisor, Dr. Royce Floyd for providing me with the opportunity to conduct research as a graduate student. The knowledge and advice he has provided throughout the duration of my studies are second to none. His passion for his research inspires me to do my best and learn something new every day. I could not have asked for a better mentor.

I would also like to thank Stephen Roswurm, Omar Yadak, Jackson Milner, Jake Choate, and any other students who helped construct and test my specimens. The scale of the research projects undertaken by graduate students in our department are too great for one individual, and my success is a reflection on the team who helped me.

I would like to thank Dr. Jeffery Volz and Dr. Philip Harvey for the advice they have provided me with as a part of my committee.

I would like to thank John Bullock for his help. As the lab manager, he has gone above and beyond his job responsibilities to help me purchase materials, cast concrete, and conduct testing. This project would have been much more difficult without his support.

Lastly, I would like to thank my parents Tammy and Terry Tiry, my grandparents, and my girlfriend Emily for supporting and believing in me throughout my academic career. Without them, none of this would be possible.

Table of Contents

List of Tables vii
List of Figures vii
Abstract xiii
1.0 Introduction 1
1.1 Application of UHPC in Bridge Construction 1
1.2 Purpose of Research 2
2.0 Literature Review 3
2.1 Prestressed Concrete 3
2.2 Ultra-High Performance Concrete 5
2.3 Girders made Continuous for Live Load 8
3.0 Methods and Approach 12
3.1 Concrete Mix Designs 12
3.2 Prestressed Girders 15
3.2.1 Prestressed Girder Design 15
3.2.2 Girder Construction 17
3.3 Composite Deck Slab 23
3.3.1 Deck Slab Design 23
3.3.2 Deck Slab Construction 24
3.4 Continuity Joints 27
3.4.1 Continuity Joint Design 27
3.4.2 Continuity Joint Construction 32
3.5 Specimen Testing 37
3.5.1 Objectives 37
3.5.2 Approach and Instrumentation 38
4.0 Results 41
4.1 Specimen Nomenclature 41
4.2 Concrete Properties 41
4.2.1 Fresh Properties 41
4.2.2 Compressive Strengths 43
4.3 Joint Testing 46
4.3.1 HSJ3-1 Negative Moment Test 47

4.3.2 HSJ3-2 Positive Moment Test 54
4.3.3 HSJ3-2 Negative Moment Test 58
4.3.4 HSDU-1 Positive Moment Test 63
4.3.5 HSDU-1 Negative Moment Test 69
4.3.6 HSDU-2 Positive Moment Test 74
4.3.7 HSDU-2 Negative Moment Test 79
4.3.8 SSDU-1 Positive Moment Test 86
4.3.9 SSDU-1 Negative Moment Test 95
4.3.10 SSDU-2 Negative Moment Test 102
4.3.11 SSDU-2 Positive Moment Test 111
5.0 Analysis 117
5.1 Negative Moment Tests 117
5.1.1 Negative Moment Test Load-Deflection and Maximum Loading 117
5.1.2 Negative Moment Test Separation at the Interface 119
5.1.3 Forces in the Negative Moment Reinforcement 122
5.2 Positive Moment Tests 124
5.2.1 Positive Moment Load-Deflection and Maximum Loading 124
5.2.2 Positive Moment Separation at the Interface 126
5.2.3 Forces in the Positive Moment Reinforcement Steel 127
6.0 Findings, Conclusions, and Recommendations 131
6.1 Findings 131
6.2 Conclusions 132
6.3 Recommendations 133
7.0 References 134

List of Tables

Table 1: Self-Consolidating Concrete Girder Mix Design (1 yd^3).....13
Table 2: Conventional Concrete Deck Mix Design (1 yd^3) 14
Table 3: J3 Ultra-High Performance Concrete Mix Design (1 yd^3).....14
Table 4: Ductal® Ultra-High Performance Concrete Mix Design (1 yd^3).....15
Table 5: Results of fresh concrete slump testing (in.) 42
Table 6: Dosage of HRWR for SCC used in girders (fl. oz/100 lb of cement).....43
Table 7: Compressive Strengths for HSJ3-1 (psi) 44
Table 8: Compressive Strengths for HSJ3-2 (psi) 44
Table 9: Compressive Strengths for HSDU-1 (psi).....45
Table 10: Compressive Strengths for HSDU-2 (psi).....45
Table 11: Compressive Strengths for SSDU-1 (psi) 45
Table 12: Compressive Strengths for SSDU-2 (psi) 45
Table 13: Maximum values for each specimen during negative moment testing119
Table 14: Calculated values for stress in negative moment reinforcement at maximum loading 123
Table 15: Maximum values for each specimen during positive moment testing 125
Table 16: Calculated values for stress in positive moment steel at maximum loading 128
Table 17: Extrapolated values of stress generated in positive steel vs embedment length 129

List of Figures

Figure 1: Superstructure of a typical bridge with precast girders made continuous (Eamon, 2016) 3
Figure 2: Loading setup for direct tension pullout testing (Graybeal, 2014) 7
Figure 3: Formation of positive restraint moment (Saadeghvaziri et al., 2004).....8
Figure 4: Variable parameters for bent strands (Noppakunwijai et al., 2002). 10
Figure 5: Cross-section of prestressed girders.....16
Figure 6: Shear reinforcement in prestressed girders 17
Figure 7: Dead (a) and live (b) prestressing abutments.....18
Figure 8: Donut load cell and chucks in place before prestressing 19
Figure 9: Elevation view (a) and plan view (b) of steel cage before casting 20
Figure 10: Two prestressed girders simultaneously cast on the prestressing bed .22
Figure 11: Wooden divider between adjacent girders.....22
Figure 12: Deck slab design for the dead (a) and live (b) end of each specimen..24
Figure 13: Deck reinforcement vertical offset (a) and adjacent lap splice alignment (b) 25
Figure 14: Deck reinforcement placed in formwork 25
Figure 15: Freshly placed deck concrete showing a close-up of the forms around the lap splice (a) and an entire set of specimens (b).....26

Figure 16: Finished concrete decks after form removal 27
Figure 17: Hooked strand continuity joint cross-section (a), elevation view (b), and plan view (c) 28
Figure 18: Negative moment lap splice cross-section (a) and elevation (b) view. 30
Figure 19: Positive moment hook cross-section (a) and elevation (b) view 31
Figure 20: Positive moment straight strand cross-section (a) and elevation (b) view 32
Figure 21: Joint reinforcement for hooked strand (a) and straight strand (b) designs 34
Figure 22: Plan views of joint formwork secured in place showing a close-up of the reinforcement (a) and zoomed-out view of the restraints (b) 36
Figure 23: Completed continuity joint before (a) and after (b) formwork removal 36
Figure 24: Alignment of the LVDTs before (a) and after (a) adding aluminum bearing plates 39
Figure 25: Detailed view of components for joint testing apparatus 40
Figure 26: Northwest (a) and southwest (b) side of the joint HSJ3-1 before testing 47
Figure 27: Northwest (a) and southwest (b) side of the joint HSJ3-1 under final loading 49
Figure 28: HSJ3-1 entire specimen showing deflection under final loading 49
Figure 29: Southeast (a) and northeast (b) side of joint HSJ3-1 after final loading 50
Figure 30: East side of HSJ3-1 joint after final loading showing locations of significant concrete spalling 51
Figure 31: Load-deflection curve for HSJ3-1 during negative moment test 52
Figure 32: Load-joint separation curve for HSJ3-1 during negative moment test 53
Figure 33: Southeast (a) and northeast (b) side of the joint HSJ3-2 before testing 54
Figure 34: Southeast (a) and northeast (b) side of the joint HSJ3-2 after testing . 55
Figure 35: Northwest (a) and southwest (b) side of the joint HSJ3-2 after testing 56
Figure 36: HSJ3-2 entire specimen showing deflection under final loading 56
Figure 37: Load-deflection curve for HSJ3-2 during positive moment test 57
Figure 38: Load-joint separation curves for HSJ3-2 during positive moment test 58
Figure 39: Flexural cracking at east side of the joint for HSJ3-2 under final loading 59
Figure 40: East side of the joint of HSJ3-2 with cracks at the interface under final loading 60
Figure 41: Visible deflection and additional flexural cracking of HSJ3-2 under final loading 61
Figure 42: Load-deflection curve for HSJ3-2 during negative moment test 62

Figure 43: Load-joint separation curves for HSJ3-2 during negative moment test 63
Figure 44: Preexisting settlement is indicated by a blue oval and preexisting cracking is indicated by a red line on the southeast (a) and northeast (b) side of the joint HSJ3-2 before testing. 64
Figure 45: As-cast top of joint before (a) and after (b) masonry sand surface prep Note: This figure shows SSDU-1 which experienced very similar settlement to HSDU-1 64
Figure 46: East side of joint (a) and northeast interface (b) of HSDU-1 after positive moment test 65
Figure 47: As-cast bottom of joint HSDU-1 showing separation at northwest interface under final loading of positive moment test 66
Figure 48: Load-deflection curve for HSDU-1 during positive moment test 67
Figure 49: Load-joint separation curves for HSDU-1 during positive moment test 68
Figure 50: East side of the joint (a) and northeast side of the interface (b) of HSDU-1 before negative moment test 69
Figure 51: Flexural cracking on northeast side of specimen HSDU-1 under final negative moment test loading 70
Figure 52: Northwest (a) and southwest (b) side of joint HSDU-1 under final negative moment test loading 71
Figure 53: Southeast interface separation of HSDU-1 during (a) and after (b) final negative moment test loading 71
Figure 54: Cracking in as-cast top face of deck (denoted by blue oval) from the west (a) and east (b) side of the joint 72
Figure 55: Load-deflection curve for HSDU-1 during negative moment test 73
Figure 56: Load-joint separation curves for HSDU-1 during negative moment test 74
Figure 57: Separation at the interface of HSDU-2 from the east (a) and west (b) side under final positive moment test loading 75
Figure 58: Cracking on the west side of HSDU-2 near the as-cast top surface of the joint 76
Figure 59: Cracking on the northwest side of HSDU-2 in the girder directly above the north roller support 77
Figure 60: Load-deflection curve for HSDU-2 during positive moment test 78
Figure 61: Load-joint separation curves for HSDU-2 during positive moment test 79
Figure 62: East (a) and southeast (b) side of joint HSDU-2 showing cracks at the interface before negative moment testing 80
Figure 63: East side of HSDU-2 showing cracks near the as-cast top face of the joint before negative moment testing 80
Figure 64: West (a) and southwest (b) side of HSDU-2 showing separation at the interface after negative moment testing 82

Figure 65: Southeast (a) and northeast (b) side of joint HSDU-2 showing cracks at the interface after negative moment testing....82
Figure 66: West side of joint HSDU-2 showing cracks near the as-cast top face of the joint after negative moment testing....83
Figure 67: East side of joint HSDU-2 showing cracks near the as-cast top face of the joint after negative moment testing....84
Figure 68: Compressive cylinder showing significant fiber settlement in the Ductal® UHPC used for joints HSDU-1 and HSDU-2....84
Figure 69: Load-deflection curve for HSDU-2 during negative moment test....85
Figure 70: Load-joint separation curves for HSDU-2 during negative moment test....86
Figure 71: East (a) and west (b) side of joint SSDU-1 showing preexisting cracks before positive moment testing....87
Figure 72: Southeast (a) and northeast (b) side of joint SSDU-1 showing the joint interface before positive moment testing....88
Figure 73: Northwest (a) and southwest (b) side of joint SSDU-1 showing the joint interface before positive moment testing....88
Figure 74: Southeast (a) and northeast (b) side of joint SSDU-1 showing cracking along the interfaces under final positive moment test loading....90
Figure 75: Northwest (a) and southwest (b) side of joint SSDU-1 showing cracking along the interfaces under final positive moment test loading....90
Figure 76: East (a) and west (b) side of joint SSDU-1 showing cracks near as-cast top face under final positive moment test loading....91
Figure 77: Northwest (a) and southwest (b) side of joint SSDU-1 showing separation at the interface near the as-cast bottom face under final positive moment test loading....92
Figure 78: Southeast (a) and northeast (b) side of joint SSDU-1 showing separation at the interface near the as-cast bottom face under final positive moment test loading....92
Figure 79: Compressive cylinder showing significant fiber settlement in the Ductal® UHPC used for joints SSDU-1 and SSDU-2....93
Figure 80: Load-deflection curve for SSDU-1 during positive moment test....94
Figure 81: Load-joint separation curves for SSDU-2 during positive moment test....95
Figure 82: East side of north girder SSDU-1 showing flexural cracks after negative moment test....96
Figure 83: East side of south girder SSDU-1 showing flexural cracks after negative moment test....96
Figure 84: West side of north girder SSDU-1 showing flexural cracks as after negative moment test....97
Figure 85: West side of south girder SSDU-1 showing flexural cracks after negative moment test....97

Figure 86: West side of joint SSDU-1 showing cracks near the as-cast top face of the joint under final negative moment test loading 98
Figure 87: East side of joint SSDU-1 showing cracks near the as-cast top face of the joint under final negative moment test loading 99
Figure 88: Southeast (a) and northeast (b) side of joint SSDU-1 showing cracking along the interfaces under final negative moment test loading 99
Figure 89: Northwest (a) and southwest (b) side of joint SSDU-1 showing cracking along the interfaces under final negative moment test loading 100
Figure 90: Load-deflection curve for SSDU-1 during negative moment test 101
Figure 91: Load-joint separation curves for SSDU-1 during negative moment test 102
Figure 92: East side of north girder of SSDU-2 showing flexural cracks under final negative moment test loading.....104
Figure 93: East side of south girder of SSDU-2 showing flexural cracks under final negative moment test loading.....104
Figure 94: West side of north girder of SSDU-2 showing flexural cracks under final negative moment test loading.....105
Figure 95: West side of south girder of SSDU-2 showing flexural cracks under final negative moment test loading.....105
Figure 96: West side of joint SSDU-2 showing cracks near the as-cast top face of the joint under final negative moment test loading 106
Figure 97: East side of joint SSDU-2 showing cracks near the as-cast top face of the joint under final negative moment test loading 106
Figure 98: As-cast top surface of joint SSDU-2 showing 0.1 in. wide cracks that formed during final negative moment test loading.....107
Figure 99: As-cast top surface of the south deck of SSDU-2 showing cracks that formed during final negative moment test loading Note: All cracks unlabeled or labeled 46 kips resulted from final loading of approximately 41.6 kips 108
Figure 100: West side of joint SSDU-2 in positive moment orientation showing undocumented cracks near the as-cast top surface caused by negative moment testing Note: All cracks unlabeled or labeled 46 kips resulted from final loading of approximately 41.6 kips 108
Figure 101: East side of joint SSDU-2 in positive moment orientation showing undocumented cracks near the as-cast top surface caused by negative moment testing Note: All cracks unlabeled or labeled 46 kips resulted from final loading of approximately 41.6 kips 109
Figure 102: Load-deflection curve for SSDU-2 during negative moment test ...110
Figure 103: Load-joint separation curves for SSDU-2 during negative moment test.....111
Figure 104: West side of joint SSDU-2 showing cracks near as-cast top face after final positive moment test loading 112
Figure 105: East side of joint SSDU-2 showing cracks near the as-cast top face after final positive moment test loading 113

Figure 106: Southeast (a) and northeast (b) side of joint SSDU-2 showing cracking along the as-cast bottom of the interfaces after final positive moment test loading 113
Figure 107: Northwest (a) and southwest (b) side of joint SSDU-2 showing cracking along the as-cast bottom of the interfaces after final positive moment test loading 114
Figure 108: Load-deflection curve for SSDU-2 during positive moment test 115
Figure 109: Load-joint separation curves for SSDU-2 during positive moment test 116
Figure 110: Load-deflection curves for all specimens during negative moment testing 118
Figure 111: Load-joint separation curves for hooked strand J3 specimens at the joint-deck interfaces during negative moment tests 120
Figure 112: Load-joint separation curves for hooked strand Ductal® specimens at the joint-deck interfaces during negative moment tests 121
Figure 113: Load-joint separation curves for straight strand Ductal® specimens at the joint-deck interfaces during negative moment tests 122
Figure 114: Load-deflection curves for all specimens during positive moment testing 124
Figure 115: Load-joint separation curves for all specimens during positive moment testing 126

Abstract

In recent years, an increased desire to improve the durability and resiliency of bridges has become an important consideration in design. Ultra-high performance concrete (UHPC) is a relatively new cementitious composite material with mechanical and durability properties far superior to conventional concrete. UHPC has high compressive and tensile strength, excellent bond strength to adjacent concrete sections, and a relatively short development length for steel reinforcement. Eliminating joints in a bridge deck with continuous spans can improve the durability of the bridge by reducing the number of pathways for water to penetrate to the bridge structure. The practice of designing connections of precast girders made continuous for live load with conventional concrete is well understood and utilized in practice, but little guidance exists on the structural design of continuity connections made of UHPC or the retrofit of simple spans to be made continuous. The desire to use UHPC is apparent because connections made of conventional concrete often crack during service and the superior properties of UHPC can lead to simpler connection details. Cracking can cause a loss of continuity and allow water to degrade both the reinforcing steel and adjacent concrete. The focus of this research was to investigate how embedment length, UHPC materials, and steel reinforcement geometry affect the performance of connections of pretensioned girders made continuous for live load. A total of six 19 ft long test specimens were constructed to represent a two-span continuous prestressed bridge system. The continuity connections were constructed using two types of UHPC material, a locally developed mix design labeled J3 and a

commercially available product. Two types of positive moment steel reinforcement details were tested: 10 in. straight strands and 16 in. long hooked strands, which are both formed as extensions of the prestressing strands in the girders. To replicate the loads a bridge system would experience during service, the specimens were tested to induce both a positive and negative moment in the connection. The measured data correlated well with the literature on the bond strength of UHPC and suggested that hooked strands and longer embedment lengths generally lead to increased load carrying capacity. Additionally, the data suggests that the required dimension and embedment lengths for continuity connections made of UHPC could be smaller than conventional concrete.

1.0 Introduction

1.1 Application of UHPC in Bridge Construction

Ultra-high performance concrete (UHPC) is a relatively recent advancement in cementitious composite materials with mechanical and durability properties which far exceed those of conventional concrete. Many of its properties have been optimized using particle packing theory and the inclusion of fibrous materials. These advancements have led to characteristics that far surpass those of conventional concrete such as high tensile strength, high compressive strength, excellent bond strength, and shorter development length to reinforcing steel. Improved performance has led to a material with numerous structural applications.

One such application is the connection of precast, prestressed concrete bridge girders to make spans continuous for live load. Prestressing concrete allows for concrete sections to go into compression in such a way that lowers service level deflection. Precast, prestressed concrete sections are constructed in a plant environment and transported to the site to be assembled, which allows for high quality control. These sections are typically simply supported and must be connected by diaphragms to create continuous spans. A major advantage to this process is that prestressed sections can be placed on the same day they arrive on the site, allowing for overall bridge construction times to be minimized.

The use of continuity connections allows bridges to be constructed with precast elements while allowing for both the structural benefits of live load continuity and

the durability benefits of reducing the number of bridge deck joints. Live load continuity effectively spreads the load out, increasing the load-carrying capacity of the girders. Conventional connections for precast girders made continuous for live load typically consist of either continuity diaphragms extending the full width of the bridge or individual linkage blocks placed between girder ends. Durability benefits are achieved by covering the ends of the girders in cementitious material, dramatically reducing the opportunity for water to seep into the joints and additionally providing improved appearance and ride quality.

1.2 Purpose of Research

The purpose of this research was to develop design guidance for bridge girders made continuous for live load using UHPC. A critical focus was to collect and analyze existing data on continuity connections of precast concrete girders and UHPC properties. Utilized data sources included the provisions provided in the *AASHTO LRFD Bridge Design Specifications* (2017), existing literature on UHPC, and other studies that identify critical parameters for UHPC. This data was considered to allow for the optimization of the live load connection. Six test specimens were constructed as detailed in the synthesized designs. Each specimen was made of two approximately half-scale AASHTO Type II girders connected with a UHPC diaphragm. They were outfitted with instruments during testing to quantify the performance, which could be used as reference in future design.

2.0 Literature Review

2.1 Prestressed Concrete

Pre-tensioned, prestressed concrete girders are commonly used in bridge construction and are one of the most critical structural elements in the bridge superstructure. Their main purpose is to support the concrete deck and transfer loading to the pier and abutments below. Pre-tensioned concrete girders have many characteristics that make them favorable over conventionally reinforced concrete. These members are cast offsite in a precast plant, which allows for better quality control during construction. The members are then transported to the site once they are ready to be installed, making them ideal for Accelerated Bridge Construction (ABC) methods. The goal of ABC construction is to minimize mobility impacts during onsite construction to improve project safety, quality, durability, costs, and environmental impact (FHWA, 2021). A general overview of the critical parts of a bridge superstructure is shown in Figure 1. This figure shows how typical diaphragms are used to connect two girders above supports.

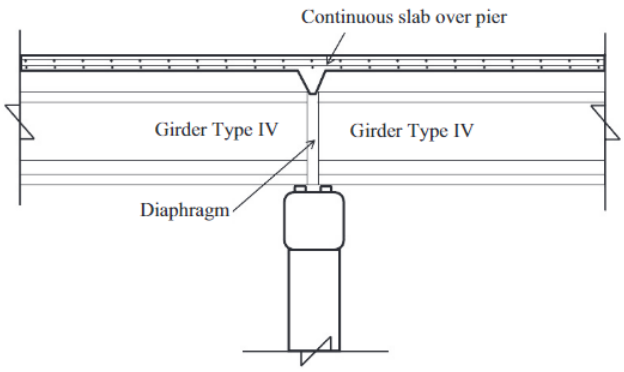

Figure 1: Superstructure of a typical bridge with precast girders made continuous (Eamon, 2016)

Prestressing occurs before service loads are applied to the member. The purpose of prestressing a concrete member is to negate deflection and add flexural capacity. Pre-tensioning is a specific type of prestressing that occurs before the concrete cures. Pre-tensioning starts by securing the prestressing strands into a prestressing bed comprised of two secured abutments on either end of concrete formwork. The dead end of the abutment remains completely stationary, while the live end of the abutment uses a series of jacks to uniformly stretch the strands. Strands are stretched incrementally to go slightly beyond the desired stress to account for prestress losses. The concrete is then poured into the formwork where it will eventually bond to the prestressing strand. Once cured, the prestressing strand is cut and the induced tension is transferred to the concrete, causing the bottom of the member to go into compression. This causes the beam to camber upwards, effectively decreasing the amount of deflection experienced during service (Saadeghvaziri et al., 2004).

However, additional moments generate in the beams in a continuous system due to time-dependent effects in the beam called creep and shrinkage. These effects are particularly important to consider during the beam-to-beam connection design process. It is best to establish continuity after the girders are 90 days old to reduce the moment caused by these time-dependent effects (Saadeghvaziri et al., 2004). UHPC can be used to help resist the stresses that may develop during this time.

2.2 Ultra-High Performance Concrete

UHPC is a revolutionary cementitious material that has dramatically superior properties compared to conventional concrete. It is defined by the FWHA as “a cementitious composite material composed of an optimized gradation of granular constituents, a water-cementitious materials ratio less than 0.25, and a high percentage of discontinuous internal fiber reinforcement” (FHWA, 2013). Mechanical properties of UHPC as defined by FHWA include a post cracking tensile strength greater than 0.72 ksi and compressive strength over 21.7 ksi. Additionally, its improved particle structure greatly reduces the ability of particles to pass through it. These factors mean that the material has significantly greater durability and application compared to other alternative forms of concrete.

Due to its increased performance, there are many applications for UHPC on structural members in highway infrastructure. It can be implemented to reduce the size of members, improve connections, and increase the durability of conventional concrete members that it is bonded to. In some cases, it has served as a replacement for conventionally reinforced concrete members, and the tensile capacity has enabled the elimination of shear stirrups (Graybeal, 2009). This has allowed for smaller members with higher capacities than previously achievable. The most common application of UHPC in bridge construction is for connections. The characteristics that make UHPC so desirable for connection design are the ability to bond well to adjacent concrete, prestressing strand, mild steel reinforcement, and its much-improved tensile capacity (Graybeal, 2009). These

factors allow for smaller connections and development lengths that can optimize the design.

The bond behavior of UHPC to reinforcing steel has been an important parameter in previous studies. A study was conducted by the FHWA to determine the bond strength of mild steel reinforcement in commonly available UHPC. Direct tension pullout tests were carried out designed to mimic a tension-tension lap slice configuration. The test utilized number 8 bars that started in precast concrete slabs and extended into a strip of UHPC that was poured on top. The part of the bars extending out of the UHPC was then tensioned using a hydraulic jack and loaded to failure. The test setup is shown in Figure 2. Over two hundred pullout tests were carried out and were varied on a select set of parameters. The tests were evaluated to test the performance of factors such as embedment length, bar size, bar spacing, and concrete compressive strength (Graybeal, 2014). It was determined that compressive strength alone is not adequate for evaluating the bond strength of reinforcing bars in UHPC. It was also observed that bond strength decreases as bar diameter increases, but bond strength increases as embedment length increases. Non-contact lap slices also displayed higher bond strength when compared to contact lap splices. This was believed to be result of the non-contact lap splices allowing UHPC fibers to fully engage around both bars (Graybeal, 2014).

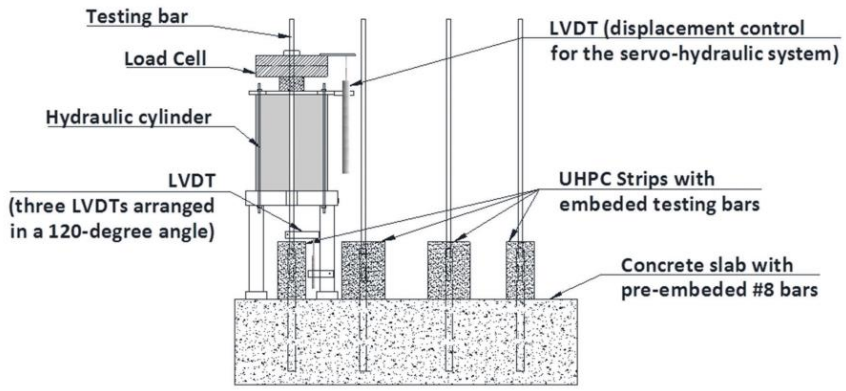

Figure 2: Loading setup for direct tension pullout testing (Graybeal, 2014)

Design practices in the United States relative to UHPC have been largely debated; thus, there has been little comprehensive design guidance provided specifically for UHPC to date. It is generally accepted to use the *AASHTO LRFD Bridge Design Specifications* (2017) as a reference when inside the bounds of the specified equations. This practice does not account for the superior properties of UHPC and cannot entirely be relied on for every aspect of design with UHPC. The need for comprehensive design guidance is apparent because, otherwise, designers cannot utilize the full capacity that UHPC has to offer. However, multiple countries have derived their own standards based on empirical data collected during testing. Countries that have developed unique solutions to model UHPC capacity include, but are not limited to France, Switzerland, and Canada (El-Helou et al., 2022).

2.3 Girders made Continuous for Live Load

A continuity joint is a type of connection that connects the ends of two simply supported beams and allows for the transfer of superimposed dead and live loads and create a continuous beam system. It is a popular technique used in bridge construction as it allows for the bridge to be prestressed offsite without sacrificing live load continuity. This style of connection can be achieved using linkage blocks or diaphragms at the joint. Continuity allows for loads to be transferred along the length of the bridge and to act as a continuous beam, effectively increasing the strength and durability of the entire system. As shown in Figure 3, girders constructed as simple spans behave differently from girders made continuous because they can rotate at their supports. Adding a continuity connection cause restraining moments to form, which are caused by concrete creep and shrinkage.

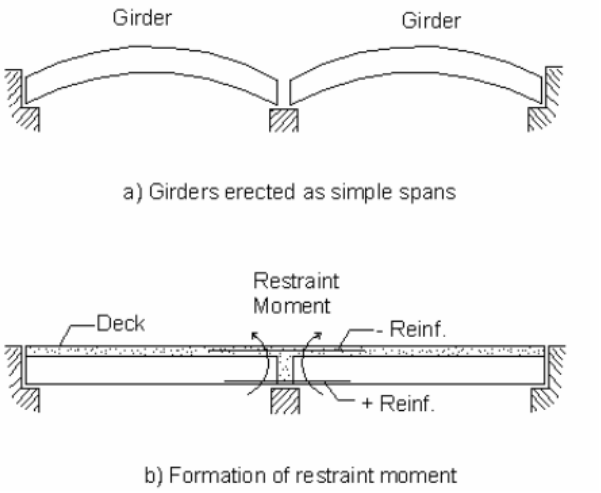

Figure 3: Formation of positive restraint moment (Saadeghvaziri et al., 2004)

A previous study by Miller (2004) examined six connection styles for continuity. This research included a survey with 51 respondents, of which, 35 had used,

fabricated, or designed continuous-for-live-load bridges. In all but one response, the negative moment continuity was established using a reinforced concrete deck slab (Miller, 2004). Included in this report were recommendations for future design and research. It was decided that the equations developed by Salmons et al. (1980) and others to approximate development of the strand were adequate for calculating the number and length of bent up strands into the diaphragm. It was noted that this design requires asymmetrical placement of the bars such that they could fit into the connection without increasing the width above the piers (Miller, 2004).

The testing carried out by Salmons et al. (1980) included fatigue testing of two different geometries of untensioned-bonded prestressing strands. The first geometry featured two overlapping strands bent in 90 degree hooks and cast into a block of conventional concrete. The second geometry featured single strand bent into a U shape with each leg of the U cast into separate concrete blocks (Salmons et al., 1980). In all cases the failure mode was fracturing of the strand. It was concluded that a fixed embedment length of 30 in. was sufficient to provide adequate anchorage in any design stress range.

Noppakunwijai et al. (2002) investigated the pullout capacity of 0.5 and 0.6 in. diameter untensioned hooked strands to determine the number and length of strands needed in conventional bridge diaphragms. It was noted that using bent up prestressing strand is simple and economical but previously recommendations were simply based on trial and adjustment (Noppakunwijai et al., 2002). Test specimens featured varied length of horizontal hook (L_h), vertical hook (L_v), and

strand diameter. These variables can be seen in Figure 4. The results of pullout tests using a hydraulic jack were used to provide design recommendations. In general, pullout capacity of bent strands increased with an increase in total embedment length. Further, it would be conservative to assume that 0.5 in. strands attain 80 percent of their specified strength with embedment lengths of 30 in. or greater. It was advised to provide a minimum embedment length of 16 in. to limit cracking at service load due to time-dependent restraint moments (Noppakunwijai et al., 2002).

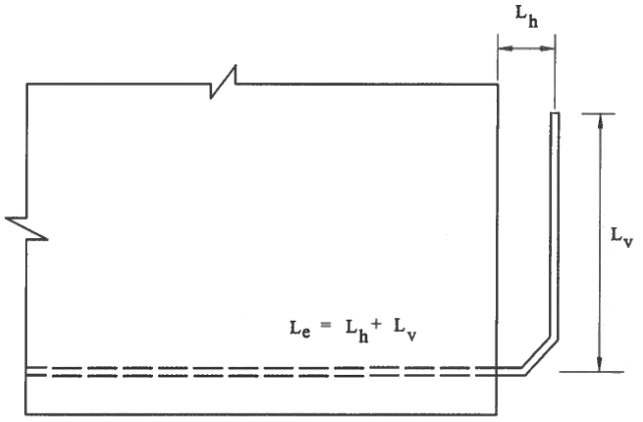

Figure 4: Variable parameters for bent strands (Noppakunwijai et al., 2002).

Previous students at the University of Oklahoma (OU) have already contributed to research efforts related to precast girders made continuous. One study utilized half-scale AASHTO Type II precast, pretensioned girders that were 18 ft long to test continuity connections made of UHPC. The study found that properties of conventional concrete can be used to adequately design both new and retrofit UHPC connections (Casey, 2019). Another study utilized half-scale AASHTO Type II precast, untensioned girders that were 9 ft long to evaluate a series of

repair materials for in-service bridges with conventional concrete continuity connections. Among the materials tested, it was concluded that UHPC provided the best balance between ease of placement and overall performance (Mesigh, 2021). The current project has been largely motivated by the desire to further investigate and optimize parameters related to these projects.

3.0 Methods and Approach

The decision was made during initial planning to divide construction into a series of phases. A total of six specimens were to be created for testing consisting of twelve pretensioned concrete girders, twelve reinforced concrete decks, and six UHPC continuity joints. Apart from minimal adjustment based on available shear steel, the deck and girder designs were reused from a previous project (Casey, 2019). Phase 1 included the construction of the prestressed girders. Phase 2 included the construction of the reinforced concrete decks. Phase 3 consisted of the construction of UHPC continuity joints. Flexural testing to evaluate positive and negative moment strength began once all joints were constructed and the first set of joints was at least 28 days old.

3.1 Concrete Mix Designs

A critical step involved selecting an appropriate mix design for the girders, deck, and joints. After analyzing the mix designs used in other projects, it was decided to make a new concrete mix design for the girders. A self-consolidating concrete (SCC) was used instead of conventional concrete to allow for easy placement during casting. A high slump flow allowed the concrete to easily flow between reinforcing steel and through the narrow web of the girders. A 28-day compressive strength of 8,000 psi and a slump flow of 26 in. were targeted during design. The water-cement ratio (w/c) of 0.35 was low enough to obtain the required strength, yet high enough to achieve adequate flowability. A high-range water reducer (HRWR), AdvaCast 575, was used to obtain the desired flow of the mix. The dosage of HRWR used for each casting varied from 8.5 – 11 oz/100 lb

of cement. HRWR was added to the mix until the desired workability was achieved based on how flowable the mix looked in the mixer. The SCC mix design used for the girders is shown in Table 1. The theoretical unit weight based on tabulated values is 149.4 lb/ft^3.

Table 1: Self-Consolidating Concrete Girder Mix Design (1 yd^3)

Material	**Weight (lb)**	**Volume (ft^3)**	**Ratio**
Type I/II Cement	825	4.20	0.156
Rock	1445	8.64	0.320
Sand	1476	8.99	0.333
Water	289	4.63	0.171
Air	0	0.54	0.020
Total	4035	27.0	1.00

The concrete used for the decks was designed by modifying a mix used on a different project with a design compressive strength of 6,000 psi. This compressive strength was selected as it is comparable to typical strengths for in-service bridge decks. A series of test batches were conducted with the goal of improving workability without sacrificing strength. The first batch was as described by the existing mix design, the second utilized a higher dosage of HRWR, and the third featured a higher w/c. The third mix design (Table 2) was ultimately selected for use in the decks with a target 28-day compressive strength of 6,000 psi and a target slump of 8 in. A w/c of 0.44 and the HRWR Glenium 7920 were used for the final mix design. Each batch of concrete used a dosage of HRWR of 5 oz/100 lb of cement. The theoretical unit weight based on tabulated values is 148.1 lb/ft^3.

Table 2: Conventional Concrete Deck Mix Design (1 yd^3)

Material	Weight (lb)	Volume (ft^3)	Ratio
Type I/II Cement	682	3.47	0.129
Rock	1725	10.32	0.382
Sand	1291	7.87	0.291
Water	300	4.81	0.178
Air	0	0.54	0.020
Total	3998	27.0	1.00

One of the parameters tested during this project was the performance of two readily available UHPC mixes, J3 and Ductal®. J3 is a UHPC mix using locally available constituent materials that was designed at OU by previous students (Looney et al., 2019). J3 was chosen as a joint material due to its well-documented characteristics and its readily available ingredients (Floyd et al., 2020). Additional tensile reinforcement is provided in the form of 0.079 in. diameter by 0.512 in. long steel fibers from Hiper Fiber at a nominal 2% by volume. This mix also used the HRWR Glenium 7920 dosed at 24 oz/100 lb of cement. The J3 mix design is shown in Table 3.

Table 3: J3 Ultra-High Performance Concrete Mix Design (1 yd^3)

Material	Mix Proportion
Silica Fume (lb)	183
Ground Granulated Blast Furnace Slag (lb)	549
Type I/II Cement (lb)	1098
Steel Fibers (lb)	263
Masonry Sand (lb)	1830
Water (lb)	366
Glenium 7920 (ml)	12992

The second UHPC mix utilized was Ductal®, a commercially available UHPC product. Ductal® is delivered as a premixed bag of ingredients, so the exact proportions of the mix are unknown. For this reason, the exact w/c and dosage of HRWR, Chryso Fluid Premia 150, used during mixing are also unknown. A series of test batches with varied amounts of water and HRWR were performed to produce a mix design that achieved the desired workability and strength needed from the material. The mix design used is provided in Table 4.

Table 4: Ductal® Ultra-High Performance Concrete Mix Design (1 yd^3)

Material	**Mix Proportion**
Premix (lb)	3700
Water (lb)	202
Steel Fibers (lb)	263
Chryso Fluid Premia 150 (ml)	22952

3.2 Prestressed Girders

3.2.1 Prestressed Girder Design

The first steps in designing the prestressed girders were to identify a suitable geometry to complement the anticipated joint design. It was determined that girder geometry used in previous work would provide enough capacity for joint testing (Connor 2019). The forms were based on approximately half-scale AASHTO Type II girders. They consisted of a 6 in. wide top flange, a 3 in. wide web, and a 9 in. wide bottom flange, with a total depth of 22.5 in. Two grade 270 low-relaxation 0.5 inch special strands were placed 2 in. from the bottom of the girder spaced at 2 in. on center. The target stress in the strands after prestress release was 75% of their ultimate strength, which was 202.5 ksi. To account for

chuck seating the stands were overstressed to 206 ksi. Two number 5 bars were placed 2 in. on center in the top flange to resist tension forces caused during prestressing and to prevent cracking. The shear reinforcement used was a wire mesh made of W2.9 on a 4 in. by 4 in. grid with a yield strength of 89 ksi. A cage comprised of two sheets of welded wire and the number 5 top bars was used in each beam. These sheets were offset to provide single vertical wires spaced at 2 in. along the length of the beam. A diagram including the welded wire configuration is shown in Figure 6. It was calculated that one sheet was adequate to induce a flexural failure in the beams in the anticipated loading configuration, but two sheets were used to ensure adequate shear capacity in the case of unanticipated failure modes. The complete cross-section of the prestressed girders is provided in Figure 5.

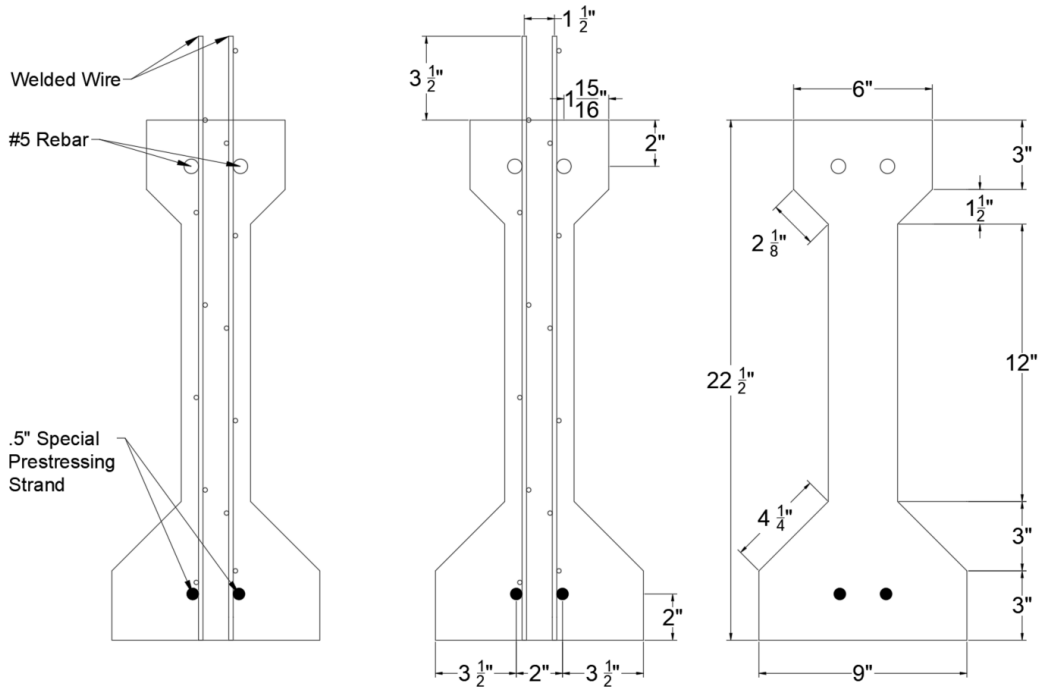

Figure 5: Cross-section of prestressed girders

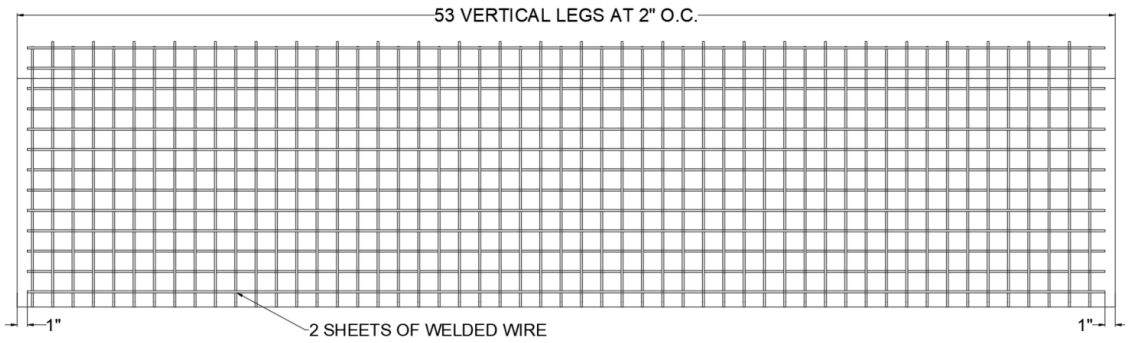

Figure 6: Shear reinforcement in prestressed girders

3.2.2 Girder Construction

The construction process started by assembling all the reinforcing steel cages ahead of time. The welded wire was cut down from its original 8 ft by 20 ft sheet into a length and height of approximately 106 in. by 26 in. This dimension allowed for 1 in. of cover along the length of the girder and 3.5 in. of welded wire to extend into the deck. Extending the welded wire into the deck ensured a strong interface between the deck and the girder, creating composite action between the two pieces. Lifting hooks, mild steel, and spacers were tied into place on the welded wire preemptively to allow the complete cages to be quickly placed on casting day.

The prestressing bed used during construction is made of three 8 ft long wooden tables set between two steel prestressing abutments. The prestressing abutments were 34 ft apart and are shown in Figure 7. Plastic sheeting was placed on the wooden tables to prevent the concrete from leaking and expedite cleanup. In order to cast two 9 ft girders at the same time using a single set of 18 ft long formwork,

a wooden divider cut to match the shape of the girders was placed in the middle of the form. The divider had to be as thin as possible, yet thick enough to allow the prestressing strand between each girder to be cut during detensioning. Next, the prestressing strand was pulled through the dead abutment, an end plate, the wooden spacer, another end plate, the live end abutment, the load cell, and finally secured in place using strand chucks. Figure 8 shows the donut load cell used to measure the force applied to one of the strands during tensioning and anchorage chucks prior to stressing. The final step before tensioning was to secure one piece of the metal formwork roughly in place on the table.

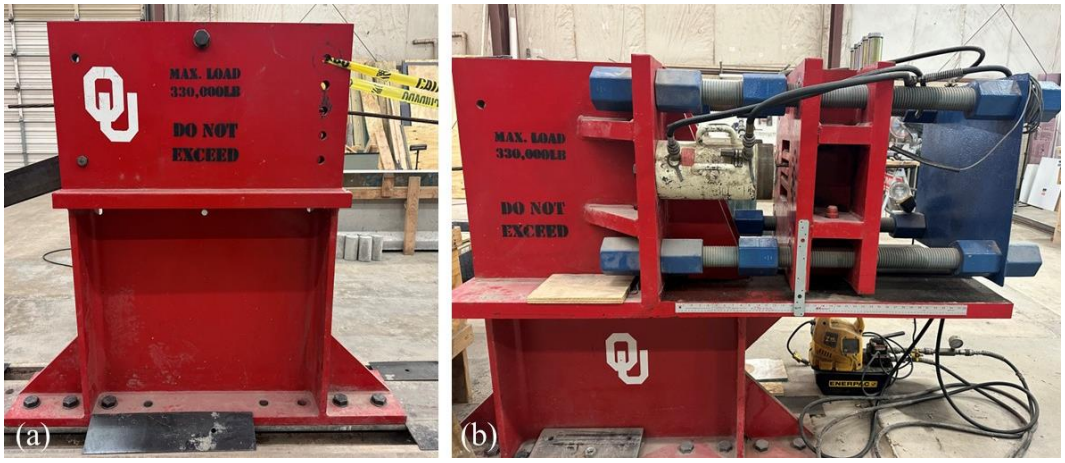

Figure 7: Dead (a) and live (b) prestressing abutments

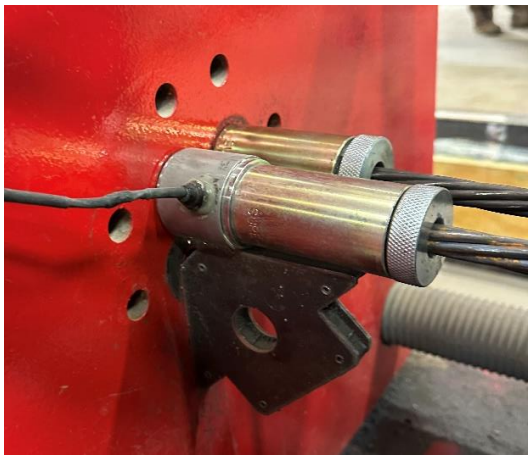

Figure 8: Donut load cell and chucks in place before prestressing

On the day of casting, the strands were tensioned at the same time to approximately 76.3% of the strands' ultimate capacity, which was roughly 206 ksi. Two hydraulic rams inside the live end abutment were used to incrementally apply load. The load was monitored using a 50 kip capacity through hole donut load cell and load was double-checked against manual displacement measurements compared to the calculated elongation. Once the required amount of stress was applied to the strands, the moving plate inside the abutment was secured in place using the large blue nuts shown in Figure 7 and the load was removed from the rams. The steel cages were then set into place and tied to the strands. The final piece of formwork was added and adjusted such that the center of strand was 3.5 in. from each edge of the bottom bell. Clamps were used to hold the top of the formwork and endplates in the correct position. The shear steel was tied to the clamps as needed to center them during casting. The formwork and steel reinforcement prior to casting can be seen in Figure 9.



Figure 9: Elevation view (a) and plan view (b) of steel cage before casting

The second stage of casting day included mixing the girder concrete. All concrete was mixed at Fears Lab to ensure the mix design was accurately followed. The concrete was mixed in a Praschak spiral blade mixer with a capacity of 21 ft^3. Each girder mix was 16 ft^3 and followed a standard conventional concrete mix procedure with a couple of exceptions. Due to the size of the mix, it was decided to not stop the mixer at any time and HRWR was added incrementally to achieve the desired slump flow. Once the concrete was removed from the mixer a slump flow test was performed in accordance with ASTM C143. Additionally, a total of eighteen 4 in. by 8 in. cylinders were made for each set of girders. The rest of the concrete was transported from the mixer and placed into the formwork using a hopper suspended by the overhead crane. A mallet was used to tap the sides of the forms to help the concrete flow into the forms. Additional consolidation

techniques such as vibrating or rodding were not required because SCC achieves adequate consolidation under its own weight.

Once the top layer of the girders started to harden a hand trowel was used to roughen the top layer to provide a rough surface for the deck to bond to in later steps. The concrete was then left to cure under wet burlap for 24 hours. At the 24-hour mark, the compressive strength was tested to ensure that the concrete had reached the 4000 psi required to release prestress. A set of girders cast simultaneously can be seen in Figure 10 at the end of the 24-hour curing period. Prestressing strands were then detensioned gradually using the live end abutment hydraulics and the prestressing force was transferred to the concrete. The strand locations closest to the abutments were then cut with an angle grinder and the strand between the girders was cut using a cutting torch due to space restraints. The wooden divider used to separate the adjacent girders and provide access to the stands can be seen in Figure 11. Strands on the end of the girders near the abutments were left approximately 5 ft long on each side to ensure an adequate length of strand was left to tie into the joint.



Figure 10: Two prestressed girders simultaneously cast on the prestressing bed



Figure 11: Wooden divider between adjacent girders

3.3 Composite Deck Slab

3.3.1 Deck Slab Design

The design of the composite concrete deck was reused from previous studies conducted at Fears Lab, namely Murray (2017) and Casey (2018). The purpose of incorporating a composite deck is to replicate the behavior of a full-scale bridge system. In the full-scale system considered by these studies, the deck would have a thickness of 8 in. and a tributary width of 96 in. At half-scale, this would be a thickness of 4 in. and a tributary width of 48 in. To simplify both construction and maneuverability of the specimens in a laboratory setting, the tributary width of the deck was decreased to 9 in. The change in tributary width was compensated by calculating the moment capacity of the theoretical half-scale system and increasing the depth of the deck to achieve an equivalent capacity. This approach resulted in a deck design that was 9 in. wide and 4.625 in. thick. Flexural steel reinforcement in the deck included four number 5 bars spaced at 2 in. on center. In order to form a contact lap splice inside the joints, the bars in each connecting deck were staggered vertically. The inside two bars were placed at one elevation, and the outside bars at another. This allowed for the centroid of the steel to be at the same location in both girders. The final deck design is provided in Figure 12.

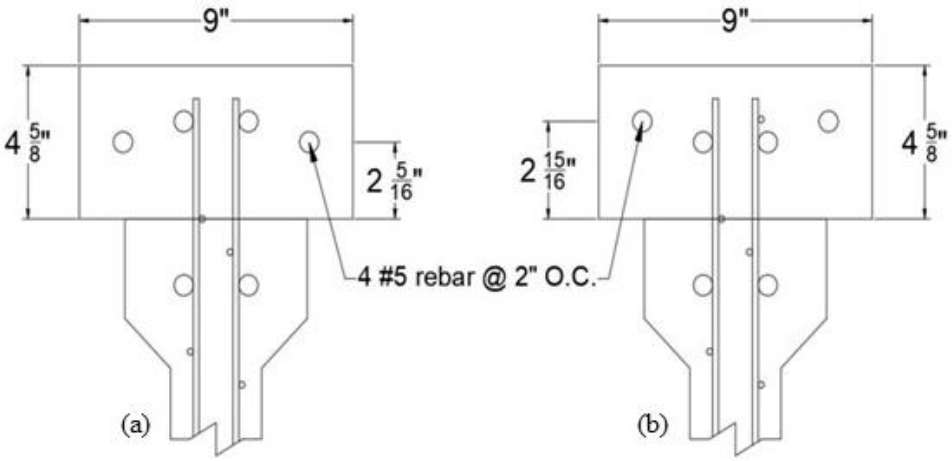

Figure 12: Deck slab design for the dead (a) and live (b) end of each specimen

3.3.2 Deck Slab Construction

The construction of the deck slab included setting the forms, placing the steel, and casting the concrete. The formwork utilized was recycled from a previous research project and was constructed using a specialty engineered finished plywood. The formwork was held together using dimensional lumber to set the desired depth and height. Small strips of oriented strand board (OSB) were then attached ¾ in. from the top of the girders using concrete screws and a hammer drill. The deck forms were secured in place on top of the OSB. The next step was adding steel reinforcement to the deck, which was extended approximately 10 in. beyond the end of the girders in the direction of the joint. Since the flexural reinforcement would eventually form a contact lap splice, careful consideration during this stage was critical to ensure the steel in each girder would line up with its counterpart once the deck concrete was placed. The beams were placed such that the ends of the lap splice were touching before being tied into place. The inside rebar was tied directly to the welded wire and outside rebar supported on

plastic chairs. All rebar was tied together to prevent lateral movement during casting. The final placement of rebar and trial fitting of the lap splice in the deck can be seen in Figures 13 and 14. Foam board insulation was used as end plates around the lap splices and plywood end plates were used on the other end.



Figure 13: Deck reinforcement vertical offset (a) and adjacent lap splice alignment (b)



Figure 14: Deck reinforcement placed in formwork

The next step was to pour the conventional deck concrete as specified in the mix design presented in Section 3.1. The concrete was mixed in the same Praschak spiral blade mixer as the girder concrete, but with a target compressive strength of

6000 psi and a slump of 8 in. Once the concrete was removed from the mixer a slump test was performed in accordance with ASTM C1611. Additionally, a total of twelve 4 in. by 8 in. cylinders were made for each set of girders. The rest of the concrete was transported from the mixer and placed into the formwork using a hopper suspended by the overhead crane. A mallet was used to tap the sides of the forms to help the concrete flow into the forms. The decks were cured for 7 days covered in wet burlap. The formwork was not removed at a specific time, but the compressive strength was checked to ensure the concrete had reached 4000 psi before the forms were removed. Various stages of the casting process can be seen in the following Figures 15 and 16.



Figure 15: Freshly placed deck concrete showing a close-up of the forms around the lap splice (a) and an entire set of specimens (b)



Figure 16: Finished concrete decks after form removal

3.4 Continuity Joints

Three pairs of continuity joints were constructed with two types of positive moment steel details and identical negative moment lap splices. Two types of UHPC were utilized: a UHPC mix developed at OU called J3, and a commercially available premixed UHPC product called Ductal®. Both UHPC mix designs are described in Section 3.1. All positive moment steel details were developed by considering both the existing code requirements for continuity joints made of conventional concrete and existing literature on the superior performance of UHPC.

3.4.1 Continuity Joint Design

Design of the continuity joint started in accordance with the *AASHTO LRFD Bridge Design Specifications* (2017) and the literature mentioned in the commentary of each section. Since the provisions provided in AASHTO are for use with conventional concrete, relationships found in other literature regarding

UHPC performance were considered in design. Figure 17 has been provided to identify pieces of the joint discussed later in this section.

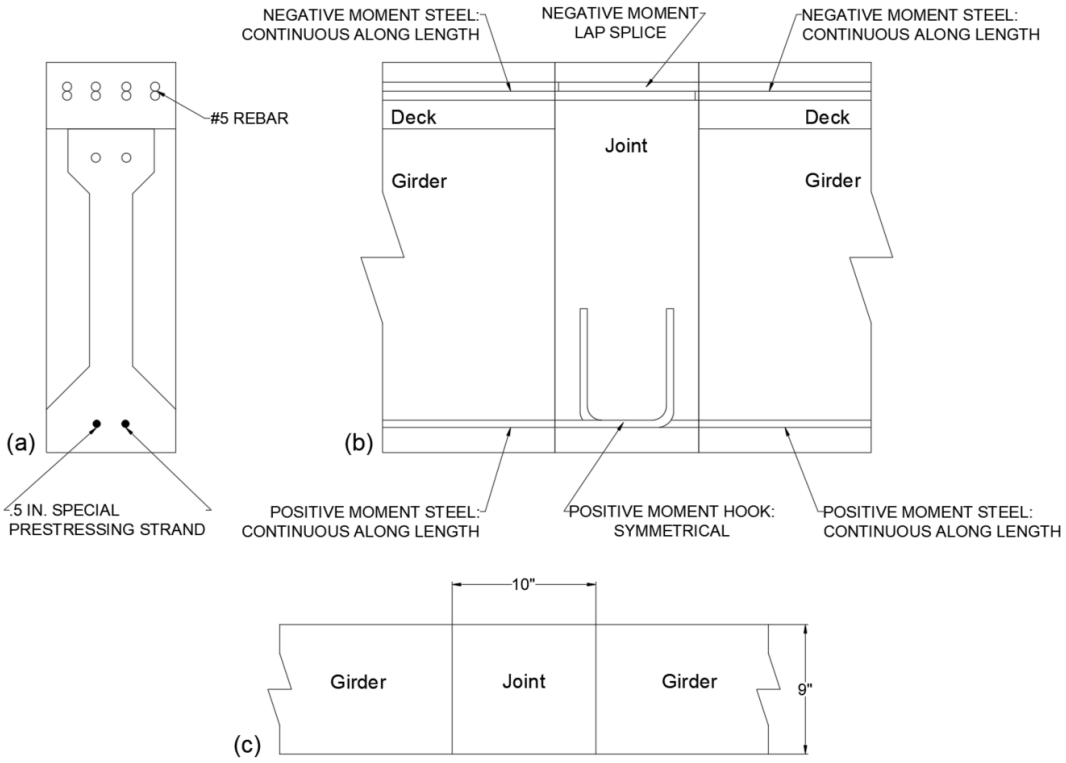

Figure 17: Hooked strand continuity joint cross-section (a), elevation view (b), and plan view (c)

3.4.1.1 Negative Moment Lap Splice Design

The negative moment steel and lap splice design was slightly modified from the design used by Casey (2019). The original design was adequate for a single point load applied at midspan of each girder, which was the worst case for a two span continuous loading. The design utilized four number 5 rebar spaced at 2 in. on center with the centroid of steel 2 in. from the top of the joint. The steel was then terminated at the point in which it was adequately developed into the deck, as specified in Section 5.10.8.1.2 of AASHTO LRFD (2017). The article states that

reinforcing steel must extend a given length past the inflection point of the moment to provide adequate development. However, due to utilizing an alternative testing setup, there is no inflection point for moment along the length of the specimen. Therefore, the steel could not be terminated and was continuous along the length of the deck.

Recommendations provided by Yuan and Graybeal (2014) were used as reference to calculate the dimensions of the lap splice in UHPC. The minimum recommended values for embedment length and splice length were $8d_b$ and $3d_b$, which resulted in 5 in. and 3.75 in., respectively, where d_b is the bar diameter. However, due to the geometry of the deck, the recommended minimum cover distance of $3d_b$ was not satisfied. Yuan and Graybeal recommended extending the embedment length to $10d_b$, or 6.25 in., for cases where the provided cover is between $2d_b$ and $3d_b$. The recommended value could not be achieved without changing the joint dimension, so the splice steel was extended 9.75 in. into the joint and resulted in embedment and splice lengths of 4.75 in. and 9.5 in. respectively. The finalized negative moment steel layout used for all specimens is provided in Figure 18.

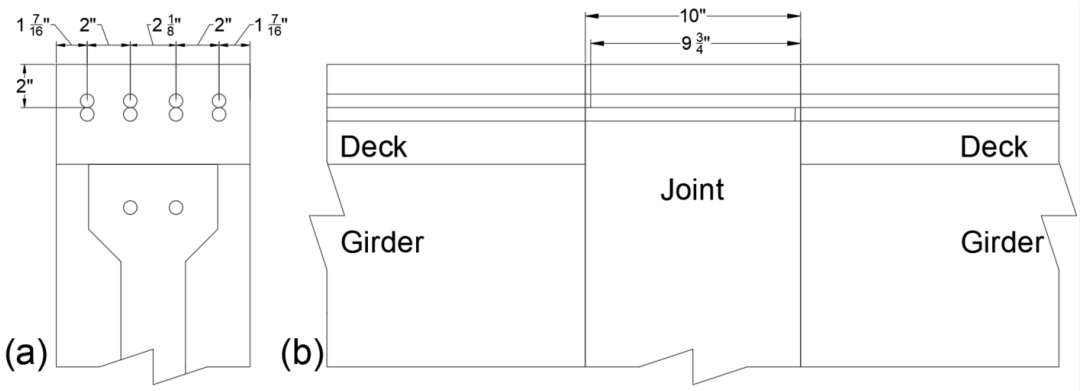

Figure 18: Negative moment lap splice cross-section (a) and elevation (b) view

3.4.1.2 Positive Moment Hooked Strand Design

Two different types of positive moment connection were constructed in order to test a range of variables within the joint. Positive moment designs were based loosely on the provisions of AASHTO LRFD (2017) and selected literature listed in the commentary. Most of the design assumptions used to optimize the joint for UHPC performance were used in the positive moment design. The decision to use hooked strands comes from existing code regarding girders made continuous with conventional concrete. Section 5.12.3.3.9c of AASHTO LRFD (2017) states that the strands shall project at least 8 in. from the face of the girder before they are bent. This section also provides equations for the maximum stress in the strands at both the service and strength limit states as a function of the total length of the strand. These equations were combined with recommendations provided in Graybeal (2014) regarding the development length of untensioned prestressing strand in UHPC to estimate the amount of strand needed to fully develop the hooked prestressing strand. Provided that the strand projection was set at 8 in. and the target stresses are known, the modified equations could be used to find the

total length of strand needed. The 8 in. embedment was then subtracted to provide the length of the vertical section of the hook. The detail used to construct bent strands to resist positive moment is provided in Figure 19. Four of the six specimens constructed utilized this design.

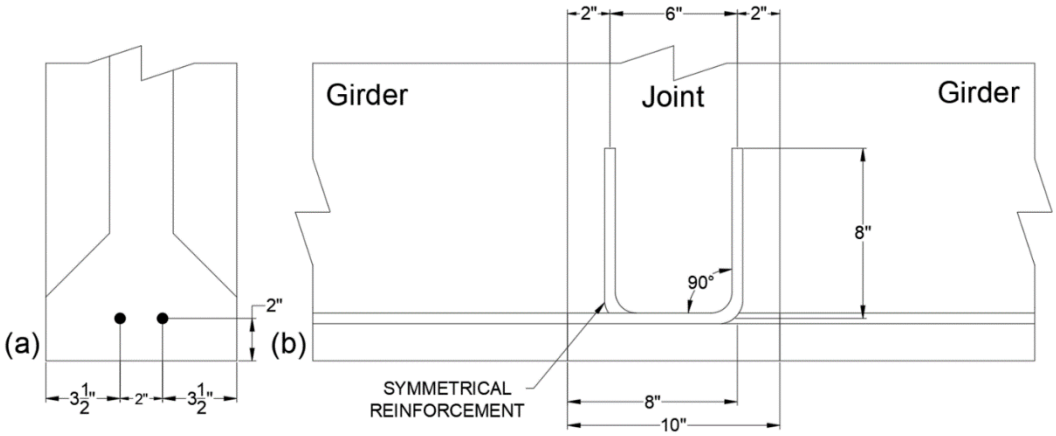

Figure 19: Positive moment hook cross-section (a) and elevation (b) view

3.4.1.3 Positive Moment Straight Strand Design

The second type of positive moment reinforcement featured a straight strand contact lap splice, which is atypical for positive moment steel in a continuous joint. This design prioritized constructability and tested whether hooked strands are needed when using UHPC. The strands extended 9.75 in. into the joint so that they could provide the longest embedment length possible without changing the geometry of the joint. Articles such as Yuan and Graybeal (2014) suggest that longer embedment lengths correlate to greater stresses developed in the strands. They also suggest that non-contact lap splices produce greater bond strength between UHPC and strand, however, bending the strand to fit in the joint would introduce additional variables to the design and was ultimately rejected. For

girders with more strands in the bottom flange, strand extensions could potentially be alternated to create a true non-contact lap splice in the joint. Ultimately, the decision to proceed with straight strands gives insight into whether the failure mode of the joint changes with varied development. It was hypothesized that this style of connection would lead to a failure mode that differs from hooked strand detailing. By investigating the maximum internal moment generated at the strands, a correlation between the bond stresses of the prestressing strand and the development length can be calculated to provide an informed recommendation regarding future design. Complete detail of the straight strand connection is provided in Figure 20.

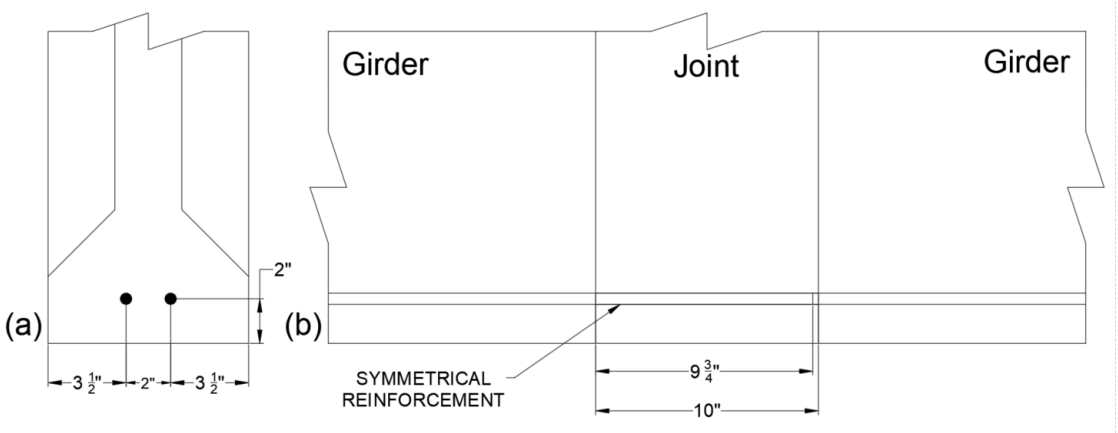

Figure 20: Positive moment straight strand cross-section (a) and elevation (b) view

3.4.2 Continuity Joint Construction

The construction of UHPC continuity joints consisted of a series of steps. The first step was to shape the prestressing strand into the desired shape for use in the joint. Each stand was bent to the desired radius with a bending tool and a piece of pipe. Next, the girders were placed into position for casting. The free ends of the

girders were supported by plywood strips and the interior supported by a square plate that would serve as the bottom piece of formwork for the joint. Once the first girder was set into place, the other would be aligned close to its final position. The target thickness of the continuity joint was set at 10 in. The concrete decks were not used as a point of reference as their shape was not perfectly uniform along their length. Any imperfections from the deck forms, as well as imperfections in the girders were also apparent in the decks. For these reasons it was determined that the exposed prestressing strands at each end of the girders would serve as the best reference point while making final adjustments. They were under significant stress during casting which provides a consistent point of reference. A string line was set up alongside the entire length of the specimens and the girders were moved into place, using the strands and string line as reference. Careful attention was taken to the alignment of the mild steel lap splices projecting from the deck, as well as the prestressing strand. If the mild steel bars did not align to form an adequate contact lap splice, a steel pipe was used to bend the mild steel bars into position. Joint reinforcement prior to casting can be seen in Figure 21. Wire and rebar ties were used to hold all steel reinforcement into position as needed.

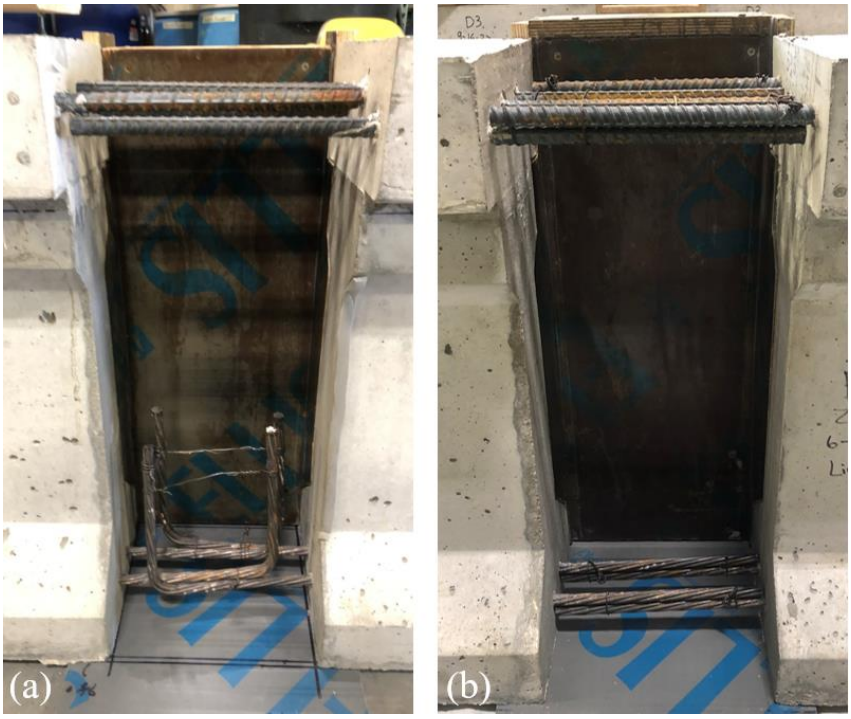

Figure 21: Joint reinforcement for hooked strand (a) and straight strand (b) designs

Once the girders were aligned and the steel reinforcement was set, formwork that followed the contour of the beam could be set perpendicular to the girders to form a rectangular joint. Due to slight variations in the shape of the girders, each piece was trial fit to determine its final placement. The forms were secured in place such that the joint corners were roughly 90 degrees. Next, these form pieces were secured in place on the bottom and the top was held in place with a bar clamp. At this point, the joint formwork was complete, and the edges were sealed using silicone. The completed formwork a can be seen in Figure 22.

The next step in construction included casting the concrete. Since there were two pairs of each type of joint being made, two joints were cast at a time. The mixer used was a gas-powered Stone HM1290 paddle type mortar mixer. Each batch was 4.5 ft^3 and proved to be just within the UHPC mixing capacity of the mixer.

Since UHPC requires much more energy to mix than conventional concrete, the batch size often must be significantly less than the design capacity of the mixer. The mixer direction was reversed intermittently and even stopped at certain points to evaluate the flowability. After the fibers were added a flow test was conducted in accordance ASTM C1437 and C1856 to validate adequate workability. The UHPC was then carted over to the joints and placed into the joints using scoops. Mallets were used to tap the sides of the forms during placement to help with consolidation. The J3 UHPC filled into the joints as expected and remained at the desired level after setting, however, the joints made of Ductal® settled more than expected. It is believed that Ductal® includes an admixture that pushes trapped air to the surface. The Ductal® utilized had also been sitting for a significant amount of time, which could have negatively impacted performance. An effort was made to overfill the joints, but the magnitude of entrapped air caused the joints to be approximately ¾ in. below the desired level. The joints were left to cure for 24 hours and the compressive strength for each specimen was at least 14,000 psi before they were moved. Completed continuity joints are shown in Figure 23.



Figure 22: Plan views of joint formwork secured in place showing a close-up of the reinforcement (a) and zoomed-out view of the restraints (b)



Figure 23: Completed continuity joint before (a) and after (b) formwork removal

3.5 Specimen Testing

3.5.1 Objectives

The specimens were tested both upright and upside down to test the capacity of both positive and negative moment, respectively. The first hooked strand specimen test was conducted to induce a negative moment in the specimen, which resulted in significant damage. Therefore, the decision was made to test the second hooked strand specimen for positive moment first. This approach proved successful, as the second hooked strand specimen was able to be tested a second time for a negative moment. This approach was used for all remaining specimens with hooked strands. To adequately test the details of the straight strand specimens, one specimen was tested in positive moment first and the second specimen was tested in negative moment first. This approach proved beneficial as it allowed each orientation to be tested without preexisting damage.

To test each specimen for both positive and negative moment, the specimens were flipped between tests. This was achieved using an overhead crane and bearing pads. First, the specimen was placed on bearing pads in its existing configuration. The chains of the crane were then wrapped around the joint such they would pick the specimens up at roughly a 60-degree angle. The specimen was then lowered onto the bearing pads laying on its side. The chains were again rearranged such that they would completely flip the specimen when lifted. The specimens were then carefully rested into their new orientation. The chains were adjusted for a final time and the specimen was moved into position for testing.

3.5.2 Approach and Instrumentation

Testing started roughly 28 days after the first set of continuity joints were cast. The girders were tested on a 17 ft span with the continuity joint at the center of the span and were simply supported on steel rollers. Both rollers could rotate but only one was free to move laterally, providing minimal restraints at the ends. The test specimens were loaded in the center of the joint for all tests using a hydraulic ram attached to a steel reaction frame. Applied loads were monitored through a load cell with a capacity of 100 kips. The load cell was supported by a swivel used to compensate for rotation of the beam and a bearing plate to allow the applied load to be evenly distributed throughout the center of the joint. In some instances, the surface of the UHPC was too uneven to be adequate for testing, so a layer of sand was used to fill in any voids and provide a level area to distribute the load.

Each girder was instrumented during testing to monitor deflection and joint movement for later analysis. Wire potentiometers (pots) were placed on the floor and connected to the load plate at the center of the joint using magnetic hooks to monitor vertical deflection throughout the duration of testing. A laser was placed on the beam to allow manual deflection measurements to be compared to data taken from the wire pots during testing. A total of four linear variable differential transformers (LVDTs) were used to monitor the relative movement of the continuity joint from the girders. The LVDTs were placed at each interface 2 in. above the extreme tension fiber, as seen in Figure 24. Concrete screws were used to hold the LVDTs on the girder and aluminum brackets were glued to the UHPC

to provide a surface for the sensors to measure from. LVDTs were not needed at the support locations because reinforced steel rollers ensured no appreciable vertical deflection occurred at these locations. All instruments were monitoring and readings recorded using a single National Instruments data acquisitions system.

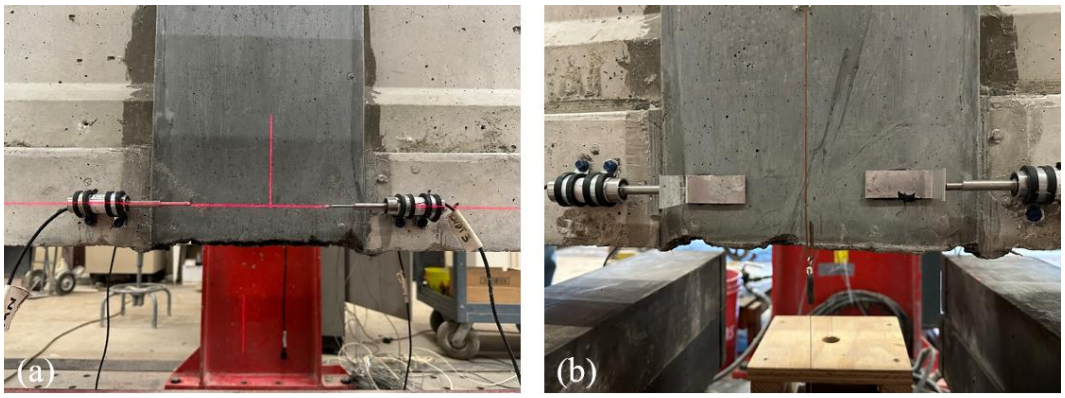

Figure 24: Alignment of the LVDTs before (a) and after (a) adding aluminum bearing plates

Before testing could begin, the specimens were set into the load frame using the overhead crane and rollers. The specimens were then carefully aligned so that they were centered in both directions on the rollers and hydraulic ram. Since there was slight variability in girder length, the roller locations were checked from the center of the joint. Any additional overhang beyond the rollers would not affect the performance of the specimens. In the interest of safety, bearing pads and lateral supports were placed under and around the joint in case it were to catastrophically fail during testing. Next, the LVDTs and wire pots would be secured to the beam, followed by the sand, swivel, spacer, and load cell. Once all instruments were in place, they were tested for accuracy by displacing them a

known amount and comparing the readout of the instrument. The apparatus used to apply the load to the joint can be seen in Figure 25.



Figure 25: Detailed view of components for joint testing apparatus

Before each test the instruments were zeroed out. The hydraulic ram was then advanced until it was almost contacting the specimen. Once the ram started applying load and stabilized at around 1500 lb the test commenced in 5 kip increments until the specimen cracked. If cracking was detected on an odd number, the next increment was 3 kips so that testing could proceed with even numbers. Beyond this point, the remainder of the test proceeded with 2 kip load increments. Between loading increments the specimens were examined for cracks and a manual deflection measurement was taken. Any new cracks were marked

with a marker and labeled with the load at which they were observed. The test was stopped once the specimen could not withstand higher loading or the specimen sustained an unsafe amount of damage.

4.0 Results

4.1 Specimen Nomenclature

The labeling of continuity connection specimens is based on the variables found in the joint. The differentiating variables found in the name include the strand geometry, the type of UHPC used, and a number to differentiate the testing order of specimens with matching details. The first two characters represent strand geometry and denote either hooked strands (HS) or straight strands (SS). The third and fourth characters represent the material used to make the UHPC joint and denote either Ductal® (DU) or J3 (J3). The following number will be either 1 or 2 and denotes the order testing was done. For example: the specimen called SSDU-2 includes a joint made with straight strands embedded in Ductal® and was the second specimen of this type tested.

4.2 Concrete Properties

4.2.1 Fresh Properties

During each casting, the workability of fresh concrete was measured by using the testing methods specified in Section 3. In some cases, the UHPC flow was greater than 10 in. and could not be accurately measured on the flow table. These cases will be denoted with a plus sign (+) in the table. The flow results for each specimen are provided in Table 5.

Table 5: Results of fresh concrete slump testing (in.)

Specimen	Girder (slump flow)	Deck (slump)	Joint (flow)
HSJ3-1	26.75	8.75	+10
HSJ3-2	26.0	8.75	+10
HSDU-1	26.5	8.00	10
HSDU-2	28.5	8.00	10
SSDU-1	24.5	8.50	10
SSDU-2	25.5	8.50	10

In most cases, the desired workability was achieved without compromising performance. The SCC used in the girders did not always meet the 26 in. target slump flow; however, the concrete was stable and achieved adequate workability for placement. The conventional concrete used in the decks was consistently close to the targeted 8 in. slump and required minimal effort to place. The J3 UHPC exceeded the targeted flow but ultimately did not result in lower performance than expected. The Ductal® UHPC achieved the desired flow, but significant segregation of the steel fibers was observed after casting and that was not apparent during fresh property testing. Without additional testing, it is difficult to say what caused this behavior.

To achieve the desired workability without compromising compressive strengths, HRWR was added to the mix based on the discretion of experienced operators at the time of mixing. The exact dosage of HRWR used for each batch of girder concrete is provided in Table 6. The dosage of HRWR used for each batch of deck concrete was 5 fl. oz/100 lb of cement. The dosage of HRWR used for the J3 joints was 24 fl. oz/100 lb of cement. The dosage of HRWR used for the two

batches of Ductal® was 974 fl. oz/yd^3 and 930 fl. oz/yd^3, respectively. The units used to describe the dosage of HRWR used in Ductal® are different from the other concrete mixes because the actual cement content is unknown.

Table 6: Dosage of HRWR for SCC used in girders (fl. oz/100 lb of cement)

Specimen	Girder
HSJ3-1	11
HSJ3-2	9
HSDU-1	9.5
HSDU-2	10
SSDU-1	8.5
SSDU-2	9.5

4.2.2 Compressive Strengths

Apart from UHPC being tested at a ramp rate of 150 psi/s based on ASTM C1856, compressive strength tests were conducted in accordance with ASTM C39 at a ramp rate of 35 psi/s. Neoprene end caps were used to prepare the ends of cylinders with a design compressive strength under 7000 psi. A cylinder grinder was used to prepare the ends for cylinders with a design compressive strength over 7000 psi. In some instances, both the 28-day strengths and test-day strengths presented are identical across multiple specimens and test days. This is because girders were cast in sets of two, decks in sets of four, and continuity joints in sets of two using the same concrete. Some connection specimens were tested twice on the same day, causing negligible changes in compressive strength between tests. Strengths listed twice based on the same set of cylinders will be denoted with an asterisk (*).

The compressive strengths of each type of concrete used for each test specimen are presented in Tables 7-12. Strengths found in each table are provided in the order in which cylinders were tested. The compressive strength of the deck and joint concrete was tested when the forms were removed instead of at a specified time, so 1-day strengths were intentionally not collected and are denoted by "--" in the compressive strength tables. The compressive strength for the decks ranged from 4600 to 4700 psi in the first 3 days, when the forms were removed. The compressive strength for the Ductal® joints ranged from 15,000 to 18,800 psi between days 3 and 4. The true strength of Ductal® cylinders may be slightly lower than measured values because they had to be ground to a height of approximately 5.25 in. due to air voids near the top surface.

Table 7: Compressive Strengths for HSJ3-1 (psi)

Day of Testing	Girder	Deck	Joint
1 Day	6670	--	14020
28 Day	9470	6670	18430
Negative Moment Test Day	10450	6560	19750

Table 8: Compressive Strengths for HSJ3-2 (psi)

Day of Testing	Girder	Deck	Joint
1 Day	6280	--	14020
28 Day	8860	6670	18430
Positive Moment Test Day	9450*	6690*	19890*
Negative Moment Test Day	9450*	6690*	19890*

Table 9: Compressive Strengths for HSDU-1 (psi)

Day of Testing	Girder	Deck	Joint
1 Day	6840	--	--
28 Day	8940	6370	27040
Positive Moment Test Day	10020	6540	29460*
Negative Moment Test Day	10120	6280	29460*

Table 10: Compressive Strengths for HSDU-2 (psi)

Day of Testing	Girder	Deck	Joint
1 Day	6940	--	--
28 Day	9320	6370	27040
Positive Moment Test Day	10320*	6240*	29700*
Negative Moment Test Day	10320*	6240*	29700*

Table 11: Compressive Strengths for SSDU-1 (psi)

Day of Testing	Girder	Deck	Joint
1 Day	6650	--	--
28 Day	9500	6220	26420
Positive Moment Test Day	9720	6100	29550*
Negative Moment Test Day	9400	6210	29550*

Table 12: Compressive Strengths for SSDU-2 (psi)

Day of Testing	Girder	Deck	Joint
1 Day	6680	--	--
28 Day	9550	6220	26420
Negative Moment Test Day	10160	6080	29550*
Positive Moment Test Day	9990	5920	29550*

4.3 Joint Testing

The primary objective of joint specimen testing was to understand how the strand details and joint materials affect joint performance under both positive and negative moment loading. All relevant data collected during testing of each specimen are presented in the appropriate section. Additionally, each of the tests are presented in chronological order. To specify the orientation of each specimen during testing, the terms positive moment or negative moment are used. Negative moment means the specimen was tested upside down to replicate a bridge system experiencing a negative moment at the joint. Positive moment means the specimen was tested right-side up to replicate a bridge system experiencing positive moment at the joint. Further details on specimen testing configuration are included in Section 3.5.2. The specimens were examined before testing to identify any pre-existing cracks that formed before loading. Any such cracks were marked and labeled with 0 kips to indicate they were not caused by loading during the test. The term interface will also be used extensively to describe the location of cracking. The interface is taken as the location in which the concrete from either the deck and joint or the girder and joint are bonded together. Additionally, words such as top and bottom will be used to describe cracking behavior. Since the orientation of the specimens changes between each test, the face of the specimen which was on the top during casting will be referred to as the “as-cast top” and the face which was on the bottom during casting will be referred to as the “as-cast bottom”.

4.3.1 HSJ3-1 Negative Moment Test

Specimen HSJ3-1 was first tested in the negative moment orientation. The joint interface before testing is shown in Figure 26. A thin layer of UHPC and silicone can be seen on the surface of the girder near the joint in Figure 26. This was an artifact on all specimens from the joint casting process and did not affect structural testing results.



Figure 26: Northwest (a) and southwest (b) side of the joint HSJ3-1 before testing

Initial flexural cracking was observed in the as-cast top face of the deck at a load of 10 kips. Initial cracks started small and were within approximately 2 ft of the joint. Cracks propagated up and into the girder as loading increased. At 10 kips, two cracks were detected in the joint, one near the joint-deck interface and one directly under the load point. Between 10 and 22 kips, these cracks grew to a length of approximately 5 in. but did not show further cracking throughout the duration of testing. At a loading of 12 kips, a crack was detected that propagated

from the point of initial cracking in the deck, into the girder, and then along the joint-girder interface to approximately half the depth of the girder. From 12 to 20 kips, the joint-girder interface opened, and cracking along the interface propagated to approximately the location of the prestressing strands. From 20 to 46 kips, the flexural cracks that started in the deck gradually extended toward the load point. Up to a loading of approximately 30 kips, new flexural cracks were detected in the deck and girder farther out from the joint along the length of the specimen. The farthest started approximately 7 ft away from the joint. Cracks would generally converge at some point in the web of the girder on their way to the load point. As loading increased the growth of flexural cracks generally slowed, and only additional separation at the joint-girder interface was observed. At 46 kips, the vertical crack along the joint-girder interface reached the as-cast bottom flange and turned toward the load point, causing horizontal cracks to form in the joint. No additional flexural cracks were detected in the girder beyond this point. Beyond 50 kips, the magnitude of deflection between loading increments increased significantly. At 52 kips, additional horizontal cracking started to occur in the joint around a location assumed to coincide with the strand location. Cracks were not marked beyond this point and any additional deflection was the result of the crack from the deck into the joint-girder interface opening. At this point, the separation at the joint was so significant it was possible to clearly see through to the other side. The test was stopped when the specimen reached a loading of 56 kips but failed to go any higher with additional deflection. The manually measured deflection was 2-3/4 in. under final loading and 2-1/8 in. after the load

was removed. The state of the specimen before the load was removed can be seen in Figures 27 and 28 including the cracks marked throughout testing.



Figure 27: Northwest (a) and southwest (b) side of the joint HSJ3-1 under final loading



Figure 28: HSJ3-1 entire specimen showing deflection under final loading

Just after the test was stopped large chunks of concrete fell out of the deck and exposed the deck reinforcement, shown in Figures 29 and 30. The specimen suffered significant damage and was deemed unfit for testing in the positive moment orientation.



Figure 29: Southeast (a) and northeast (b) side of joint HSJ3-1 after final loading



Figure 30: East side of HSJ3-1 joint after final loading showing locations of significant concrete spalling

Figure 31 shows the load-deflection curve for specimen HSJ3-1 during negative moment testing. The readings from two wire pots, one on each of the east and west sides of the specimen at the load point, were averaged to provide the data included in the figure. Initial cracking was visually detected at a load of 10 kips. However, initial cracking only resulted in a minor loss of stiffness. From 10 to 42 kips the curve followed a slightly lower slope which coincides with the development of flexural cracks in the girders. A great change in stiffness occurred at around 42 kips, which was when cracking shifted from flexure in the girders to joint separation at the interface.

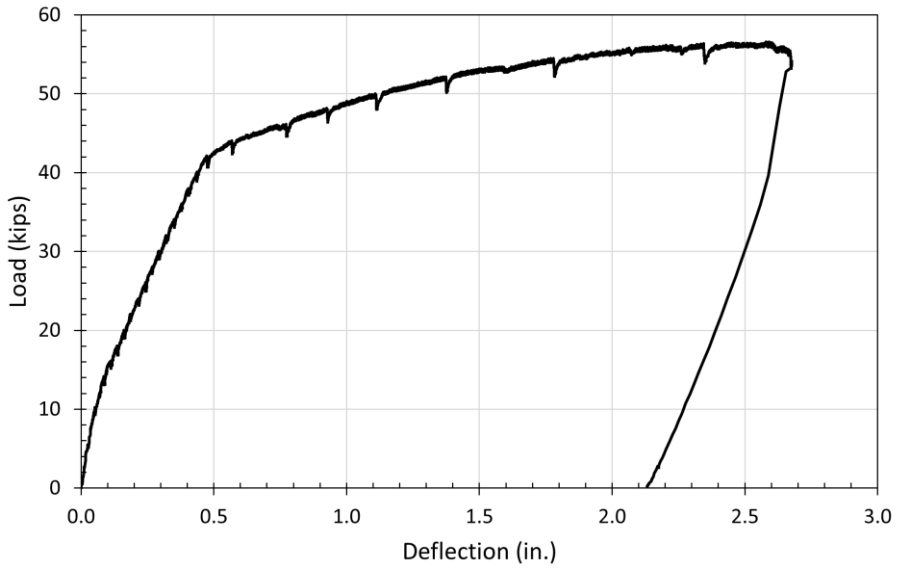

Figure 31: Load-deflection curve for HSJ3-1 during negative moment test

The load-joint separation curves for both the north and south joint-deck interfaces are presented in Figure 32. A total of four LVDTs were placed 2 in. above the extreme tension fiber of the deck to monitor separation at the interface. The data shown is the average measurement of the two LVDTs across the same interface, either the north or south side of the joint. The measured magnitude of joint separation on specimen HSJ3-1 was expected to be much larger than what was measured due to large visible separation at the joint-girder interface. However, because the joint separation propagated from cracks that started in the deck outside the LVDT locations the large visible separation was not measured. The part of the deck where the LVDTs were mounted was so well bonded to the joint that significant cracking occurred through the deck beyond the location where the LVDTs could measure. The separation that was measured followed similar trends at both interface locations. The south interface did show slightly greater

separation than the north interface for loads beyond 44 kips, which coincides with an overall decrease in stiffness for the entire specimen.

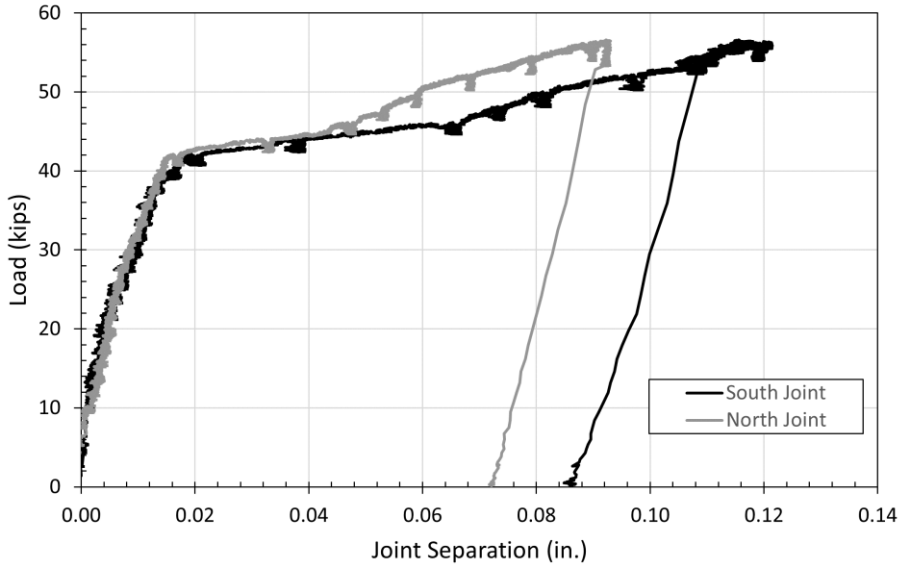

Figure 32: Load-joint separation curve for HSJ3-1 during negative moment test

4.3.2 HSJ3-2 Positive Moment Test

Specimen HSJ3-2 was first tested in the positive moment orientation. The joint interface before testing is shown in Figure 33.

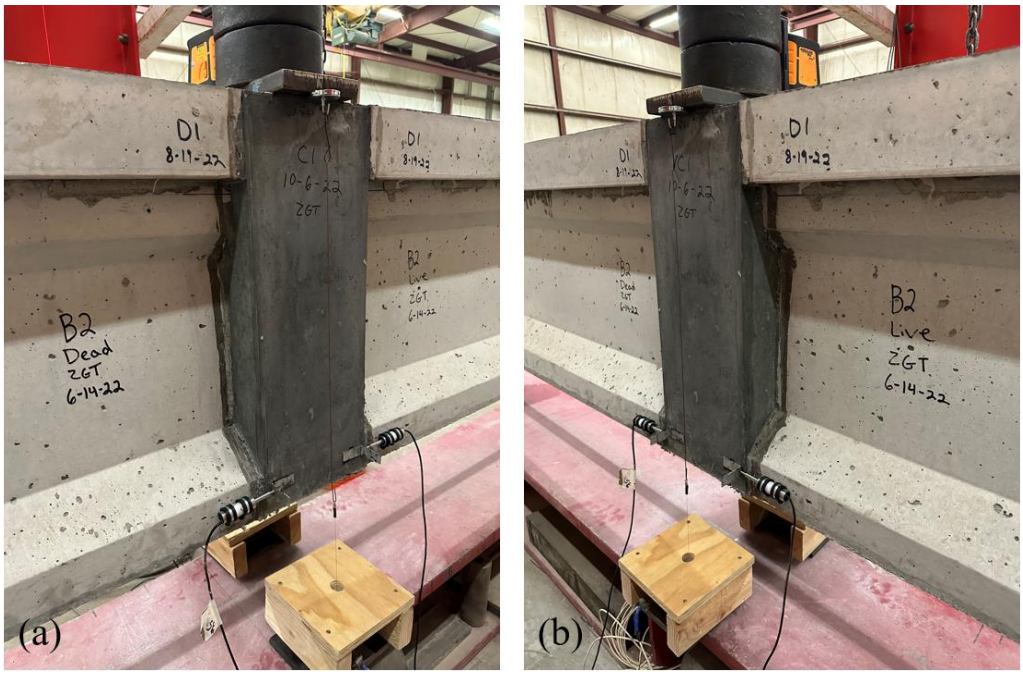

Figure 33: Southeast (a) and northeast (b) side of the joint HSJ3-2 before testing

Initial cracking was observed at a load of 5 kips and was present on both sides of the joint-girder interface along the as-cast bottom flange. The initial cracks propagated up the joint-girder interface as loading increased and were the only locations where cracks started throughout the duration of the test. From 5 to 10 kips, the initial cracks grew to the bottom of the as-cast top flange. At a loading of 12 kips, the cracks reached the bottom of the deck. At 14 kips, the crack opened halfway up the deck, to the approximate location of the mild steel lap splice. At 26 kips, the cracks turned toward the load point and caused horizontal cracks to form in the UHPC joint. For the remaining duration of the test, small cracks were observed around the existing crack at the joint-girder interface and large openings

at the joint-girder interface were observed. The state of the specimen before the load was removed can be seen in Figures 34-36 including the cracks marked throughout testing.



Figure 34: Southeast (a) and northeast (b) side of the joint HSJ3-2 after testing



Figure 35: Northwest (a) and southwest (b) side of the joint HSJ3-2 after testing

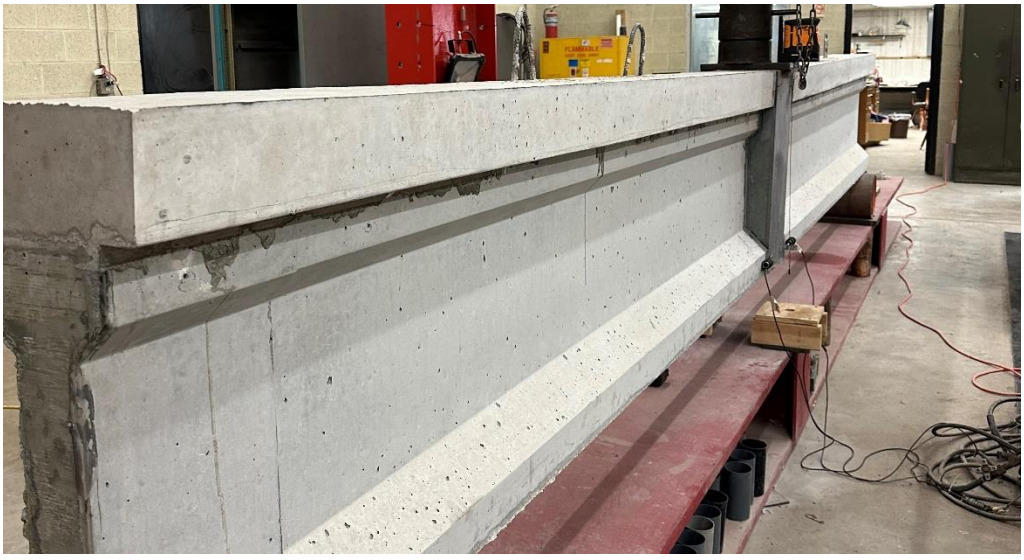

Figure 36: HSJ3-2 entire specimen showing deflection under final loading

The manually measured deflection was 1-3/16 in. under final loading and 3/8 in. after the load was removed. It was believed that the prestressing strands started to

slip in the joint before the test was stopped, but this conclusion was not supported by the significant rebound experienced by the specimen.

Figure 37 shows the load-deflection curve for specimen HSJ3-2 during positive moment testing. Initial cracking was visibly detected at a load of 5 kips. However, initial cracking only resulted in a minor loss of stiffness. At 12 kips, cracking was visibly detected at the bottom of the deck and resulted in a greater loss of stiffness. From 12 to 38 kips the curve followed a much lower slope which coincides with additional separation of the cracks that formed at the interface. For the remaining duration of the test, the load curve started to flatten out until the specimen failed to resist additional load. After the load was removed the deflection of the specimen rebounded significantly, suggesting that the strands in the as-cast bottom flange of the girder were adequately anchored in the joint.

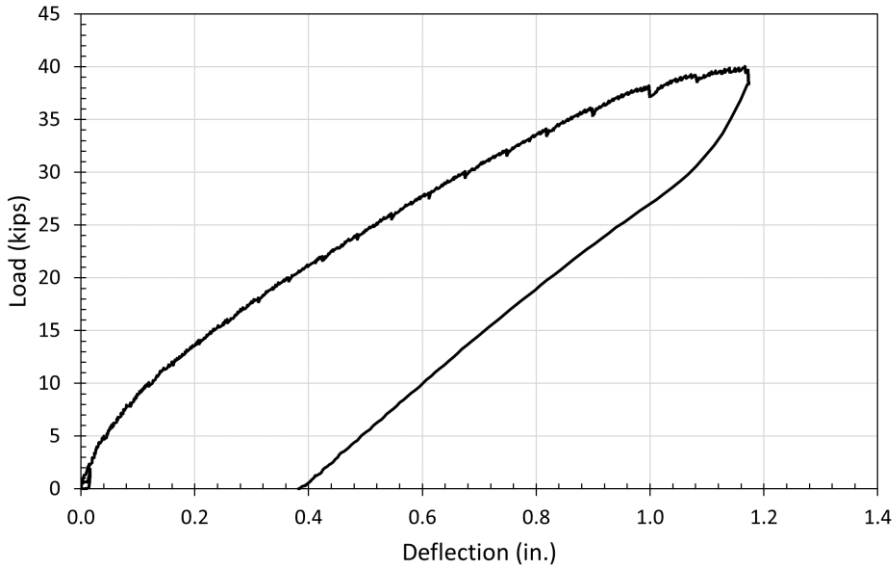

Figure 37: Load-deflection curve for HSJ3-2 during positive moment test

The load-joint separation curves for both the north and south joint-girder interfaces are presented in Figure 38. The measured magnitude of joint separation

on specimen HSJ3-2 during the positive moment test matched what was expected based on the cracking detected at the interface during testing. The separation that was measured followed similar trends at both interface locations during testing. However, the south interface showed a slightly greater magnitude of separation than the north interface beyond a load of approximately 38 kips. The load-deflection and load-joint separation curves show similar behavior, suggesting that cracking at the interface locations was the primary cause of overall specimen deflection.

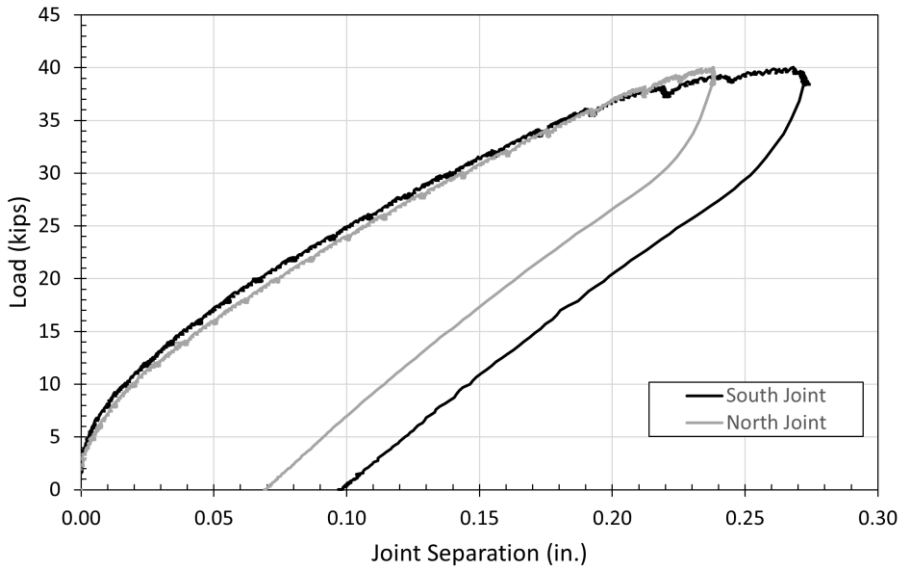

Figure 38: Load-joint separation curves for HSJ3-2 during positive moment test

4.3.3 HSJ3-2 Negative Moment Test

Specimen HSJ3-2 was removed from the load frame, flipped upside down, and placed back in the load frame to be tested in the negative moment orientation. No damage was observed while flipping the specimen. The state of the joint interface after positive moment testing, but before negative moment testing is identical to

that shown in Figures 34 and 35 in Section 4.3.2. Initial cracking was observed as flexural cracks in the as-cast top face of the deck at a load of 8 kips. Initial cracks started small and were dispersed within approximately 2 ft of the joint. Between 8 and 14 kips, the initial cracks started to propagate up through the deck toward the load point. From 14 to 20 kips, new flexural cracks beyond the initial cracks formed and extended from the as-cast top face of the deck to approximately the middle of the girder web. From 20 to 34 kips, small new cracks propagated intermittently out of existing cracks and connected to other existing cracks. From 36 to 48 kips, existing flexural cracks propagated up toward the load point and stopped at the as-cast bottom flange of the girder. The extent of flexural cracks in the girder due to negative moment loading is shown in Figure 39.



Figure 39: Flexural cracking at east side of the joint for HSJ3-2 under final loading

At 46 kips the joint interface, which was already extensively cracked due to positive moment testing, started to open greatly at the extreme tension fiber as

shown in Figure 40. Cracks were not documented after this point and significant deflection occurred with increased loading. The test was stopped after the specimen failed to reach a load of 52 kips. The final deflection of the specimen is shown in Figure 41. The manually measured deflection was 2-1/8 in. under final loading and 1-1/2 in. after the load was removed.

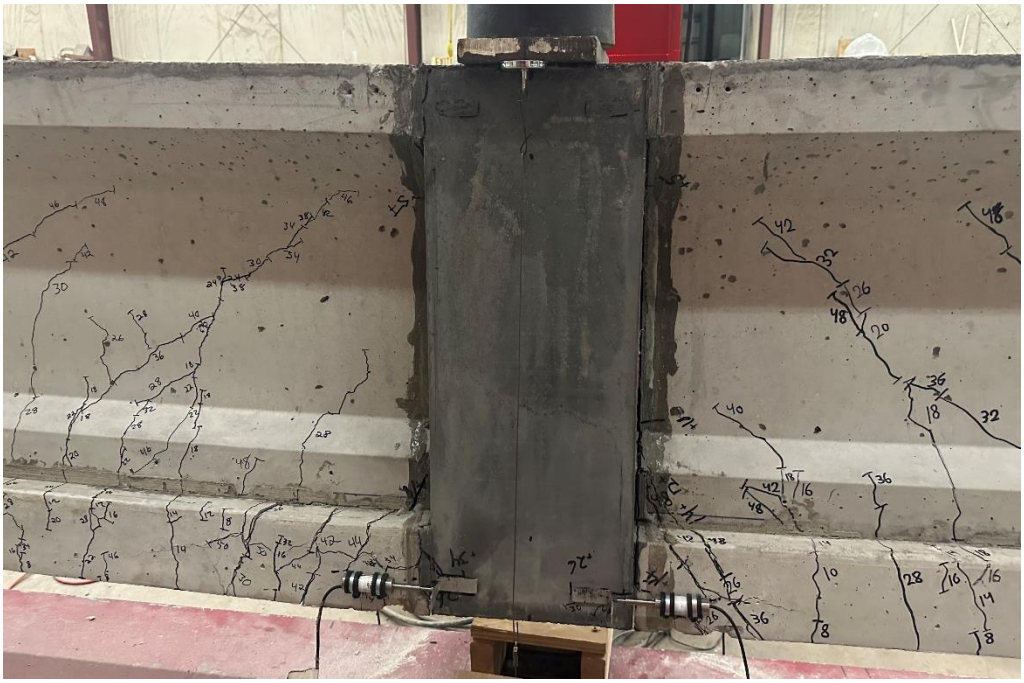

Figure 40: East side of the joint of HSJ3-2 with cracks at the interface under final loading



Figure 41: Visible deflection and additional flexural cracking of HSJ3-2 under final loading

Figure 42 shows the load-deflection curve for specimen HSJ3-2 during negative moment testing. Initial cracking was visibly detected at a load of 8 kips. However, a minimal loss of stiffness is shown in the graph at a load of 10 kips. From 10 to 42 kips the curve followed a lower slope which coincides with the development of flexural cracks in the girders. A great change in stiffness occurred at around 42 kips, which coincides with when cracking shifted from flexure in the girders to joint separation at the interface.

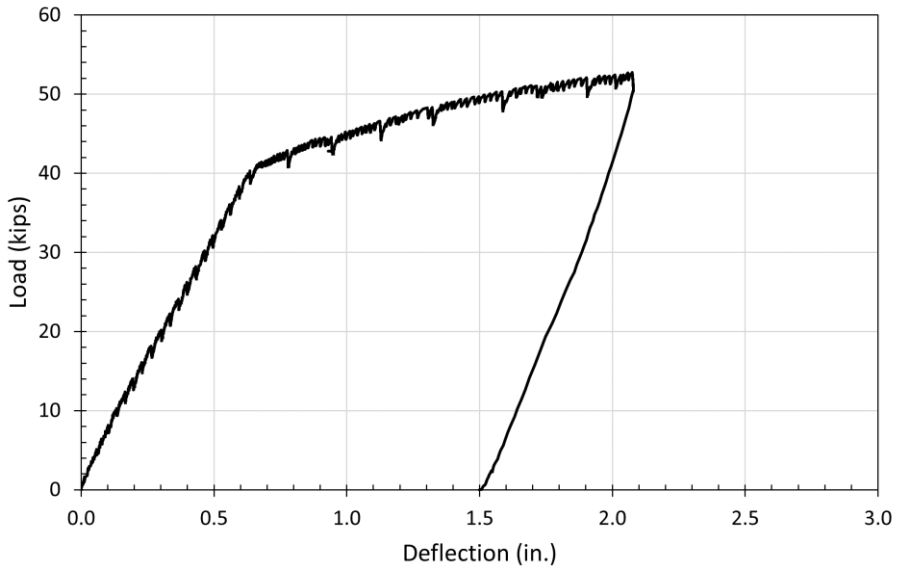

Figure 42: Load-deflection curve for HSJ3-2 during negative moment test

The load-joint separation curves for both the north and south joint-deck interfaces are presented in Figure 43. The measured magnitude of joint separation on specimen HSJ3-2 during the negative moment test was expected to be higher due to cracks at the interface that were caused by positive moment testing. However, flexural cracking was the primary failure mechanism observed during testing. The measured separation followed similar trends at both interface locations. The south interface did show slightly greater separation than the north interface for loads beyond 44 kips, which coincides with an overall decrease in stiffness for the entire specimen.

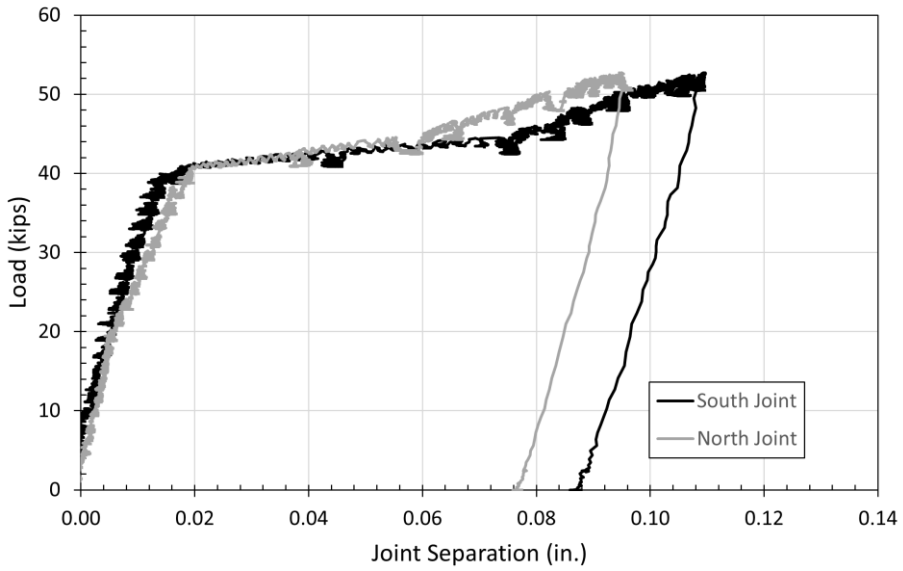

Figure 43: Load-joint separation curves for HSJ3-2 during negative moment test

4.3.4 HSDU-1 Positive Moment Test

Before testing, it was discovered that the as-cast top surface of the joint material for HSDU-1 had experienced approximately 3/4 in. of settlement. The magnitude of the settlement could be distinguished from above the specimen as well as due to a noticeable change in color along the depth. Additionally, a single preexisting crack was marked near the top of the joint. Figure 44 shows the joint before testing and includes the settlement circled in blue and the extent of preexisting cracking highlighted in red. Figure 45 shows the surface of the UHPC joint material before and after being prepped for testing in the positive moment orientation. A layer of sand was used to prepare the rough surface left by the settlement to evenly distribute the load from the bearing plate to the joint.

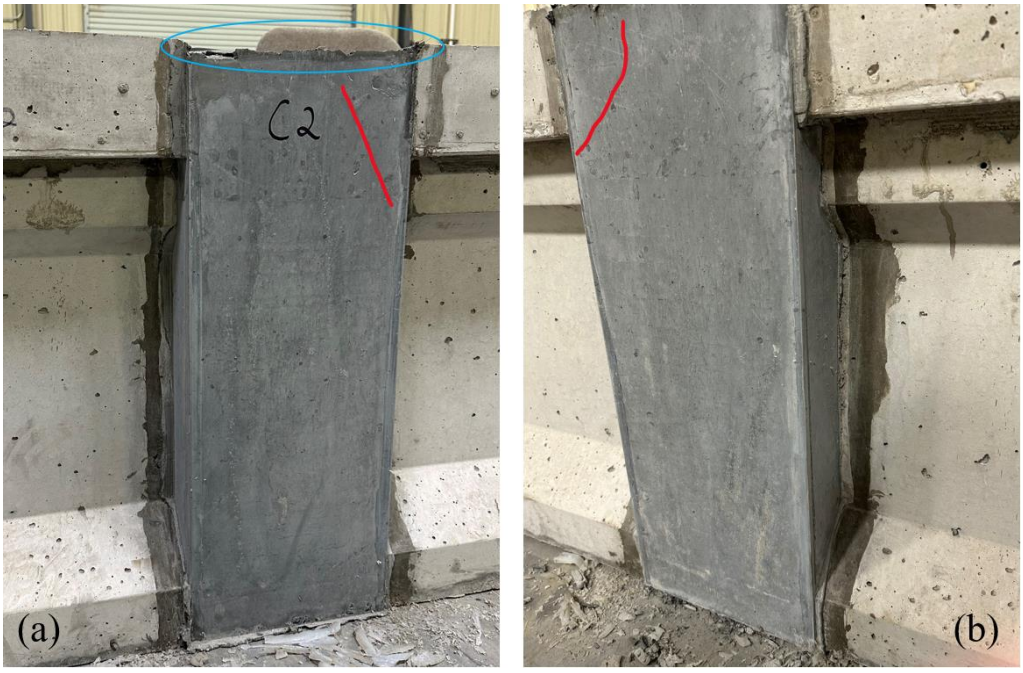

Figure 44: Preexisting settlement is indicated by a blue oval and preexisting cracking is indicated by a red line on the southeast (a) and northeast (b) side of the joint HSJ3-2 before testing.

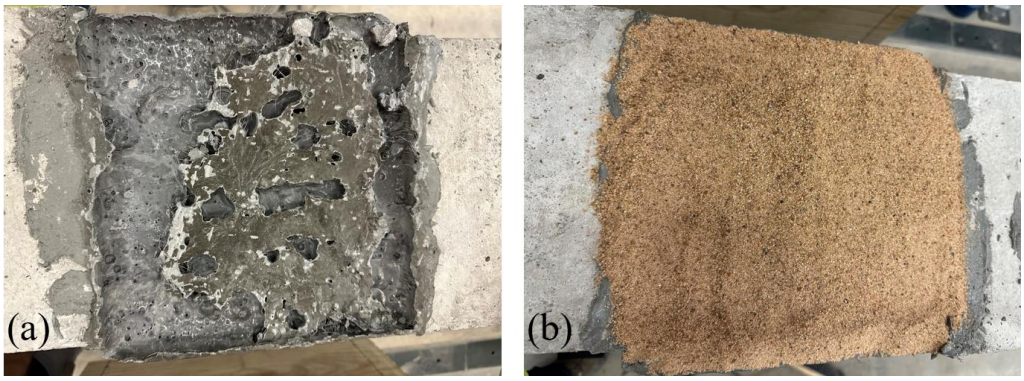

Figure 45: As-cast top of joint before (a) and after (b) masonry sand surface prep
Note: This figure shows SSDU-1 which experienced very similar settlement to HSDU-1

Specimen HSDU-1 was first tested in the positive moment orientation. Initial cracking was observed at a load of 5 kips on both sides of the joint-girder interface along the as-cast bottom flange. As shown in Figure 46, the initial cracks propagated up the joint-girder interface as loading increased and were the only

locations where cracks started throughout the duration of the test. At 8 kips, the initial cracks grew to the web of the girder. From 10 to 16 kips, the cracks followed the joint interface to the as-cast bottom of the deck. At 18 kips, the crack opened halfway up the deck, to the approximate location of the mild steel lap splice. At 20 kips, the crack turned toward the load point and caused horizontal cracks to form in the UHPC joint. From 22 to 46 kips, the horizontal cracks slowly turned up towards the load point in increments of less than 1 in. as seen in Figure 46. Simultaneously, the crack at the interface opened a considerable amount that could clearly be seen through. Separation at final loading is shown in Figure 47. The test was stopped when the specimen failed to reach 44 kips. The manually measured deflection was 1-5/8 in. under final loading and 11/16 in. after the load was removed.

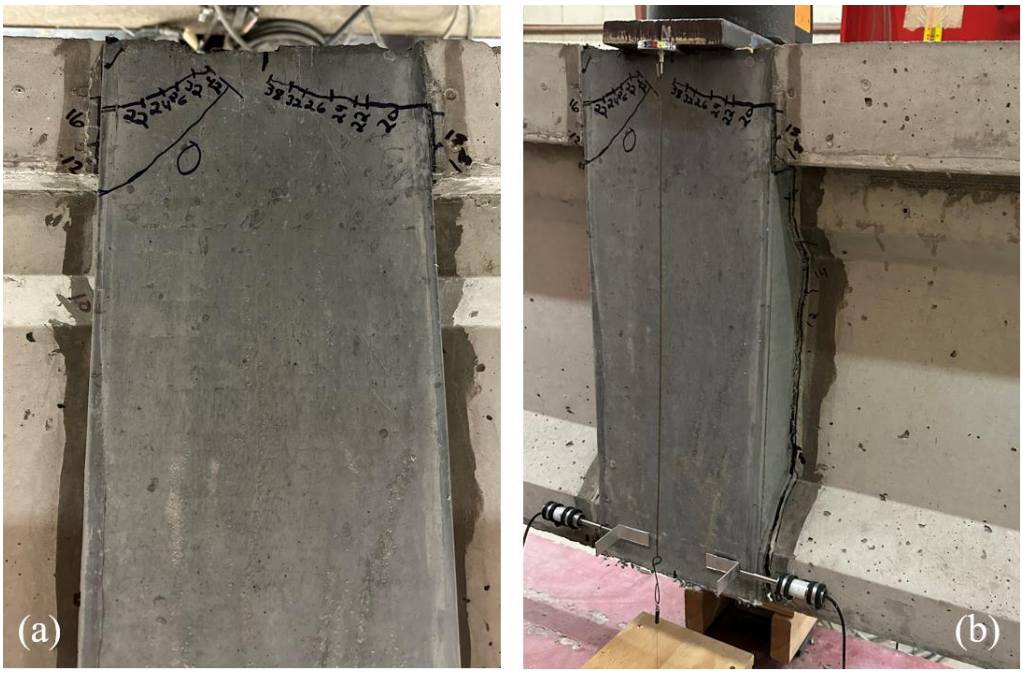

Figure 46: East side of joint (a) and northeast interface (b) of HSDU-1 after positive moment test

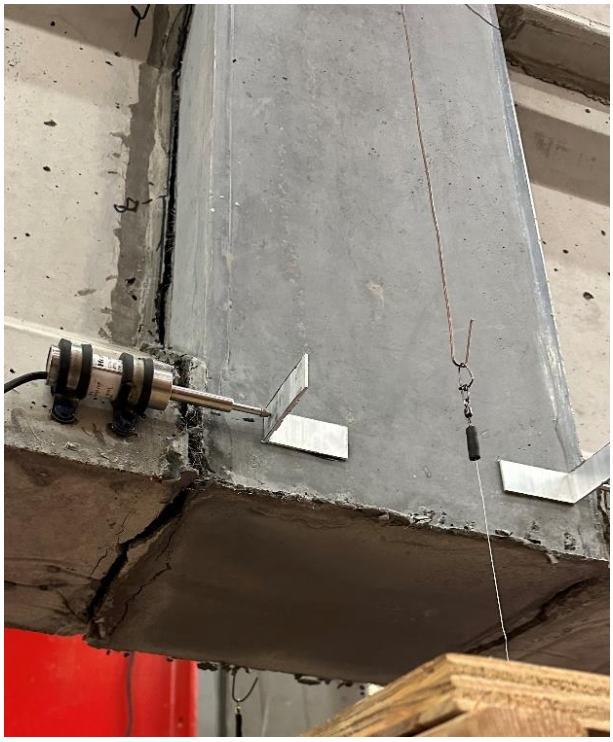

Figure 47: As-cast bottom of joint HSDU-1 showing separation at northwest interface under final loading of positive moment test

Figure 48 shows the load-deflection curve for specimen HSDU-1 during positive moment testing. Initial cracking was visibly detected at a load of 5 kips. However, initial cracking only resulted in a minor loss of stiffness. From 10 to 16 kips, cracking was detected up the interfaces toward the deck and resulted in a greater loss in stiffness. From 16 to 40 kips the curve followed a lower slope which coincides with cracking along the mild steel lap splice in both the joint and the deck, suggesting a bond failure. For the remaining duration of the test, the load curve started to flatten out until the specimen failed to resist additional load. After the load was removed the deflection of the specimen rebounded significantly, suggesting that the strands in the as-cast bottom flange of the girder were substantially anchored in the joint.

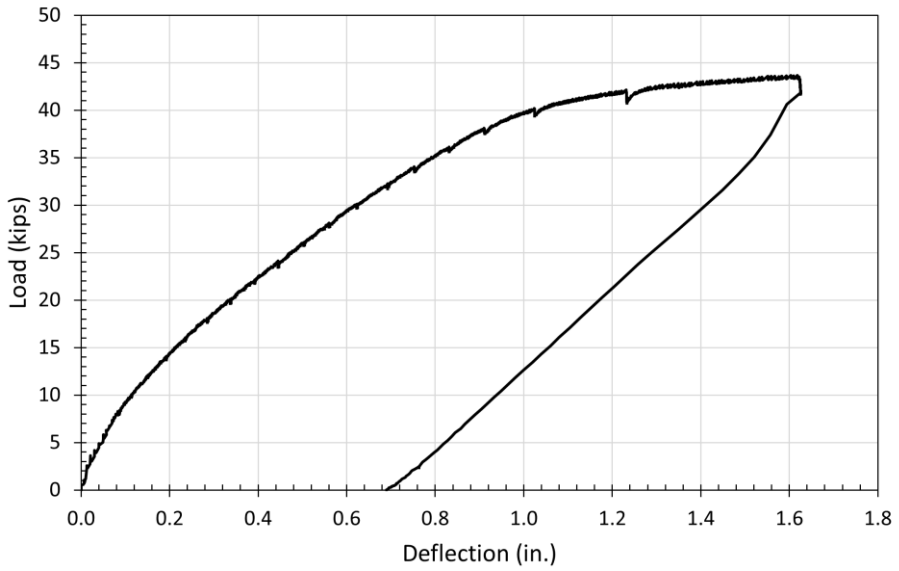

Figure 48: Load-deflection curve for HSDU-1 during positive moment test

The load-joint separation curves for both the north and south joint-girder interfaces are presented in Figure 49. The measured magnitude of joint separation on specimen HSDU-1 matched what was expected based on the cracking observed at both interfaces during testing. The measured separation followed similar trends at both interface locations during testing. However, the south interface showed a greater magnitude of separation than the north interface beyond a loading of 25 kips. The load-deflection and load-joint separation curves show similar behavior, suggesting that cracking at the interface locations was the primary cause of overall specimen deflection.

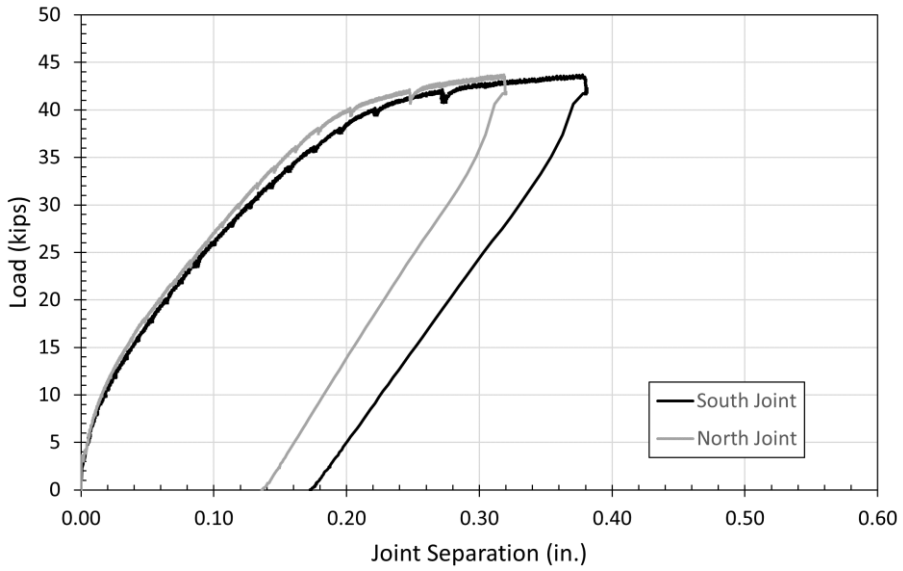

Figure 49: Load-joint separation curves for HSDU-1 during positive moment test

4.3.5 HSDU-1 Negative Moment Test

Specimen HSDU-1 was removed from the load frame, flipped upside down, and placed back in the load frame to be tested in the negative moment orientation. No damage was observed while flipping the specimen. The east side of the joint and the northeast side of the interface before testing is shown in Figure 50.



Figure 50: East side of the joint (a) and northeast side of the interface (b) of HSDU-1 before negative moment test

Initial cracking was observed as two flexural cracks that started near the as-cast top face of the deck at a load of 5 kips. One crack was approximately 1-1/2 ft from the joint and propagated halfway through the web of the girder toward the load point. The second crack was approximately 3 ft from the load point and propagated halfway through the deck. At 8 kips, horizontal cracks caused by positive moment testing near the as-cast top of the joint converged directly under the load point. From 10 to 16 kips, intermittent flexural cracking continued from

the as-cast top of the deck into the girder. From 18 to 22 kips, flexural cracks reached approximately halfway up the web of the girder and bent toward the load point. Additionally, new horizontal cracks formed on the south side of the joint in the center of the deck and extended approximately 5 in. away from the joint. Flexural cracking on the east side of the north girder is shown in Figure 51.

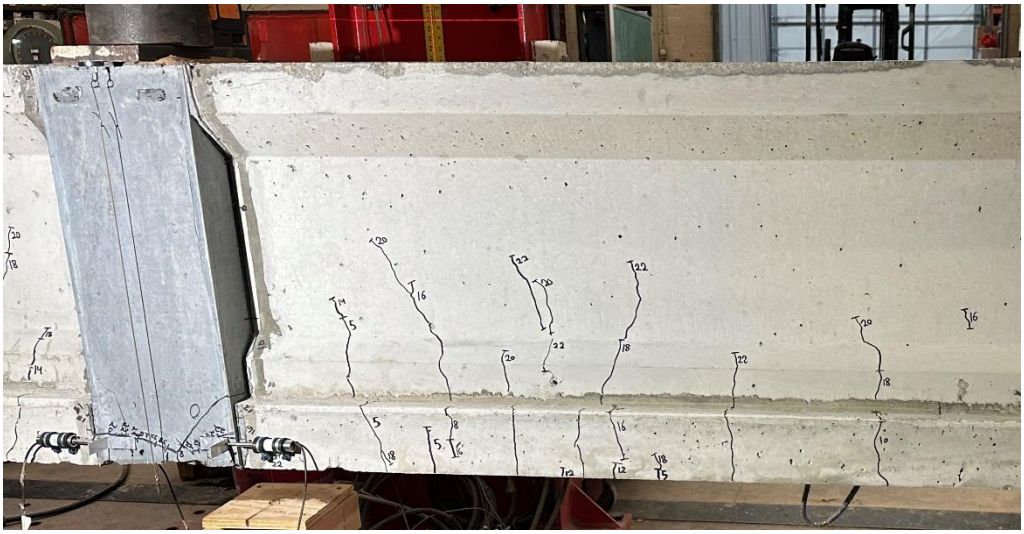

Figure 51: Flexural cracking on northeast side of specimen HSDU-1 under final negative moment test loading

The specimen reached a maximum load of 22.7 kips and the crack at the south joint interface, which was originally caused by positive moment testing, started to open substantially. Separation at the joint interfaces during and after testing is shown in Figures 52 and 53. The specimen was pushed to a deflection of 1-1/8 in. and the test was stopped. The deflection did not rebound after loading was removed.



Figure 52: Northwest (a) and southwest (b) side of joint HSDU-1 under final negative moment test loading

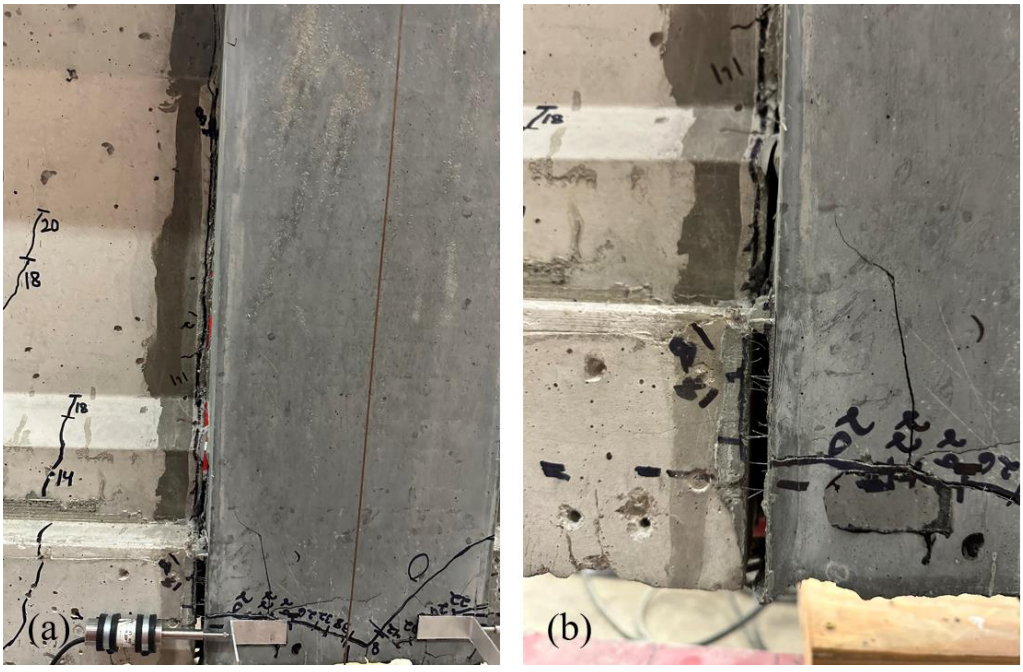

Figure 53: Southeast interface separation of HSDU-1 during (a) and after (b) final negative moment test loading

Closer examination of the specimen after testing revealed an unaccounted-for crack on the north side of the joint in the as-cast top surface of the deck that was not easily visible during testing. Figure 54 shows the unaccounted-for crack from both sides of the joint. This crack is believed to have formed at 20 kips with other vertical cracks in the deck and suggests a bond failure in the joint around the lap splice.

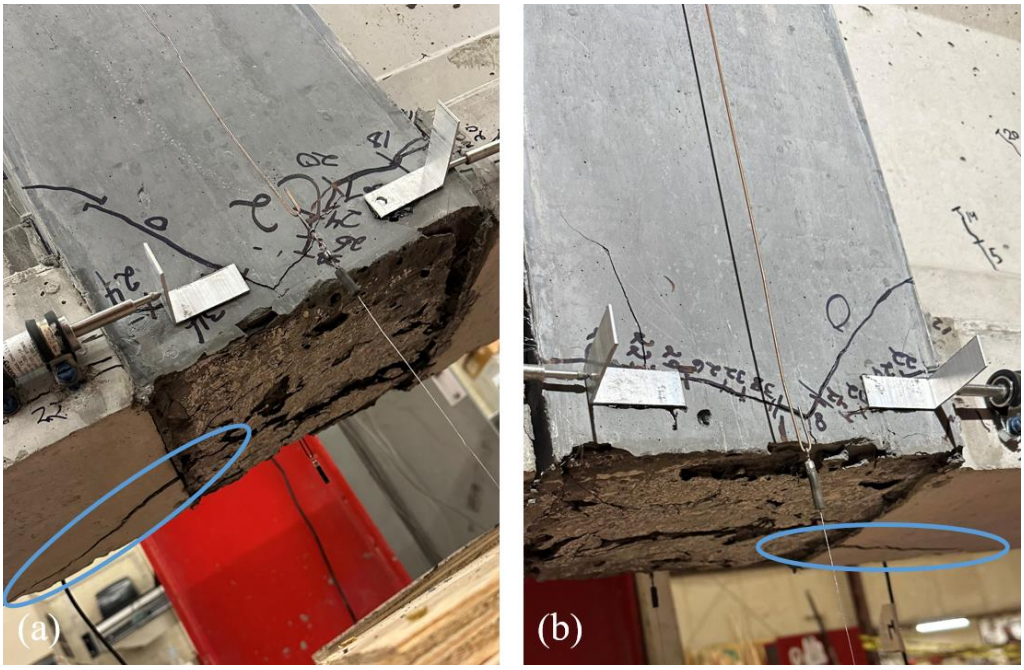

Figure 54: Cracking in as-cast top face of deck (denoted by blue oval) from the west (a) and east (b) side of the joint

Figure 55 shows the load-deflection curve for specimen HSDU-1 during negative moment testing. Initial cracking was visibly detected at a load of 5 kips. However, initial cracking did not result in a noticeable loss of stiffness. From 5 to 18 kips the curve followed a nearly linear slope which coincides with the development of flexural cracks in the girder. At 18 kips horizontal cracks started forming on the south side of the joint but did not result in a significant loss of stiffness. The

sudden loss of load carrying capacity and horizontal cracking at approximately 22 kips suggest that the full flexural capacity of the lap splice was not developed. It is believed that the bond between the lap splice and the joint material could have been compromised due to air voids near the as-cast top surface. Significant segregation of steel fibers in the joint material was also detected, which could have caused reduced tensile strength of the joint material and resulted in bond failure.

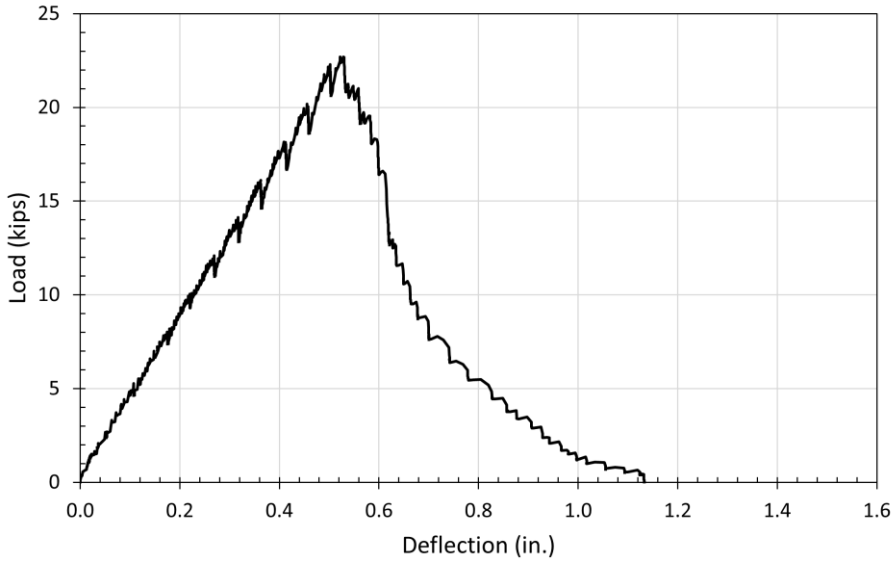

Figure 55: Load-deflection curve for HSDU-1 during negative moment test

The load-joint separation curves for both the north and south joint-deck interfaces are presented in Figure 56. The measured magnitude of joint separation on specimen HSDU-1 was similar to what was expected based on observations during testing. Enough separation was observed at the south interface for it to easily be seen through at the end of testing. The north joint showed very little separation by comparison. The magnitude of separation at both joint locations was minimal until the maximum load was reached. After the maximum load was

reached, the separation of the south joint increased rapidly until the test was stopped. This behavior suggests a sudden bond failure occurred that resulted from pullout of the south side of the lap splice.

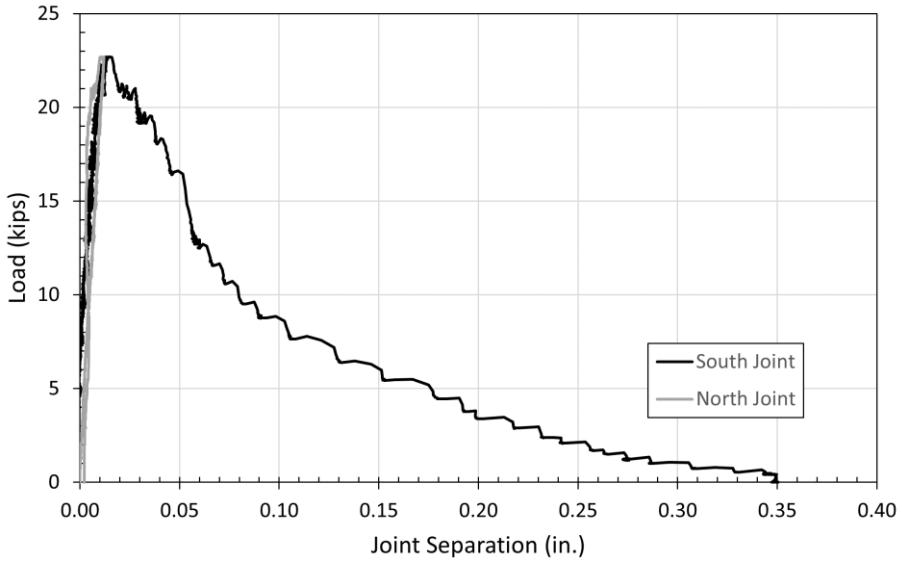

Figure 56: Load-joint separation curves for HSDU-1 during negative moment test

4.3.6 HSDU-2 Positive Moment Test

Settlement and preexisting cracks identical to those on specimen HSDU-1 were detected before testing near the as-cast top surface of the joint material. Therefore, the same process outlined in Section 4.3.4 was followed to prep the surface and mark cracks before testing.

Specimen HSDU-2 was first tested in the positive moment orientation. Initial cracking was observed at a load of 5 kips on both sides of the joint-girder interface along the as-cast bottom flange. As shown in Figure 57, the initial cracks propagated up the joint-girder interface as loading increased.



Figure 57: Separation at the interface of HSDU-2 from the east (a) and west (b) side under final positive moment test loading

At 8 kips, the cracks at the interface propagated up through the bottom flange and approximately 3 in. up the web. From 10 to 16 kips, the crack at the north interface propagated through the remaining depth of the girder, halfway up the deck, and turned horizontally into the joint toward the load point. The location of the initial horizontal cracking is the approximate location of the mild steel lap splice. For the rest of the test, the north horizontal crack slowly turned up towards the load point in increments of less than 1 in. From 10 to 22 kips, the crack at the south interface propagated through the remaining girder depth and halfway up the deck. At 30 kips, the crack turned horizontal and propagated into the UHPC and toward the load point. The location of the south horizontal crack is the approximate location of the mild steel lap splice. For the remainder of the test, the horizontal crack slowly turned up towards the load point in increments of less

than 1 in. Final horizontal cracking near the as-cast top surface of the joint, which propagated from both the north and south interfaces, is shown in Figure 58.



Figure 58: Cracking on the west side of HSDU-2 near the as-cast top surface of the joint

At 44 kips, the specimen experienced significant joint separation and both wire pots were removed for their protection before testing continued. The test was stopped when significantly higher deflections were needed to reach the next loading increment. The manually measured deflection was 2-5/16 in. under final loading and 1-3/16 in. after the load was removed.

At a loading of 23 kips, cracks shown in Figure 59 suddenly appeared on the northwest side of the girder at the roller location and propagated both toward and away from the load point. Extensions of these cracks occurred intermittently from 30 to 38 kips and were monitored closely alongside separation at the joint. These

cracks initially exhibited shear-like behavior but were ultimately believed to have been caused by uneven bearing at the load point.



Figure 59: Cracking on the northwest side of HSDU-2 in the girder directly above the north roller support

Figure 60 shows the load-deflection curve for specimen HSDU-2 during positive moment testing. Initial cracking was visibly detected at a load of 5 kips. However, initial cracking did not result in a significant change in stiffness. From 10 to 16 kips, horizontal cracking was visibly detected near the as-cast top surface of the joint material and resulted in a greater loss of stiffness. From 16 to 40 kips the curve followed a nearly linear slope which coincides with additional cracking in the joint. For the remaining duration of the test, the load curve started to flatten out and exhibited flexural behavior until the specimen failed to resist additional load. The rebound behavior of the specimen is not shown in Figure 60 because the wire pots were removed before the test was stopped.

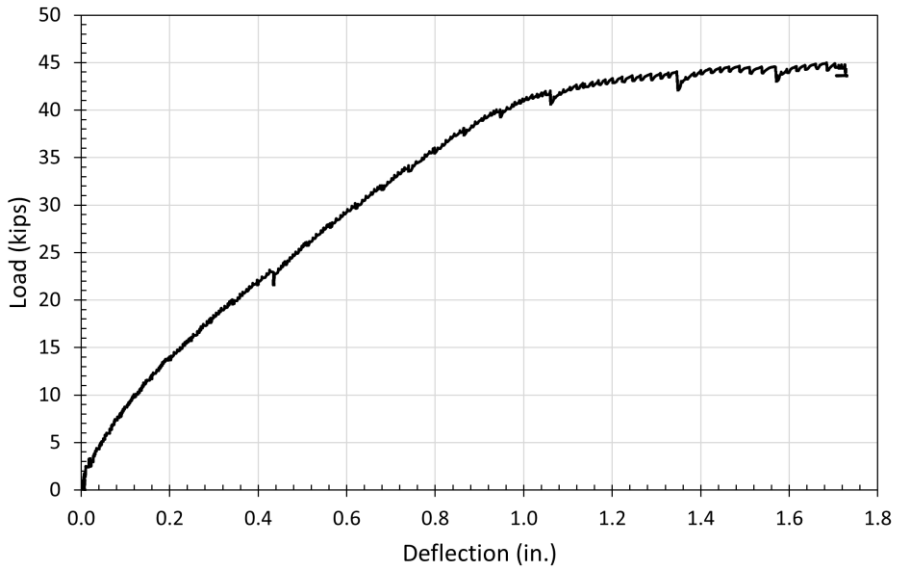

Figure 60: Load-deflection curve for HSDU-2 during positive moment test

The load-joint separation curves for both the north and south joint-girder interfaces are presented in Figure 61. The measured magnitude of joint separation on specimen HSDU-2 was as expected based on observations during testing. The joint separation at both interface locations could easily be seen through at the end of testing. The measured separation followed similar trends at both interface locations. From 0 to approximately 43 kips, the north interface showed slightly greater separation than the south interface. However, the south interface experienced greater separation than the north joint for loads beyond 43 kips. The load-deflection and load-joint separation curves show similar behavior, suggesting that cracking at the interface locations was the primary cause of overall specimen deflection.

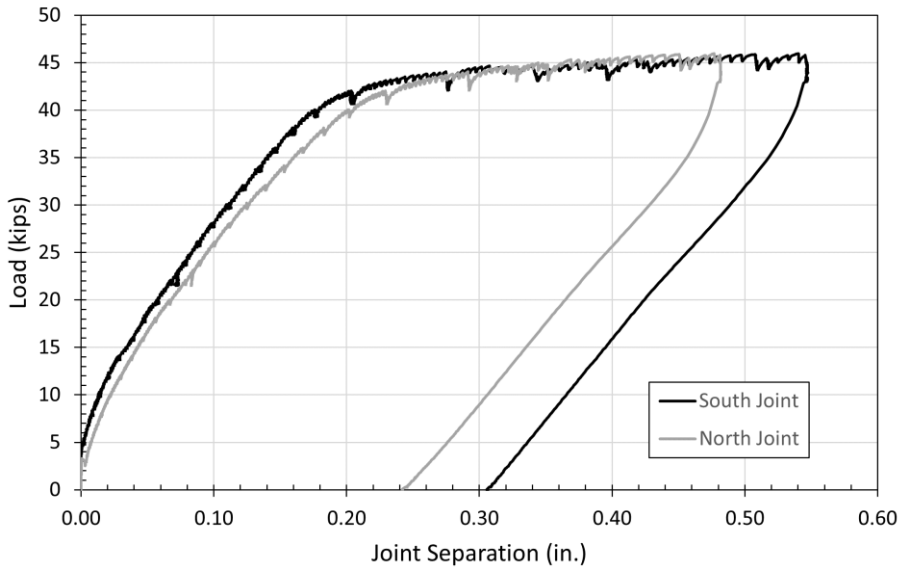

Figure 61: Load-joint separation curves for HSDU-2 during positive moment test

4.3.7 HSDU-2 Negative Moment Test

Specimen HSDU-2 was removed from the load frame, flipped upside-down, and placed back in the load frame to be tested in the negative moment orientation. No damage was observed while flipping the specimen. Cracking near the as-cast bottom and as-cast top of the specimen before negative moment testing are shown in Figures 62 and 63, respectively.



Figure 62: East (a) and southeast (b) side of joint HSDU-2 showing cracks at the interface before negative moment testing

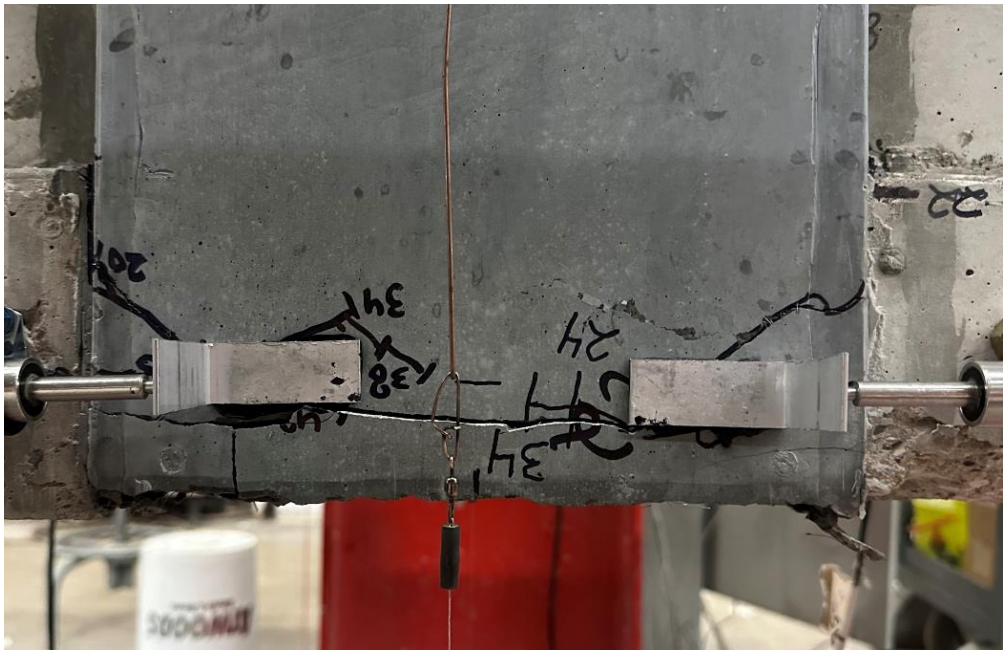

Figure 63: East side of HSDU-2 showing cracks near the as-cast top face of the joint before negative moment testing

It is likely that cracks caused by positive moment testing opened further during the duration of negative moment testing but were indistinguishable from previous cracks and therefore not marked. At 5 kips, initial cracks were observed in the south girder as a series of cracks near the joint. One of these cracks was a horizontal crack starting from the mid-depth of the deck at the joint-deck interface that propagated toward the supports for approximately 1 ft. Two flexural cracks with lengths of approximately 1 in. started 2 ft away from the joint in the as-cast top face of the deck. From 8 to 10 kips, additional flexural cracks formed along the length of the south girder. Additionally, cracks caused by positive moment testing started opening from the as-cast top of the interface and continued to do so throughout the duration of the test. At 12 kips, the first cracks were observed in the north girder and followed the same pattern as the initial cracking in the south girder. At 14 kips, small, isolated cracks occurred in the center of the web in both girders and this cracking in both girders was identical in magnitude. Flexural cracks reached the as-cast bottom of the deck and propagated toward the load point. From 16 to 18 kips, flexural cracks continued through the as-cast top flange and to approximately the middle of the web. The test was stopped when the specimen could not resist additional load. Significant separation along the entire south interface was clearly visible at the conclusion of the test and is shown in Figures 64 and 65.

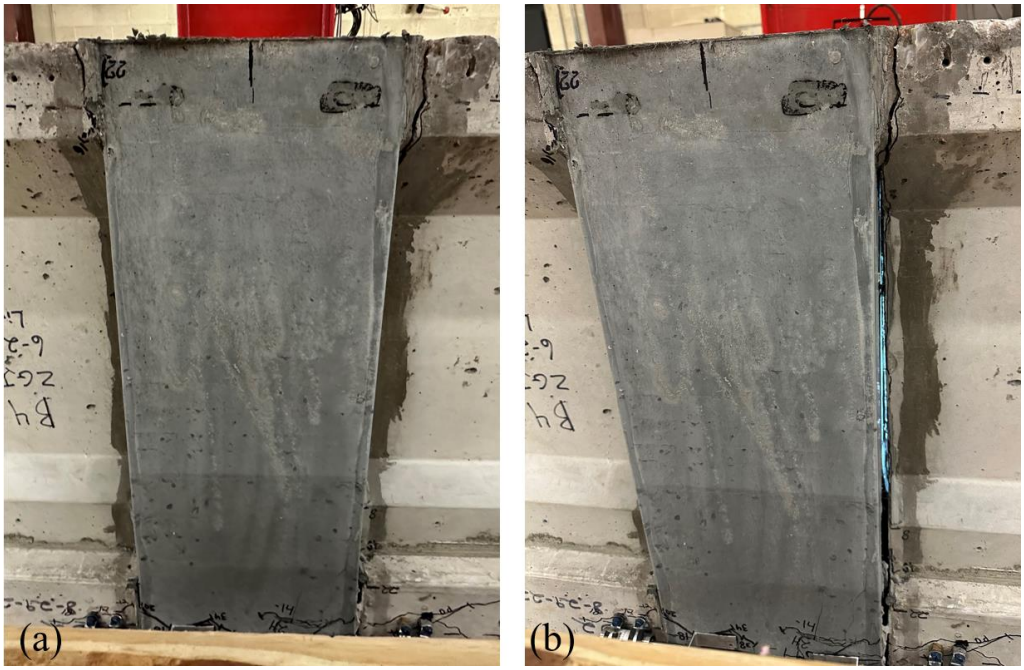

Figure 64: West (a) and southwest (b) side of HSDU-2 showing separation at the interface after negative moment testing



Figure 65: Southeast (a) and northeast (b) side of joint HSDU-2 showing cracks at the interface after negative moment testing

A closer examination of the specimen after testing revealed that the cracks that formed near the as-cast top surface of the joint during positive moment testing grew together. These cracks can be seen in Figures 66 and 67. Additionally, deep spiderweb like cracking was observed in the as-cast top surface of the joint. Figure 66 shows a piece of the joint material approximately 2 in. thick that was able to be easily removed from the surface. The removed piece of joint material had no fibers below the surface, which suggests that the fibers were not evenly distributed throughout the joint.

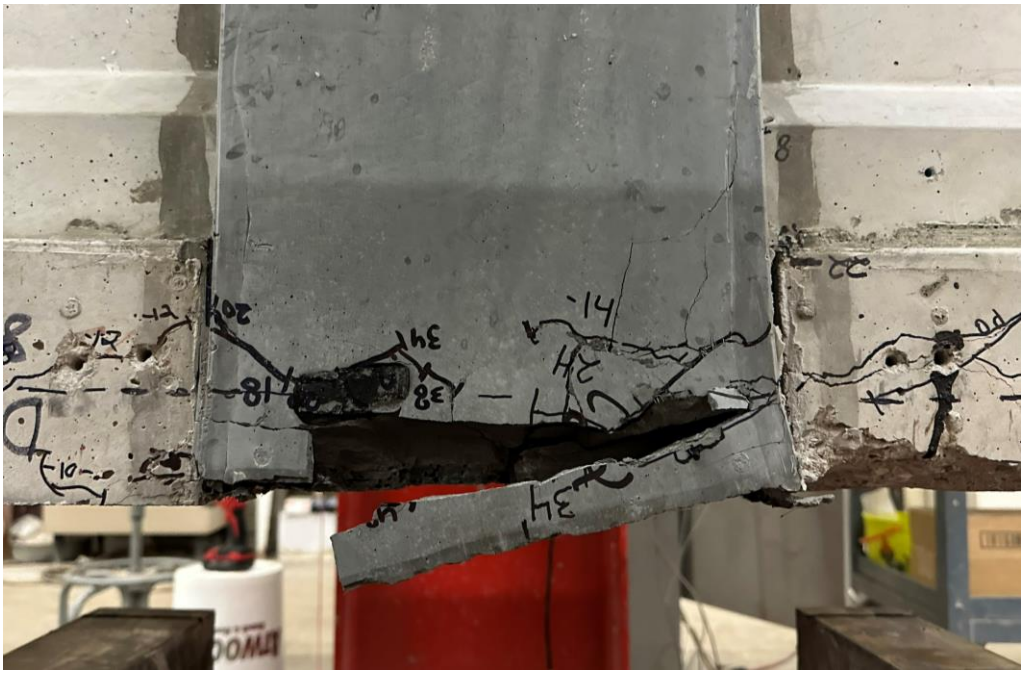

Figure 66: West side of joint HSDU-2 showing cracks near the as-cast top face of the joint after negative moment testing

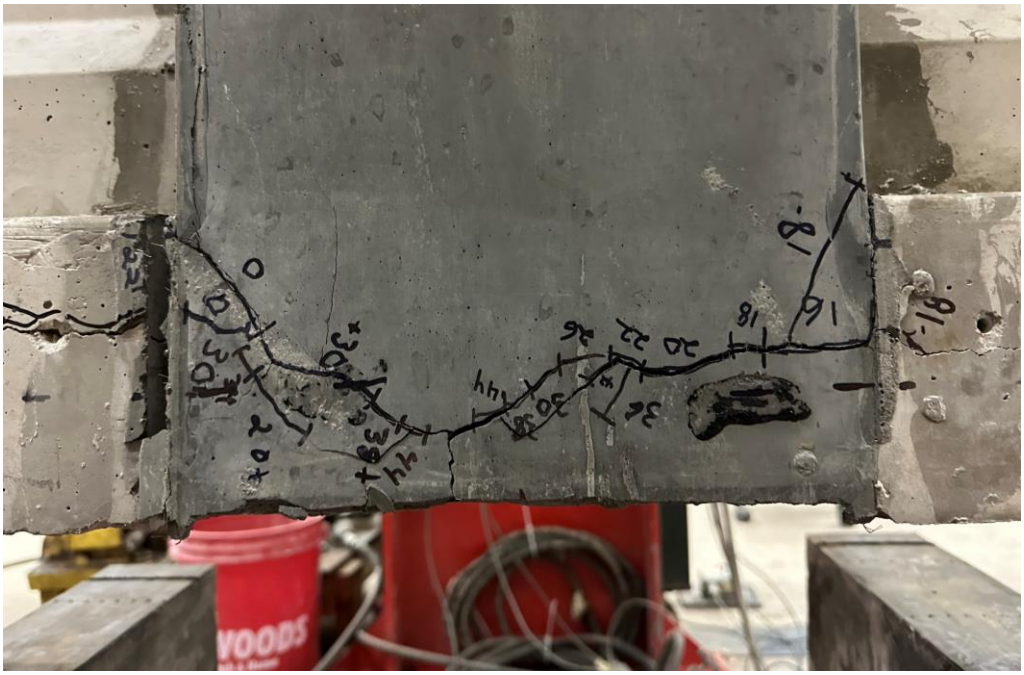

Figure 67: East side of joint HSDU-2 showing cracks near the as-cast top face of the joint after negative moment testing

Figure 68 shows a split open compression testing cylinder from the batch of Ductal® UHPC used in joints HSDU-1 and HSDU-2, which confirms that fibers were only present in the bottom half of the specimen.



Figure 68: Compressive cylinder showing significant fiber settlement in the Ductal® UHPC used for joints HSDU-1 and HSDU-2

Figure 69 shows the load-deflection curve for specimen HSDU-2 during negative moment testing. Initial cracking was visually detected at a load of 5 kips. However, initial cracking did not result in a noticeable loss of stiffness. From 5 to 18 kips the curve followed a nearly linear slope which coincides with the development of flexural cracks in the girder. At 18 kips horizontal cracks started forming near the as-cast top surface of the joint resulting in a significant loss of stiffness. The sudden loss of load carrying capacity and horizontal cracking at 18 kips suggest that the full flexural capacity of the lap splice was not developed. It is believed that the bond between the lap splice and the joint material could have been compromised due to air voids near the as-cast top surface. Significant fiber settlement in the joint material could also have negatively impacted the performance of the joint material and resulted in bond failure.

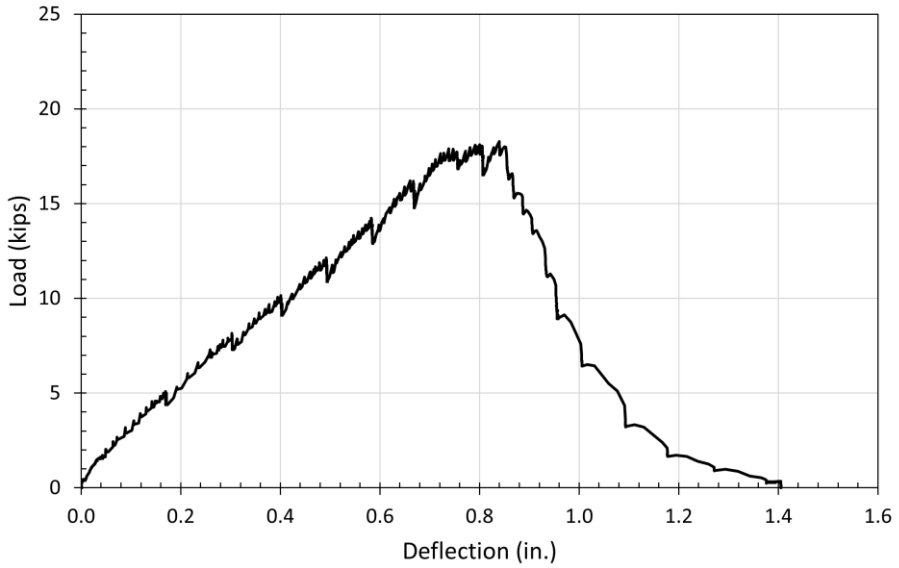

Figure 69: Load-deflection curve for HSDU-2 during negative moment test

The load-joint separation curves for both the north and south joint-deck interfaces are presented in Figure 70. The measured magnitude of joint separation on

specimen HSDU-2 was similar to what was expected based on observations during testing. The separation at the south interface could easily be seen through at the end of testing, and by comparison the north joint showed very little separation. The magnitude of separation at both joint locations was very minimal until the max load was reached. After the max load was reached, the separation of the south joint increased rapidly until the test was stopped. This behavior suggests a sudden bond failure occurred that resulted in pullout of the south side of the lap splice.

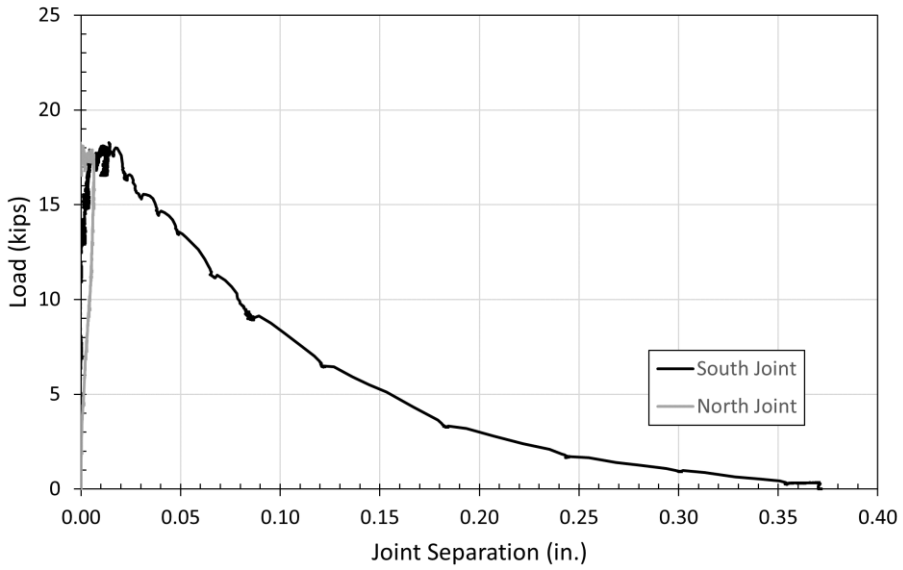

Figure 70: Load-joint separation curves for HSDU-2 during negative moment test

4.3.8 SSDU-1 Positive Moment Test

Settlement and preexisting cracks identical to other Ductal® specimens were detected near the as-cast top surface of the joint before testing. Therefore, the same process outlined in Section 4.3.4 was followed to prepare the surface and mark preexisting cracks before testing. Figure 71 shows two preexisting cracks

that started from the as-cast bottom of the deck on both sides of the joint up to the center of the as-cast top face of the joint. Additional cracks were detected on the as-cast top face of the joint but could not be seen from the sides to determine their severity. The joint-girder interfaces were uncracked before testing and are shown in Figures 72 and 73.



Figure 71: East (a) and west (b) side of joint SSDU-1 showing preexisting cracks before positive moment testing



Figure 72: Southeast (a) and northeast (b) side of joint SSDU-1 showing the joint interface before positive moment testing

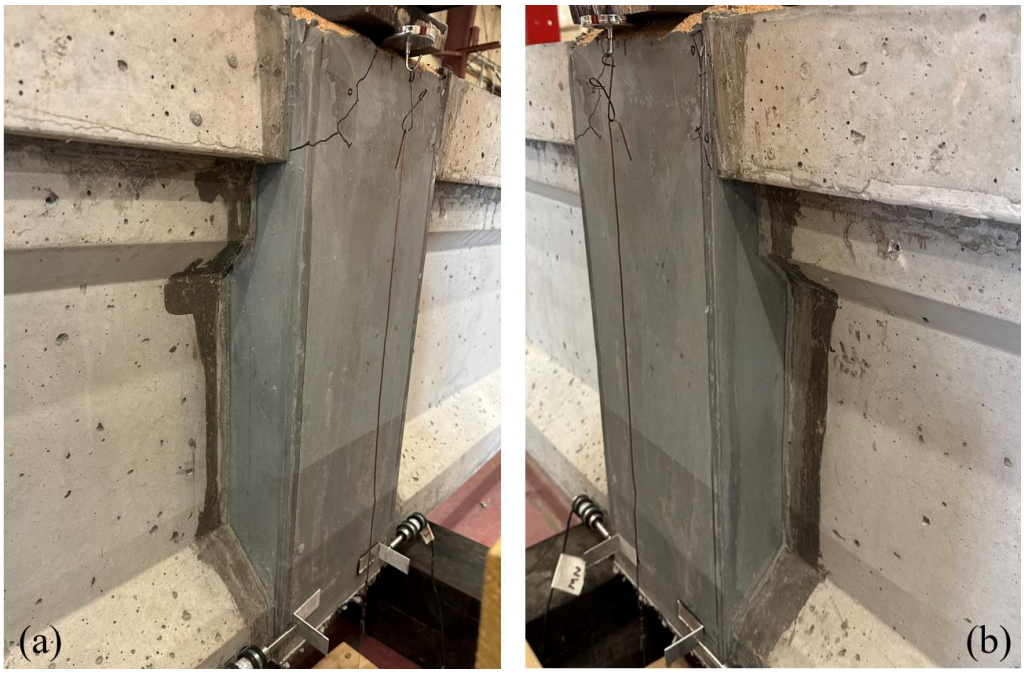

Figure 73: Northwest (a) and southwest (b) side of joint SSDU-1 showing the joint interface before positive moment testing

Specimen SSDU-1 was first tested in the positive moment orientation. Initial cracking was observed at a load of 8 kips, which is shown in Figures 72 and 73. Cracking occurred on both sides of the joint-girder interface and started from the as-cast bottom flange to the as-cast top flange. The joint separation started along the bottom of both interfaces and separation increased as the test continued. At 14 kips, the cracks followed along the interface up to the as-cast bottom of the deck. At 16 kips, the crack along the south interface reached the approximate location of the mild steel lap splice and stopped propagating upward. At 22 kips, the crack along the north interface reached the approximate location of the mild steel lap splice and stopped propagating upward. At 24 kips, new cracks in the joint started from the preexisting cracks and generally propagated toward the load point. The test was stopped at 26 kips due to the specimen experiencing increasingly larger deflections between load increments. Figures 74 and 75 show significant cracking along both interface locations, where signs of strand pullout could be seen under final loading. Cracking near the as-cast top face of the joint is shown in Figure 76.



Figure 74: Southeast (a) and northeast (b) side of joint SSDU-1 showing cracking along the interfaces under final positive moment test loading



Figure 75: Northwest (a) and southwest (b) side of joint SSDU-1 showing cracking along the interfaces under final positive moment test loading

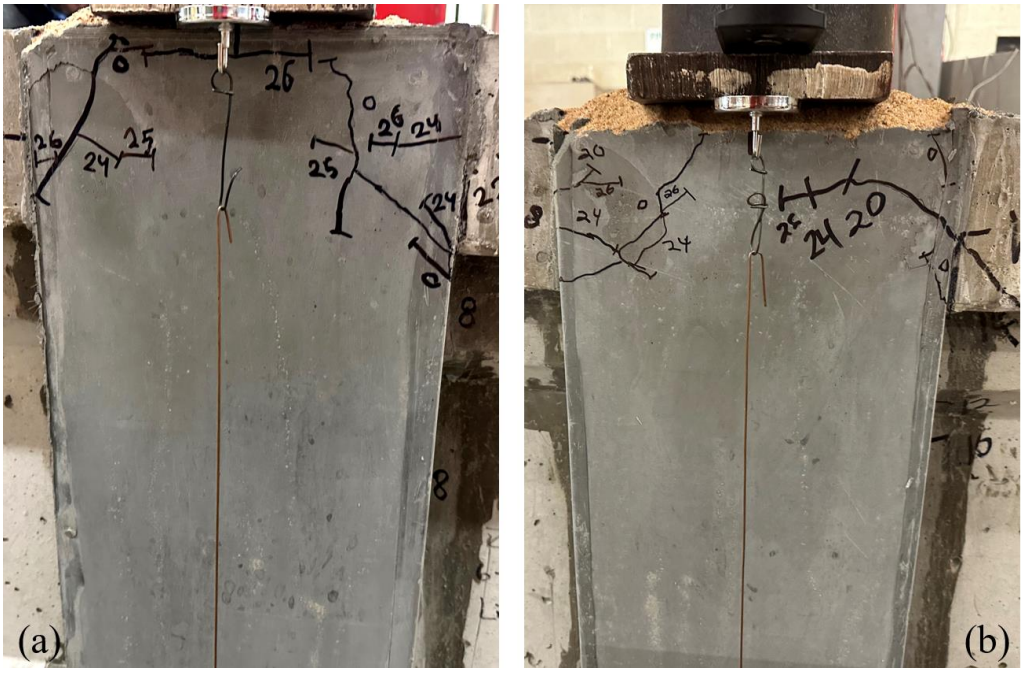

Figure 76: East (a) and west (b) side of joint SSDU-1 showing cracks near as-cast top face under final positive moment test loading

The manually measured deflection was 1-5/16 in. under final loading and 15/16 in. after the load was removed. Figures 77 and 78 show joint separation on both sides of the specimen under final loading.

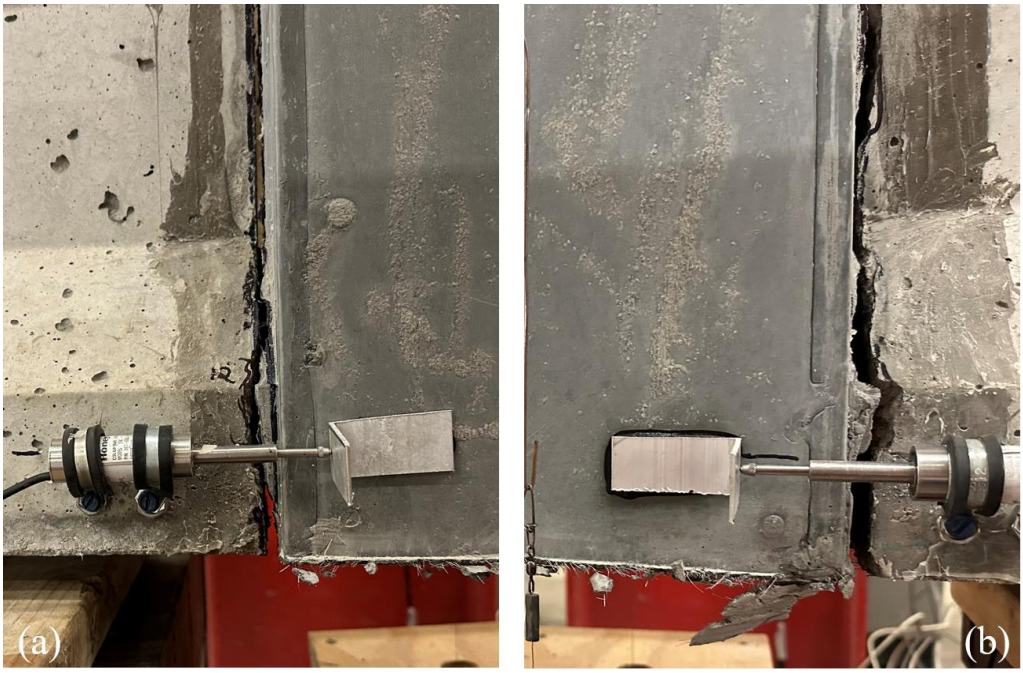

Figure 77: Northwest (a) and southwest (b) side of joint SSDU-1 showing separation at the interface near the as-cast bottom face under final positive moment test loading



Figure 78: Southeast (a) and northeast (b) side of joint SSDU-1 showing separation at the interface near the as-cast bottom face under final positive moment test loading

Since the as-cast top surface of all the joints constructed with Ductal® UHPC looked identical, the decision was made to split open compression testing cylinders from all batches. Figure 79 shows a cylinder from the batch of Ductal® UHPC that was used in joints SSDU-1 and SSDU-2, which confirms that fibers were only present in the bottom half of the specimen. This type of fiber distribution was not noticed while using Ductal® for previous projects.



Figure 79: Compressive cylinder showing significant fiber settlement in the Ductal® UHPC used for joints SSDU-1 and SSDU-2

Figure 80 shows the load-deflection curve for specimen SSDU-1 during positive moment testing. Initial cracking was visibly observed at a load of 8 kips, which resulted in a noticeable change in stiffness and loss of load. From 8 to 24 kips the slope of the graph changed from linear to an increasing curvature, which signified a gradual loss in stiffness and coincides with cracking along the interfaces up to the mild steel lap splice. For the remaining duration of the test, new cracks formed near the as-cast top face of the joint and the load curve showed an increase in

stiffness until the specimen suddenly failed to resist additional load. After the load was removed the deflection of the specimen showed a small rebound. A small rebound suggests that the strands in the as-cast bottom flange of the girder were still somewhat bonded, but not adequately anchored in the joint.

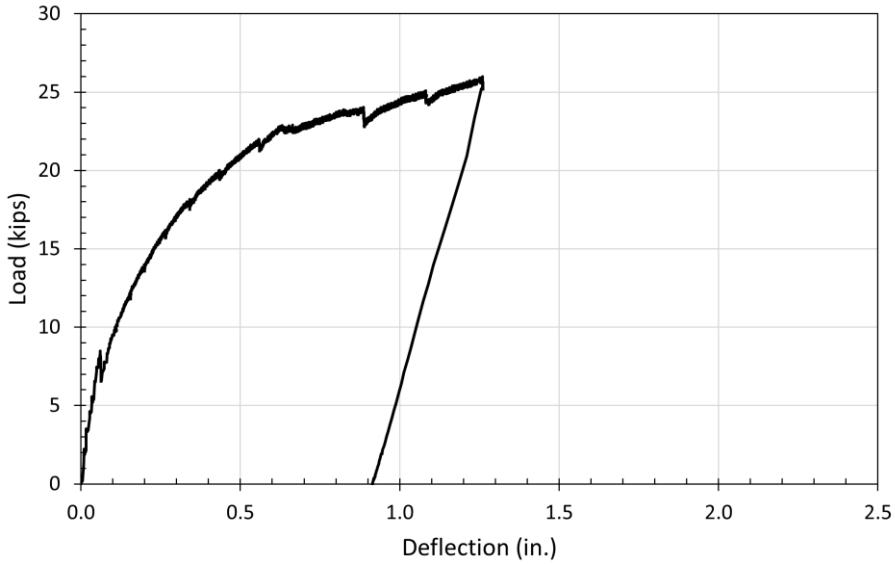

Figure 80: Load-deflection curve for SSDU-1 during positive moment test

The load-joint separation curves for both the north and south joint-girder interfaces are presented in Figure 81. The measured magnitude of joint separation on specimen SSDU-2 matched what was expected based on the cracking visually observed at both interfaces during testing. The measured separation followed similar trends at both interfaces during testing. However, the south interface showed a greater magnitude of separation than the north interface beyond a loading of approximately 22 kips. The load-deflection and load-joint separation curves show similar behavior, suggesting that cracking at the interface locations was the primary cause of overall specimen deflection.

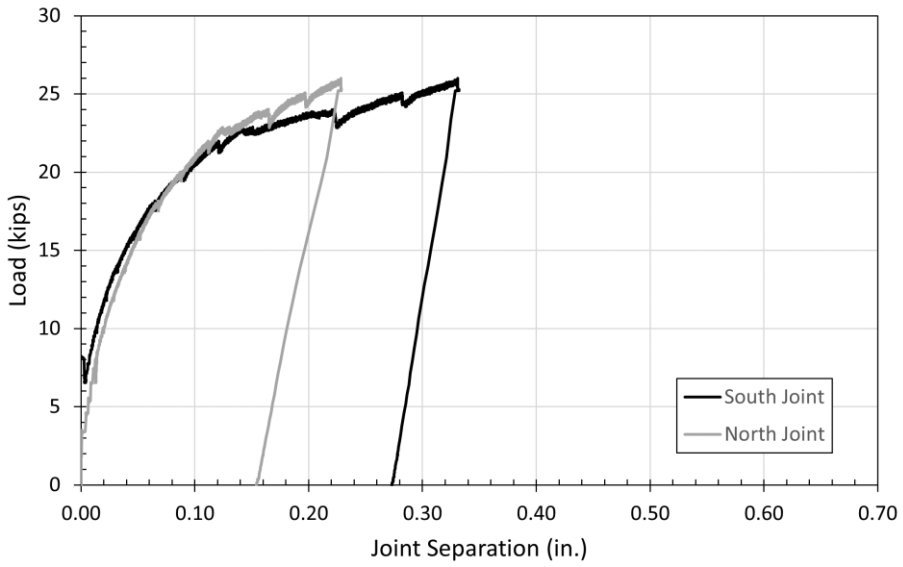

Figure 81: Load-joint separation curves for SSDU-2 during positive moment test

4.3.9 SSDU-1 Negative Moment Test

Specimen SSDU-1 was removed from the load frame, flipped upside down, and placed back in the load frame to be tested in the negative moment orientation. No damage was observed while flipping the specimen. At 5 kips, small initial flexural cracks were observed in the as-cast top face of both girder decks approximately 3 ft away from the joint. From 5 to 8 kips, additional flexural cracks started intermittently along the length of the girder from the as-cast top face of the decks. From 8 to 14 kips, the cracks propagated through the deck and into the girder. At 20 kips, most of the existing flexural cracks closest to the joint propagated to the middle of the web of the girder. From 20 to 26 kips, new flexural cracks formed beyond existing cracks and propagated from the as-cast top surface of the deck to approximately the mid-depth of the web of the girder. From 26 to 36 kips, existing flexural cracks propagated up toward the load point and the rate of

cracking for each increment slowed. All flexural cracks that developed during testing are shown in Figures 82 through 85.

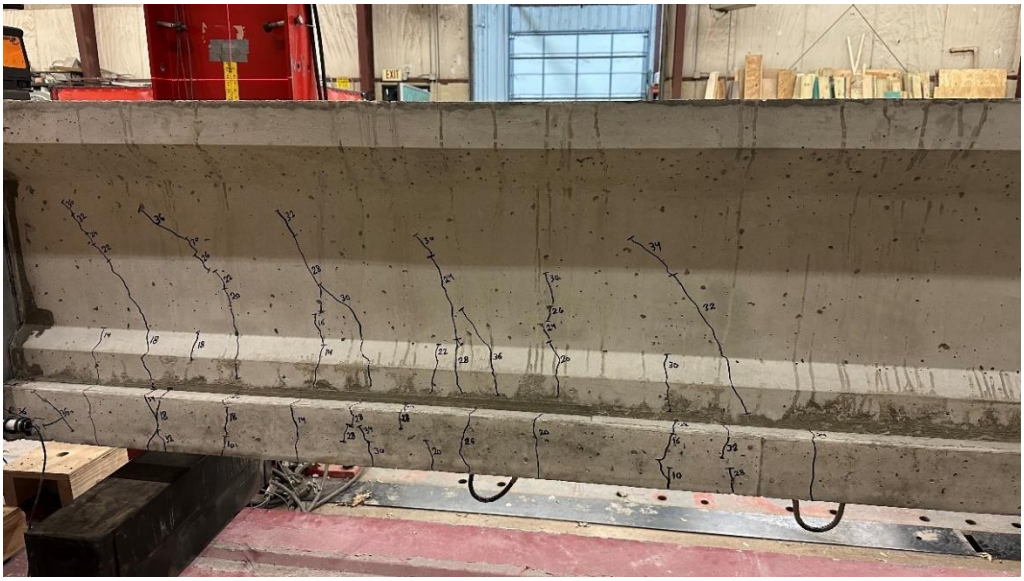

Figure 82: East side of north girder SSDU-1 showing flexural cracks after negative moment test



Figure 83: East side of south girder SSDU-1 showing flexural cracks after negative moment test



Figure 84: West side of north girder SSDU-1 showing flexural cracks as after negative moment test



Figure 85: West side of south girder SSDU-1 showing flexural cracks after negative moment test

A sudden deflection occurred during the increment after 36 kips resulting in half of the applied load being lost trying to reach 38 kips. The test continued in an attempt to reload the specimen but only resulted in additional deflection. At 12.6 kips and a manually measured deflection of 1-1/8 in., it was determined that the

specimen would not withstand additional load and the test was stopped. The specimen did not rebound after the load was removed.

After the test, the unmarked cracks shown in Figures 86 and 87 were discovered near the as-cast top face of the joint. The cracks are believed to have formed near the end of testing. Cracks that formed at the interface during the test are shown in Figures 88 and 89 under final loading.

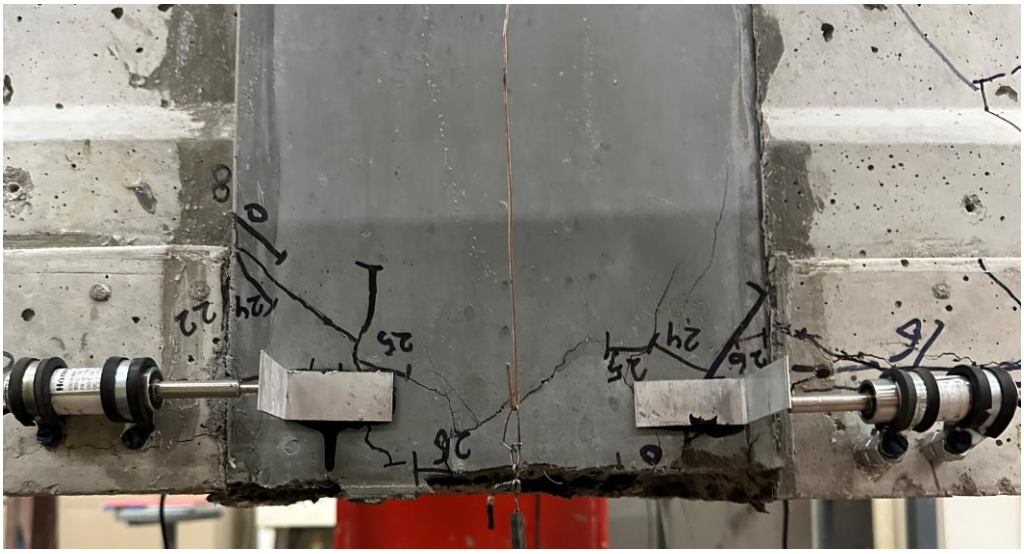

Figure 86: West side of joint SSDU-1 showing cracks near the as-cast top face of the joint under final negative moment test loading

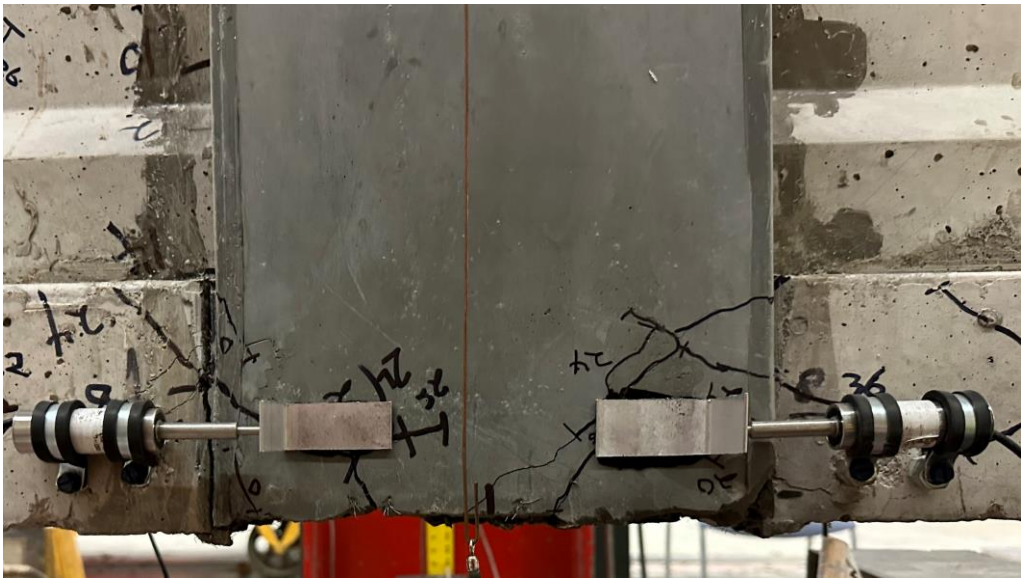

Figure 87: East side of joint SSDU-1 showing cracks near the as-cast top face of the joint under final negative moment test loading

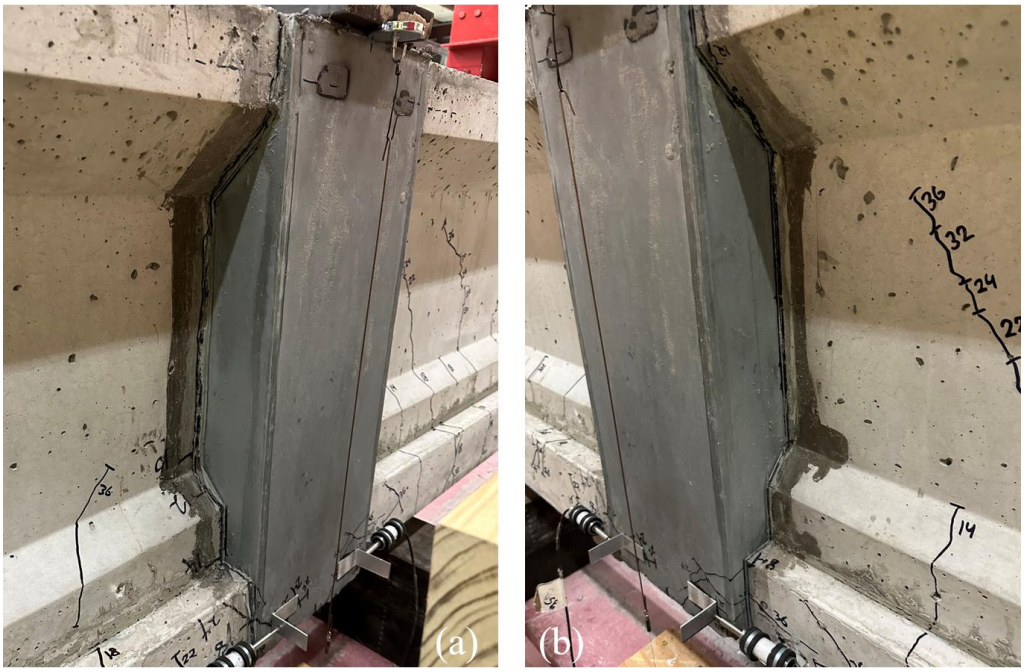

Figure 88: Southeast (a) and northeast (b) side of joint SSDU-1 showing cracking along the interfaces under final negative moment test loading



Figure 89: Northwest (a) and southwest (b) side of joint SSDU-1 showing cracking along the interfaces under final negative moment test loading

Figure 90 shows the load-deflection curve for specimen SSDU-1 during negative moment testing. Initial cracking was visually detected at a load of 5 kips. However, initial cracking only resulted in a minor loss of stiffness. From 5 to 36 kips the curve follows a slightly lower slope which coincides with the development of flexural cracks in the girders. At 36 kips a significant loss of stiffness occurred that could have been caused by the cracks that were detected after testing near the as-cast top surface of the joint. The sudden loss of load carrying capacity at the end of the test suggests that the full flexural capacity of the lap splice was not developed. It is believed that the bond between the lap splice and the joint material could have been compromised due to air voids near the as-cast top surface. Significant fiber settlement in the joint material also may

have negatively impacted the performance of the joint material and resulted in bond failure.

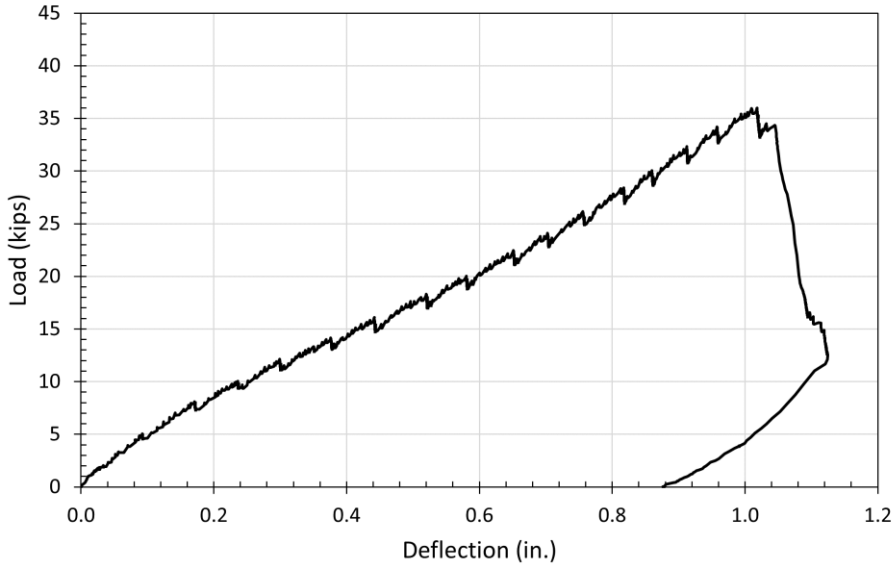

Figure 90: Load-deflection curve for SSDU-1 during negative moment test

The load-joint separation curves for both the north and south joint-deck interfaces are presented in Figure 91. The measured magnitude of joint separation on specimen SSDU-1 was similar to what was expected based on observations during testing. The magnitude of separation at both interface locations was very minimal until the maximum load was reached. After the maximum load was reached, the separation of the south joint increased rapidly until the test was stopped. This behavior suggests a sudden bond failure occurred that resulted in pullout of the south side of the lap splice.

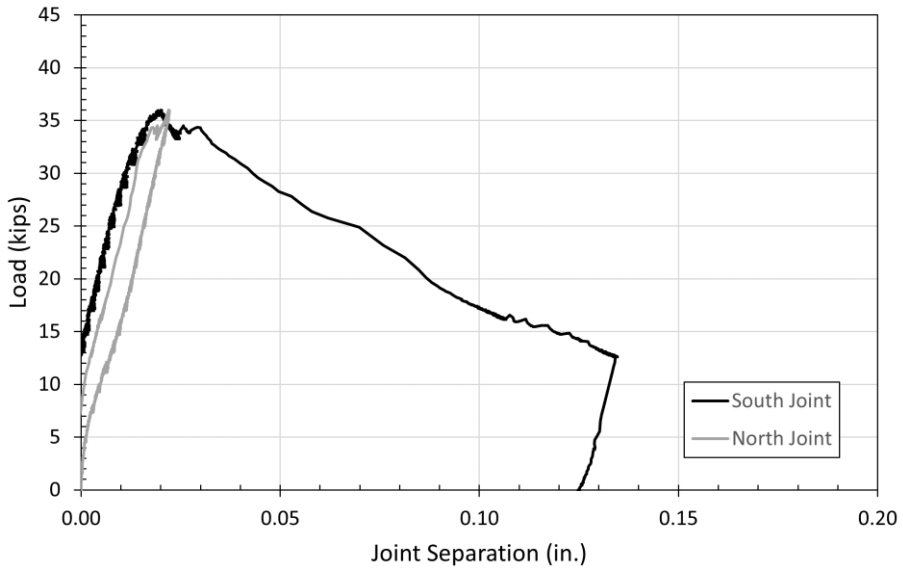

Figure 91: Load-joint separation curves for SSDU-1 during negative moment test

4.3.10 SSDU-2 Negative Moment Test

Specimen SSDU-2 was flipped upside down and placed in the load frame to be tested in the negative moment orientation first. No damage was observed while flipping the specimen. Settlement and preexisting cracks identical to those on other Ductal® specimens were detected before testing near the as-cast top surface of the joint. Therefore, the same process outlined in Section 4.3.4 was followed to mark preexisting cracks before testing. It was not necessary to prep the surface in the negative moment orientation because settlement was only present in the top surface. The preexisting cracks, which were only present in the joint near the joint-deck interface, can be seen in Figure 97. The joint-girder interfaces were confirmed to be visually uncracked before testing.

At 5 kips, initial cracking was detected on the west side of the joint near the as-cast top surface. These cracks were identical to the preexisting cracks identified

on the east side of the joint, so they were potentially formed before testing. Additionally, small flexural cracks were identified intermittently along the east side of the girders near the as-cast top surface of the deck. From 8 to 16 kips, the flexural cracks propagated through the deck and into the as-cast top flange of the girder toward the load point. At 18 kips, new flexural cracks appeared from the as-cast top of the deck into the as-cast top flange of the girder. In general, the farther away a crack was from the joint, the faster it propagated through the girder toward the load point. At 20 kips, most of the existing flexural cracks closest to the joint propagated to the mid-depth of the web of the girder. From 20 to 26 kips, new flexural cracks formed beyond existing cracks and extended from the as-cast top face of the deck to approximately the mid-depth of the web of the girder. From 26 to 36 kips, existing flexural cracks propagated up toward the load point and the rate of propagation for existing cracks slowed. From 36 to 40 kips, new flexural cracks formed beyond existing cracks and extended from the as-cast top face of the deck to approximately the mid-depth of the web of the girder. The test was stopped when the specimen could not resist additional loading. All flexural cracks that developed during testing are shown in Figures 92 through 95. Cracks that formed near the as-cast top surface of the joint are shown in Figures 96 and 97. The manually measured deflection was 9/16 in. under final loading and 3/8 in. after the load was removed.



Figure 92: East side of north girder of SSDU-2 showing flexural cracks under final negative moment test loading



Figure 93: East side of south girder of SSDU-2 showing flexural cracks under final negative moment test loading

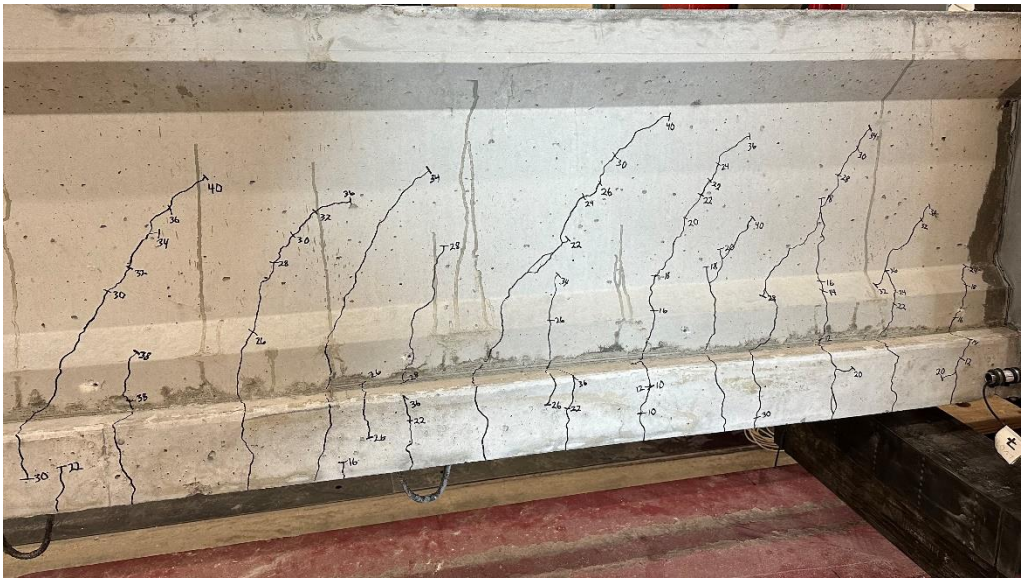

Figure 94: West side of north girder of SSDU-2 showing flexural cracks under final negative moment test loading



Figure 95: West side of south girder of SSDU-2 showing flexural cracks under final negative moment test loading



Figure 96: West side of joint SSDU-2 showing cracks near the as-cast top face of the joint under final negative moment test loading

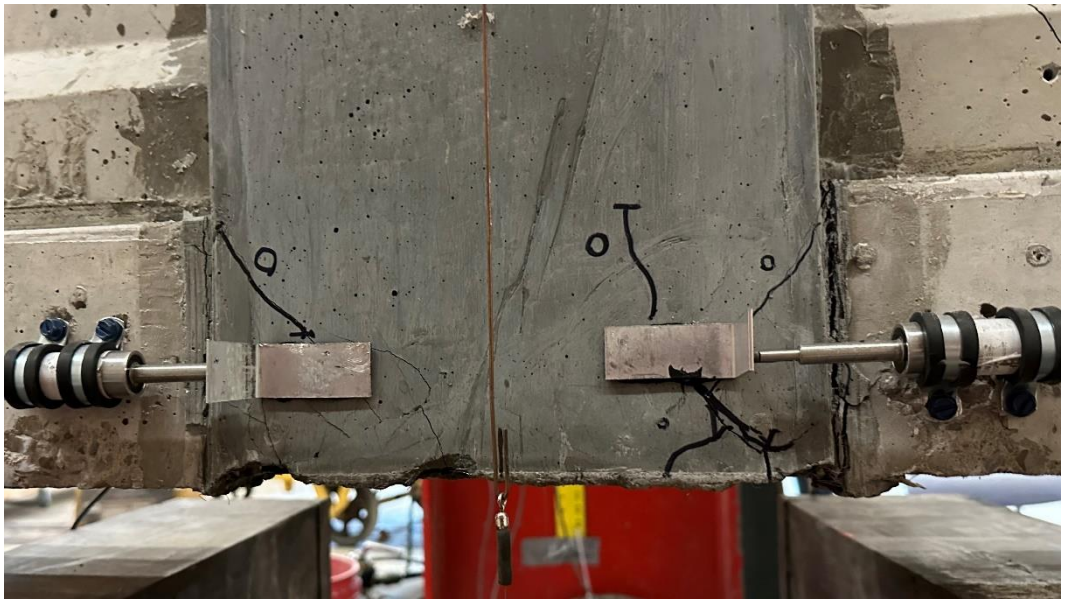

Figure 97: East side of joint SSDU-2 showing cracks near the as-cast top face of the joint under final negative moment test loading

Specimen SSDU-2 was removed from the load frame, flipped upright, and placed back in the load frame to be tested in the positive moment orientation. A closer examination of the specimen in the positive moment orientation revealed that undocumented cracks formed in multiple places near the joint. Figure 98 shows significant cracking on the as-cast top surface of the joint. The cracks at the as-cast top surface of the joint measured 0.1 in. across the widest point using a crack gauge. Figure 99 shows cracks that formed on the as-cast top face of the deck. Figures 100 and 101 show cracks that propagated along the sides of the joint. These cracks were marked before the start of positive moment testing but were mistakenly marked 46 kips. Since the maximum load recorded by the data acquisitions system was 41.6 kips, all cracks marked 46 kips should be considered to have formed between 40 and 41.6 kips, the final increment of loading.

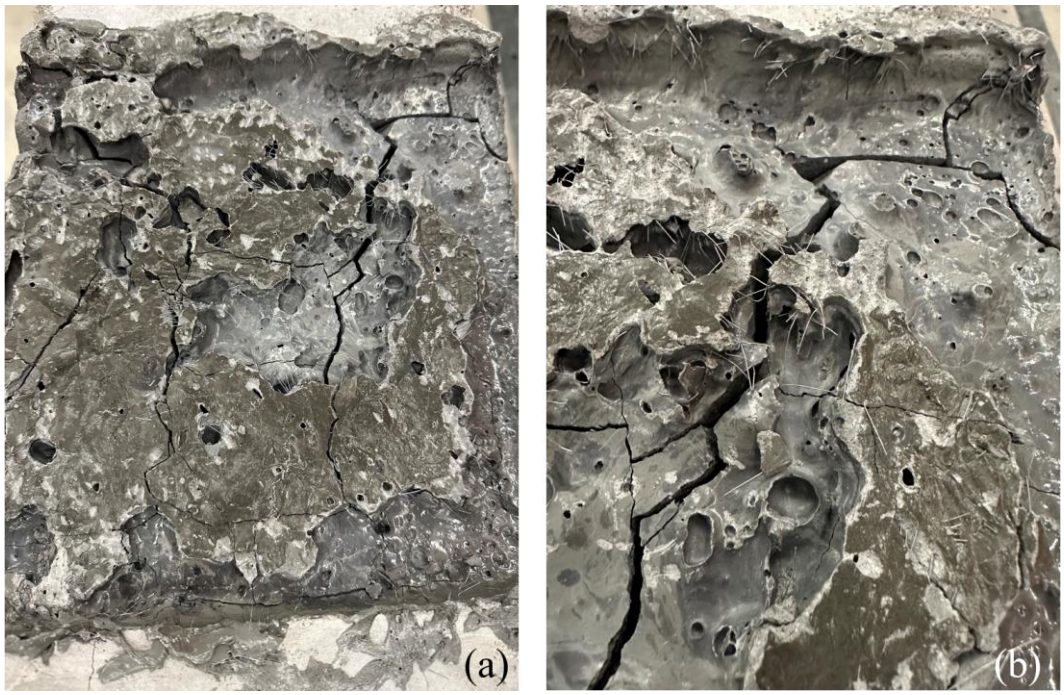

Figure 98: As-cast top surface of joint SSDU-2 showing 0.1 in. wide cracks that formed during final negative moment test loading



Figure 99: As-cast top surface of the south deck of SSDU-2 showing cracks that formed during final negative moment test loading Note: All cracks unlabeled or labeled 46 kips resulted from final loading of approximately 41.6 kips



Figure 100: West side of joint SSDU-2 in positive moment orientation showing undocumented cracks near the as-cast top surface caused by negative moment testing Note: All cracks unlabeled or labeled 46 kips resulted from final loading of approximately 41.6 kips



Figure 101: East side of joint SSDU-2 in positive moment orientation showing undocumented cracks near the as-cast top surface caused by negative moment testing Note: All cracks unlabeled or labeled 46 kips resulted from final loading of approximately 41.6 kips

Figure 102 shows the load-deflection curve for specimen SSDU-2 during negative moment testing. Initial cracking was visually detected at a load of 5 kips. However, initial cracking only resulted in a minor loss of stiffness. At 12 kips the south joint started to separate and resulted in a substantial loss of stiffness. From 12 to 42 kips the curve follows a noticeably lower slope which coincides with the development of flexural cracks in the girders. At 42 kips a significant loss of stiffness occurred that could have been caused by the cracks that were detected after testing near the as-cast top surface of the joint. The sudden loss of load carrying capacity at the end of the test suggests that the full flexural capacity of the lap splice was not developed. It is believed that the bond between the lap splice and the joint material could have been compromised due to air voids near the as-cast top surface. Significant fiber settlement in the joint material also could

have negatively impacted the performance of the joint material and resulted in bond failure.

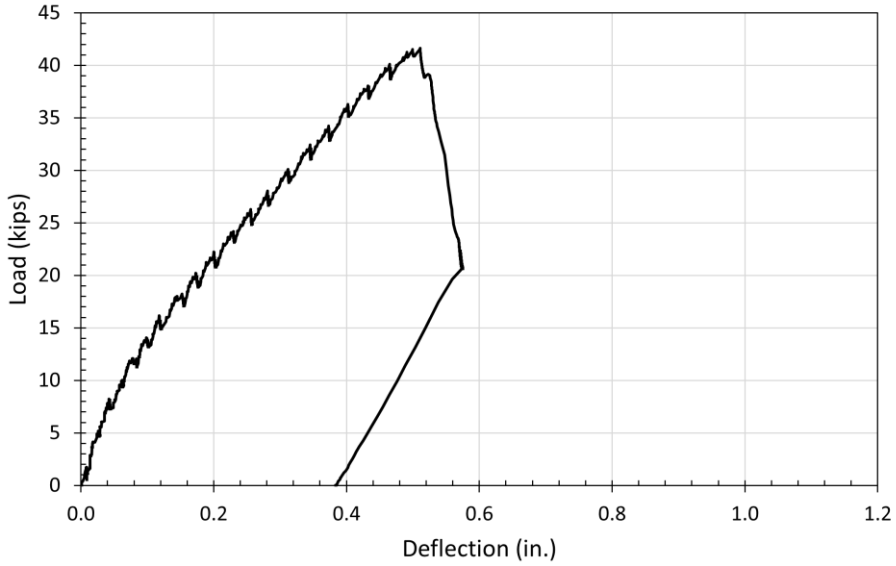

Figure 102: Load-deflection curve for SSDU-2 during negative moment test

The load-joint separation curves for both the north and south joint-deck interfaces are presented in Figure 103. The measured magnitude of joint separation on specimen SSDU-2 was similar to what was expected based on observations was during testing. The magnitude of separation at both interface locations was minimal until the maximum load was reached. After the maximum load was reached, the separation of at north joint interface increased rapidly until the test stopped. This behavior suggests a sudden bond failure occurred that resulted in pullout of the north side of the lap splice.

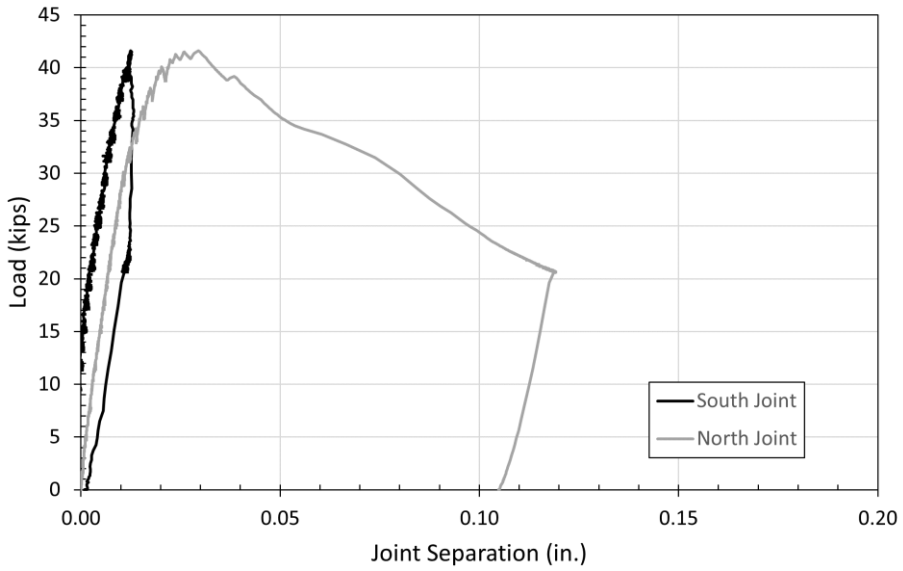

Figure 103: Load-joint separation curves for SSDU-2 during negative moment test

4.3.11 SSDU-2 Positive Moment Test

Settlement identical to other Ductal® specimens was detected before testing near the as-cast top surface of the joint. Therefore, the same process outlined in Section 4.3.4 was followed to prepare the surface.

Initial cracking was observed at a load of 5 kips on both sides of the joint-girder interface along the as-cast bottom flange. The joint separation started along the bottom of both interfaces and separation increased as the test continued. From 5 to 10 kips, the cracks propagated up the interface and reached the approximate location of the mild steel lap splice in the deck. Additionally, existing horizontal cracks in the deck started to propagate away from the load point. From 10 to 16 kips, existing horizontal cracks near the as-cast top surface of the joint started to propagate toward the load point. At 20 kips, additional cracking occurred at the joint-deck interface propagating away from the load point. No additional cracking

was marked beyond this point. At 22 kips, very distinct cracking sounds were heard from existing cracks near the as-cast top surface of the joint and strand locations. Just before reaching 26 kips, a popping sound was heard coming from near the strand locations and the applied load decreased. The test was stopped just beyond 26 kips due to the specimen experiencing a significant decrease in load-carrying capacity and showing signs of strand pullout. Cracking near the as-cast top surface of the joint is shown in Figures 104 and 105. The manually measured deflection was 2-1/2 in. under final loading and 2-1/16 in. after the load was removed. Figures 106 and 107 show joint separation on both sides of the specimen after loading was removed.

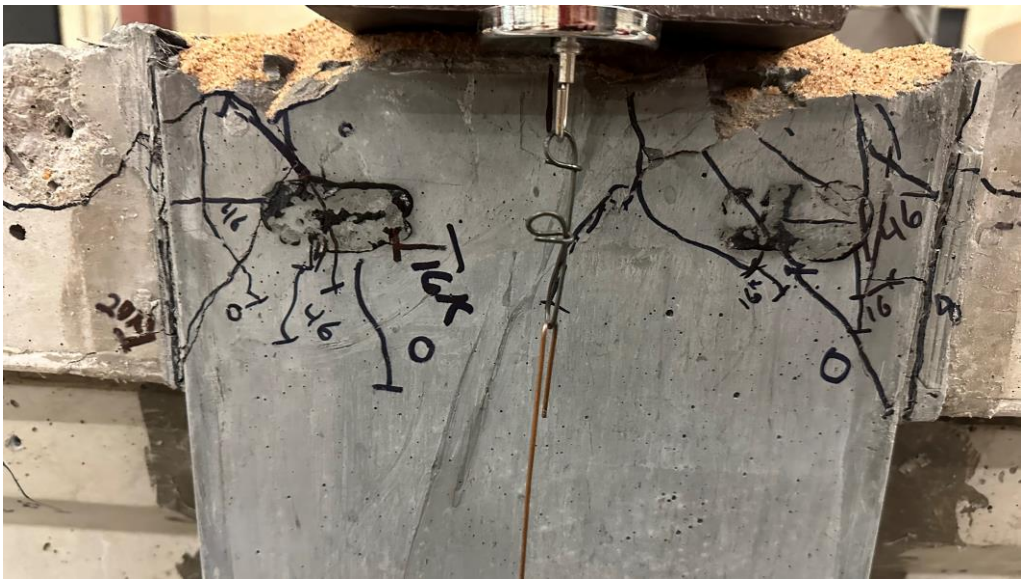

Figure 104: West side of joint SSDU-2 showing cracks near as-cast top face after final positive moment test loading

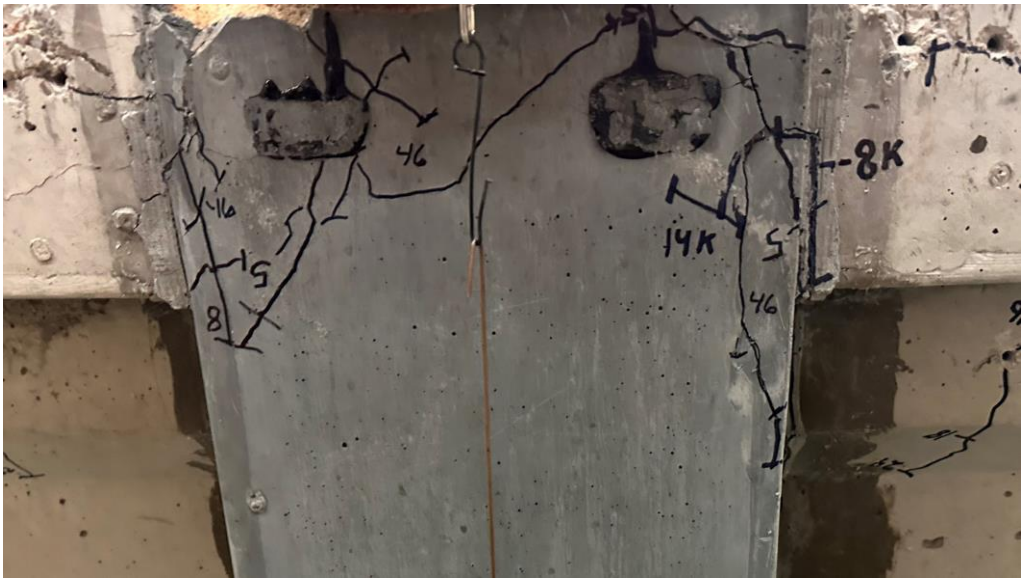

Figure 105: East side of joint SSDU-2 showing cracks near the as-cast top face after final positive moment test loading



Figure 106: Southeast (a) and northeast (b) side of joint SSDU-2 showing cracking along the as-cast bottom of the interfaces after final positive moment test loading



Figure 107: Northwest (a) and southwest (b) side of joint SSDU-2 showing cracking along the as-cast bottom of the interfaces after final positive moment test loading

Figure 108 shows the load-deflection curve for specimen SSDU-2 during positive moment testing. Initial cracking was visibly detected at a load of 5 kips. However, initial cracking did not result in a noticeable loss of stiffness. From 10 to 20 kips a significant loss of stiffness is visible on the load curve which coincides with cracking along the mild steel lap splice in both the joint and the deck, suggesting a bond failure. From 20 to 26 kips the load curve followed a relatively linear path with a much reduced stiffness as both loading and deflection increased. Just before 26 kips the curve dipped and some of the applied load was lost, which coincides with popping sounds originating near the strand locations. For the remaining duration of the test, the load curve followed a similar slope until the specimen suddenly failed to resist additional load. After the load was removed the deflection of the specimen showed a small rebound. A small rebound suggests

that the strands in the as-cast bottom flange of the girder were still somewhat bonded, but not adequately anchored in the joint.

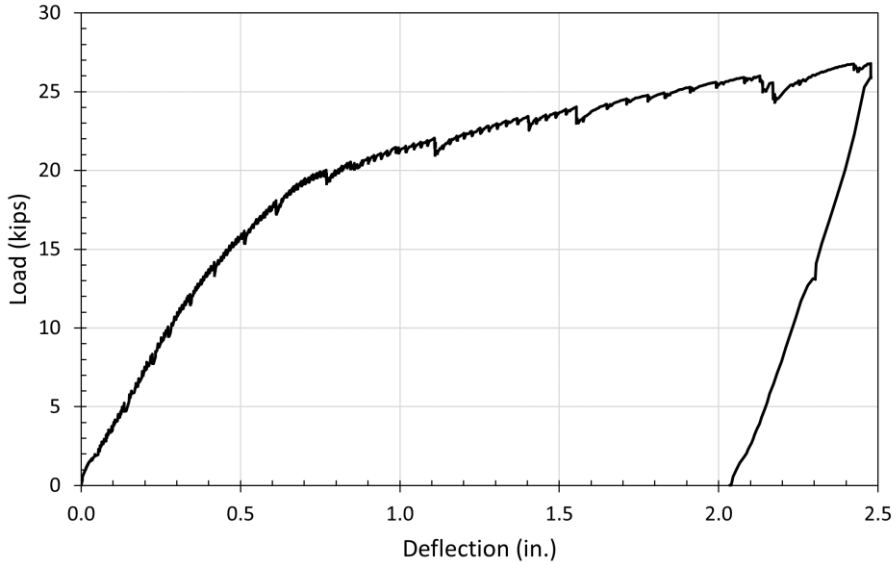

Figure 108: Load-deflection curve for SSDU-2 during positive moment test

The load-joint separation curves for both the north and south joint-girder interfaces are presented in Figure 109. The measured magnitude of joint separation of specimen SSDU-2 matched what was expected based on the cracking observed at both interfaces during testing. The measured separation followed similar trends at both interface locations during testing. Although it was not observed visually, the figure shows the north interface opened suddenly at a load of 8 kips and showed a slightly greater magnitude of separation for the remaining duration of the test. This may have been caused by an issue with the LVDT and may not accurately represent the behavior of the specimen. Otherwise, both curves follow the same shape. The load-deflection and load-joint separation

curves show similar behavior, suggesting that cracking at the interface locations was the primary cause of overall specimen deflection.

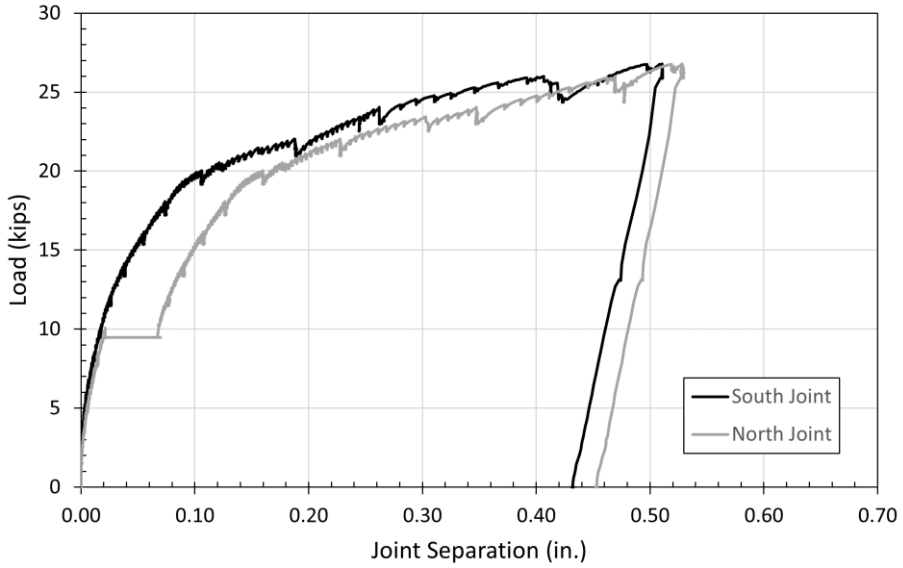

Figure 109: Load-joint separation curves for SSDU-2 during positive moment test

5.0 Analysis

Section 5 will compare and analyze the raw data presented in Section 4. Load-deflection graphs and load-joint separation graphs are included in the appropriate sections for comparison. The graphs will present data from the same tests as in Section 4 but have been presented on the same scale to allow for easier comparison. Additionally, the maximum moment experienced at the joint interface of each section was calculated based on the maximum applied point load and specimen geometry for use in comparison.

5.1 Negative Moment Tests

5.1.1 Negative Moment Test Load-Deflection and Maximum Loading

Figure 110 shows the load-deflection curves for all specimens during negative moment testing. All specimens had identical negative moment steel details, but joints cast with the same batch of UHPC are identified on the graph with the same color line. The first specimen tested with a particular detail is shown as a solid line and the second specimen tested is shown as a dotted line.

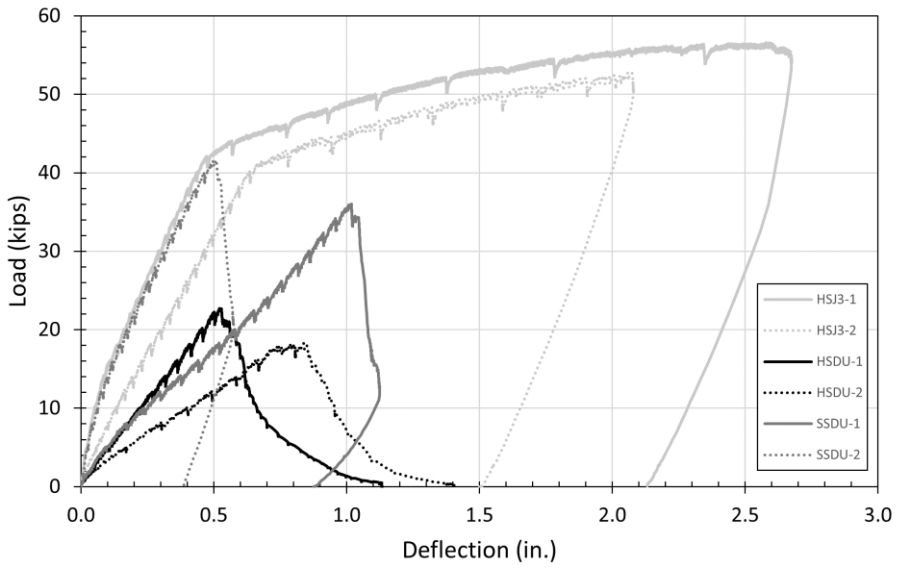

Figure 110: Load-deflection curves for all specimens during negative moment testing

Specimens with joints made with J3 UHPC achieved higher loads and had a much more gradual, flexure-like loss of stiffness and failure behavior when compared to joints made with Ductal® UHPC. All the joints made with Ductal® achieved their maximum loading and experienced a sudden and total loss of load-carrying capacity, which correlated with the pullout of one side of the mild steel lap splice. This behavior is believed to have been caused by the significant fiber segregation and preexisting cracking observed.

Table 13 shows the maximum values recorded during negative moment testing for each specimen. The load was recorded from the load cell by the data acquisition system during each test and later converted to a moment both under the load point and at the interface location using the loading configuration and considering the system to be uniform beam. The joints cast with J3 had a greater load carrying capacity than the joints cast with Ductal®. Although all specimens had identical negative moment details, the straight strand Ductal® specimens displayed twice

the load-carrying capacity of the hooked strand Ductal® specimens. This behavior was most likely due to damage caused by positive moment testing and artificially suggests that hooked positive moment reinforcement results in a lower negative moment load-carrying capacity. Since the hooked strand specimens had a greater load-carrying capacity during positive moment testing it is believed that greater damage was sustained around the negative moment steel regions. Alternatively, this behavior could have been caused by differences between the two batches of Ductal®. Differences such as the amount of void space near the as-cast top surface of the joint or uneven fiber distribution throughout the joint could have disproportionally affected the bond strength of reinforcing steel.

Table 13: Maximum values for each specimen during negative moment testing

Specimen	Load (kip)	Moment at Load (kip-ft)	Moment at Interface (kip-ft)
HSJ3-1	56.6	240.5	228.7
HSJ3-2	52.7	224.1	213.1
HSDU-1	22.7	96.5	91.8
HSDU-2	18.3	77.7	73.9
SSDU-1	36.0	153.0	145.5
SSDU-2	41.6	176.9	168.3

5.1.2 Negative Moment Test Separation at the Interface

Figures 111 through 113 show the load-joint separation curves for each specimen with identical positive moment steel details. The letter following the name of each specimen differentiates the north interface (N) from the south interface (S). The curves for each set of specimens are shown on their own figure for clarity and use the same scale for comparison. The hooked strand J3 specimens shown in Figure

111 displayed the greatest load carrying capacity both before and after a significant loss of stiffness occurred around 40 kips. The slight rebound behavior of both specimens was nearly identical in both tests, particularly the rebound of the south joint interfaces which are almost indistinguishable in the figure. This behavior would be expected for specimens with identical details and damage.

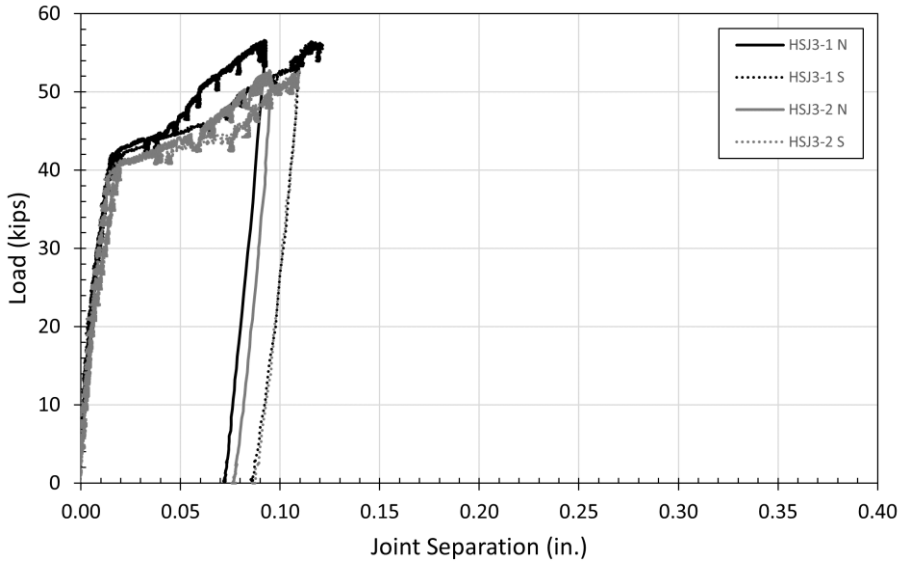

Figure 111: Load-joint separation curves for hooked strand J3 specimens at the joint-deck interfaces during negative moment tests

The hooked strand Ductal® specimen results shown in Figure 112 displayed the lowest load carrying capacity as previously mentioned. Once both specimens reached their maximum load an immediate loss of stiffness occurred and the south side interface separated substantially, suggesting a bond failure in the mild steel lap splice region. There was negligible change in the separation at the north side interface during both tests. The behavior of both interfaces before and after the significant loss of stiffness was nearly identical in both cases.

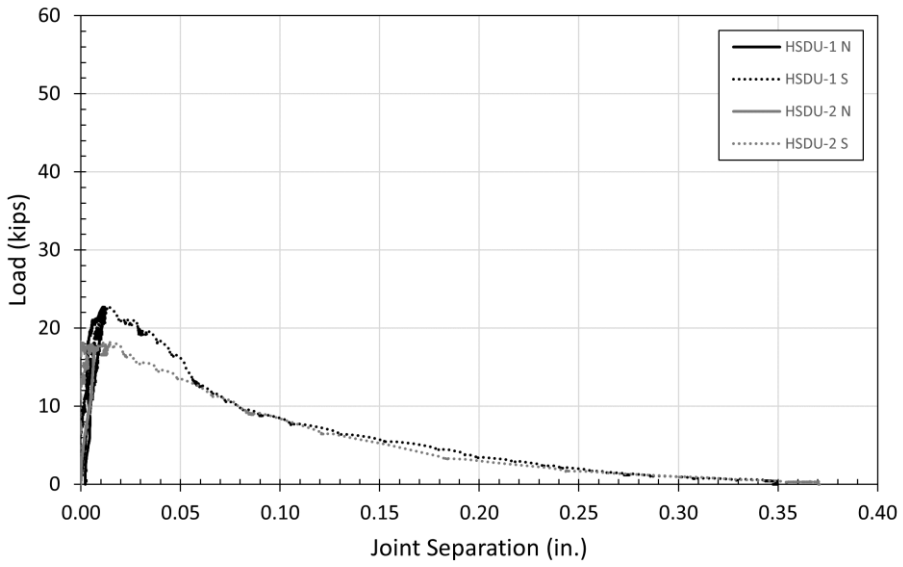

Figure 112: Load-joint separation curves for hooked strand Ductal® specimens at the joint-deck interfaces during negative moment tests

The straight strand Ductal® specimen results shown in Figure 113 displayed a load carrying capacity that falls between the hooked strand J3 specimens and the straight strand Ductal® specimens. Once both specimens reached their maximum load an immediate loss of stiffness occurred and one interface location started to separate substantially, suggesting a bond failure in the mild steel lap splice region. For SSDU-1 the south interface exhibited this behavior and for SSDU-2 the north exhibited this behavior. There was negligible change in the opposite interface during either test. The behavior of both interfaces before and after the significant loss of stiffness followed similar trends and both showed a slight rebound during unloading.

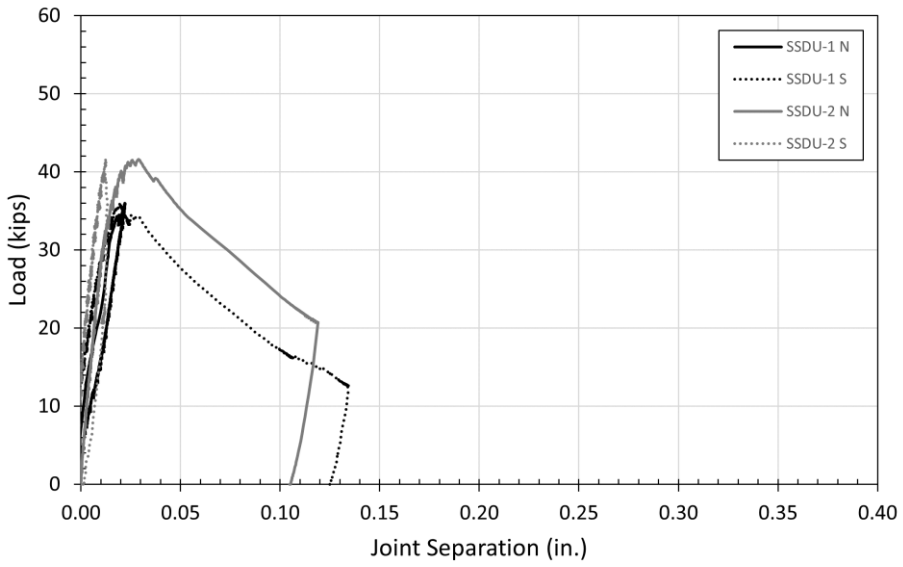

Figure 113: Load-joint separation curves for straight strand Ductal® specimens at the joint-deck interfaces during negative moment tests

5.1.3 Forces in the Negative Moment Reinforcement

Table 14 shows the calculated stresses in the negative moment steel during negative moment testing. The stress in the steel was calculated using strain compatibility, where the internal moment was set equal to the externally applied moment at the interface. Each moment was calculated using the maximum load and compressive strength measured on each day of joint testing. The compressive strength of the girder was used for negative moment tests and the compressive strength of the deck was used for positive moment tests. The compressive force was approximated by assuming a Whitney Equivalent Rectangular Stress Distribution. If the calculated stress in the steel was greater than the specified yield strength for the steel, it was assumed that the steel was either close to being fully developed or was yielding. The true yield strength of the steel was not tested and was assumed to equal the specified strength. Therefore, due to the

assumptions made to simplify analysis the true stress in the steel and the existence of yielding is unknown.

Table 14: Calculated values for stress in negative moment reinforcement at maximum loading

Specimen	Stress in Steel (ksi)
HSJ3-1	89.7
HSJ3-2	83.6
HSDU-1	35.4
HSDU-2	28.4
SSDU-1	56.6
SSDU-2	65.5

As shown in Table 14, the calculated stress in the steel for specimens HSJ3-1, HSJ3-2, and SSDU-2 surpassed the 60 ksi specified yield strength of the steel. However, the actual stress in the steel is considered to not exceed the actual yield strength of the steel. The calculated values are included to show the stress required for strain compatibility to hold true with the assumption used in this research. Without knowing the actual yield strength of the steel, it is speculated that the steel in specimens HSJ3-1 and HSJ3-2 yielded. This is also supported by the shape of the load-deflection curves for these specimens. Specimen SSDU-2 showed signs of bond failure during testing but was likely close to yielding.

5.2 Positive Moment Tests

5.2.1 Positive Moment Load-Deflection and Maximum Loading

Figure 114 shows the load-deflection curves for all specimens during positive moment testing. The first specimen tested of a particular set is shown as a solid line and the second specimen tested is shown as a dotted line. Specimen HSJ3-1 is not represented in the figure because it was not tested in the positive moment orientation due to damage caused by the negative moment test.

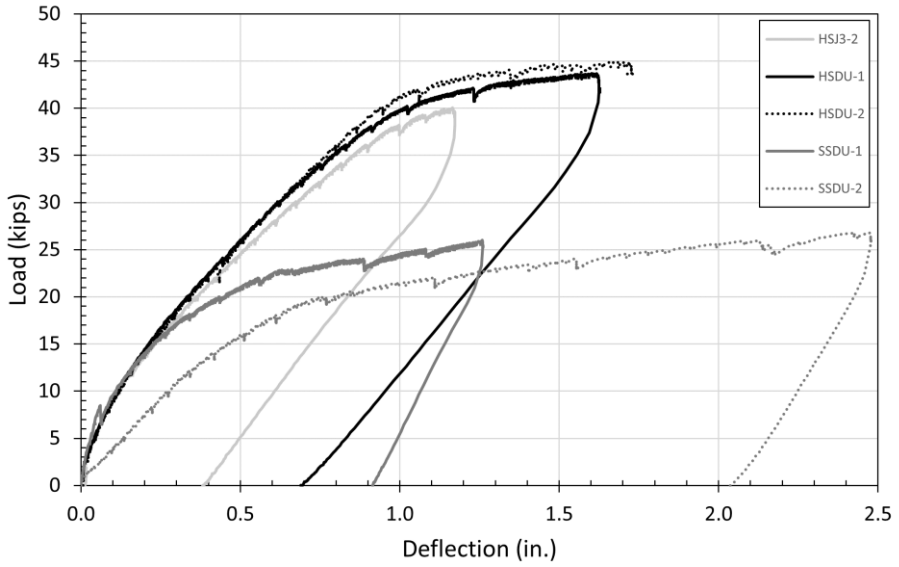

Figure 114: Load-deflection curves for all specimens during positive moment testing

All load-deflection graphs followed a similar trend and exhibited a similar loss of stiffness throughout the duration of testing. All specimens demonstrated some level of rebound after unloading, which suggests that there were no cases where the positive moment steel was entirely debonded due to testing. The rebound curve for HSDU-2 is not shown because the wire pots were removed before the test was stopped. The hooked strand Ductal® specimens achieved the highest loads, followed closely by the one hooked strand J3 specimen tested. The straight

strand specimens demonstrated less than half the load carrying capacity of the hooked specimens. Specimen SSDU-2 experienced twice the deflection of SSDU-1 for a given load yet demonstrated a similar load carrying capacity. This was likely because SSDU-2 was tested in the negative moment orientation first and SSDU-1 was tested in the positive moment orientation first. If the specimens followed the same order of testing the load-deflection curves would likely be similar.

Table 15 shows the maximum values recorded during negative moment testing for each specimen. The hooked strand Ductal® specimens had a slightly greater load carrying capacity than the hooked strand J3 specimens. The straight strand Ductal® specimens had a significantly lower capacity compared to both the hooked strand J3 and hooked strand Ductal® specimens. The results suggest that the addition of a hook significantly increases load carrying capacity for the given strand embedment.

Table 15: Maximum values for each specimen during positive moment testing

Specimen	**Load (kip)**	**Moment at Load (kip-ft)**	**Moment at Interface (kip-ft)**
HSJ3-2	40.0	170.2	161.9
HSDU-1	43.7	185.7	176.6
HSDU-2	46.0	195.3	185.7
SSDU-1	26.0	110.5	105.1
SSDU-2	26.8	113.9	108.3

5.2.2 Positive Moment Separation at the Interface

Figure 115 shows the load-joint separation curves for all specimens during positive moment testing. The first specimen tested for a particular set is shown as a solid line and the second specimen tested is shown as a dotted line. Specimen HSJ3-1 is not represented in the figure because it was not tested in the positive moment orientation due to damage caused by the negative moment test.

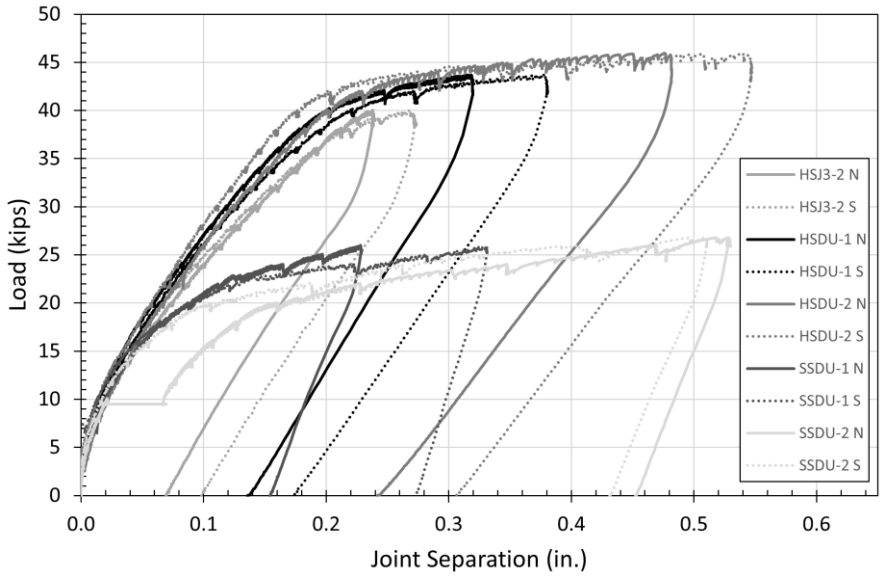

Figure 115: Load-joint separation curves for all specimens during positive moment testing

A strong correlation between hooked strands and increased load carrying capacity can be seen in Figure 115, similar to that shown in Figure 114. The hooked strand Ductal® specimens and the hooked strand J3 specimen showed a very similar loss of stiffness around 40 kips. After the significant loss of stiffness, all specimens maintained some level of load carrying capacity until the test was stopped. The J3 specimen was tested until the stiffness dropped, but not to the same extent as the Ductal® specimens, in order to allow for negative moment testing. The straight

strand Ductal® specimens showed a loss of stiffness at a lower load than all hooked strand specimens but followed a similar trend to the hooked strand specimens. Only specimen SSDU-2 showed any signs of a sudden bond loss. All specimens showed some magnitude of rebound after the test was stopped, but the hooked strand specimens showed a greater magnitude of rebound. This behavior suggests that either the addition of a hook or a longer length of embedded strand increases the pullout capacity of the strands. Specimen HSDU-2 showed a slightly higher load carrying capacity yet significantly higher joint separation than HSDU-1. The reason for this behavior is unknown but may be linked to the order of testing or the duration of testing. Both specimens were tested for positive moment first and both tests were stopped after the specimens reached their load carrying capacity. However, HSDU-2 took a longer amount of time to reach its load carrying capacity and may have resulted in greater deflections.

5.2.3 Forces in the Positive Moment Reinforcement Steel

Table 16 shows the calculated stresses in the positive moment steel during positive moment testing. The stress in the steel was calculated using the same method and assumptions outlined in Section 5.1.3. For specimens with straight strands where the load-displacement curve suggests a bond failure, the bond stress along the steel in tension was calculated to approximate the development achieved by the embedment. For specimens with hooked strands, the bond stress could not be directly calculated due to the contribution of the hook and are denoted by “--” in the table.

Table 16: Calculated values for stress in positive moment steel at maximum loading

Specimen	Stress in Steel (ksi)	Bond Stress (ksi)
HSJ3-2	236.8	--
HSDU-1	259.1	--
HSDU-2	273.8	--
SSDU-1	152.3	1.17
SSDU-2	157.2	1.20

As shown in Table 16, the calculated values of stress in the strands for the hooked strand specimens were significantly higher than the straight strand specimens. The calculated value for specimen HSDU-2 exceeded the 270 ksi specified rupture strength of the prestressing strand, so it is assumed that the strand was fully developed and close to rupturing. The hooked strand J3 specimen performed similarly to the hooked strand Ductal® specimens but will not be included when making comparisons between hooked and straight strands.

The calculated values for SSDU-1 and SSDU-2 are very similar to recommendations made in a study on the development of prestressing strands in UHPC lap splices, which was conducted using a direct tension test. The study states that 0.5 in. and 0.6 in. diameter prestressing strands can be developed in 20 in. and 24 in., respectively (Graybeal, 2014). Additionally, it states that with greater confinement full development may be possible in 16 in. or less. Interpolating between the provided values yields an approximate development of 21 in. for 0.5 in. special prestressing strands with a diameter of 0.52 in. Using the interpolated value for development length and setting the stress in the strands to 270 ksi, the equivalent bond stress at rupture according to the study would be

approximately 0.98 ksi. The average of the calculated bond stresses for specimens SSDU-1 and SSDU-2 was 1.19 ksi, which correlates to a required development length of 17.5 in. to fully develop the strands. The validity of this result is supported by the fact that the joint provided greater confinement than a typical direct tension specimen. Additionally, using internal moments to stress the strands provides a more realistic stress state around the embedded element than a direct tension test and may have caused the deviations between results from the testing methods in this research and the literature.

Table 17 shows extrapolated values assuming a linear relationship between stress in the steel and embedment length. The average calculated stress in the 10 in. straight strand specimens tested in this research was used to provide this relationship solely based on bond strength. It is important to note that only two specimens were used to derive the values listed in Table 17.

Table 17: Extrapolated values of stress generated in positive steel vs embedment length

Embedment Length (in.)	**Stress in Steel (ksi)**
0	0
8	123.8
10	154.8
16	247.7
17.5	270.9

The average calculated value for stress in the steel of the hooked strand Ductal® specimens was 266.5 ksi, which is only 18.8 ksi greater than the extrapolated value for 16 in. straight strands. However, the extrapolated value for 8 in. straight strand is 123.8 ksi. When comparing the hooked strand specimens, which had an

8 in. embedment to the back of the hook and an 8 in. extension on the hook, the inclusion of a hook potentially doubled the resistance to pullout. There is not enough information to definitively comment on the contribution of the hook because all hooked specimens included a straight embedment before the bend of the hook. Based on tests described in this thesis the inclusion of a hook is not necessary in cases where adequate development can be provided by straight strands. However, a hook would be useful in cases where space in the joint is limited or additional resistance to pullout is needed.

6.0 Findings, Conclusions, and Recommendations

This section summarizes the findings, conclusions, and recommendations based on the testing outlined in Section 4 and the analysis outlined in Section 5. The conclusions given in this section are limited to the materials and conditions utilized during testing. These conditions include the UHPC used in the joints, similar reinforcement within the joint, and the loading configuration of the joint specimens.

6.1 Findings

- Joints made with the Ductal® UHPC formed cracks near the as-cast top surface before testing.
- The fiber distribution during casting of UHPC does not always accurately represent the fiber distribution in the hardened material.
- Initial cracking occurred at a load between 5 and 10 kips for all tests, which corresponds to a moment of 21.3 and 42.5 kip-ft.
- Initial cracking occurred at 51-102% of the cracking moment of the girder and 18-36% of the cracking moment of the joint.
- The most common location of initial cracking during positive moment testing was at the extreme tension fiber of the joint-girder interface.
- All specimens showed some magnitude of rebound after positive moment testing.
- The most common location of initial cracking during negative moment testing was in the extreme tension fiber of the deck.
- All specimens with hooked strands showed some magnitude of rebound after negative moment testing.

- The stress generated in the strands at the joint interface of the hooked strand Ductal® specimens with an 8 in. embedment and 8 in. hook extension was approximately 70% greater than the stress generated in the straight strand Ductal® specimens with a 10 in. embedment.
- Only specimens with joints made of J3 UHPC showed behavior that suggested yielding of the lap splice during negative moment testing.
- No cracking was observed near the top of the girders after prestress release.
- No shear cracking was observed for any specimens.

6.2 Conclusions

- The performance of the Ductal® UHPC suggests that it may have been beyond its shelf life. The material was left over from a project in the field and was at least several months old before it was obtained.
- Factors such as bond strength, resistance to cracking, and fiber distribution contribute to the performance of joints made of UHPC more than compressive strength.
- Joints made with J3 showed greater bond strength than joints made with Ductal® during negative moment testing.
- Joints made with J3 and Ductal® showed very similar performance during hooked strand positive moment testing.
- Providing a hook is an effective way to significantly increase the capacity of the UHPC joint with a fixed horizontal length of strand embedment.
- Extrapolated data suggests that hooked strands provide a similar capacity to straight strands of equal total length.
- The provided mild steel in the top flange of the girders was adequate to prevent cracking after prestress release.
- The provided shear reinforcement was adequate to ensure a flexural failure in the girders.

6.3 Recommendations

- Sandblasting or alternative methods should be used to prep the ends of the girders to enhance the bond of UHPC to the girder concrete.
- Joints made with Ductal® UHPC should be overfilled and ground down to prevent void space from forming around the negative moment reinforcement.
- Cured specimens from UHPC test batches should be checked for both compressive strength and fiber distribution.
- Beam end pullout tests should be conducted with a variety of embedment lengths and hook lengths to optimize the hook design for UHPC.
- This project should be repeated with joints that include strain gauges in the joint, non-contact mild steel lap splices, and non-contact prestressing steel details.

7.0 References

AASHTO. (2017). *AASHTO LRFD Bridge Design Specification (8th Edition)*. American Association of State Highway and Transportation Officials (AASHTO), Washington, DC.

ASTM Standard C1437 (2015) *Standard Test Method for Flow of Hydraulic Cement Mortar,* ASTM International, West Conshohocken, PA.

ASTM Standard C1856 (2017) *Standard Practice for Fabricating and Testing Specimens of Ultra-High Performance Concrete,* ASTM International, West Conshohocken, PA.

Casey, Conner. (2019). *Ultra-High Performance Concrete for Connections of Precast, Prestressed Girders Made Continuous for Live Load.* Master's Thesis, Civil Engineering and Environmental Science, University of Oklahoma, Norman, OK: University of Oklahoma.

Eamon, C., Chehab, A., & Parra-Montesinos, G. (2016). *Field Tests of Two Prestressed-Concrete Girder Bridges for Live-Load Distribution and Moment Continuity*. Journal of Bridge Engineering, Vol. 21, No. 5.

El-Helou, Rafic G., and Benjamin A. Graybeal. (2022). *Flexural Behavior and Design of Ultrahigh-Performance Concrete Beams*, Journal of Structural Engineering 148.4: 04022013.

FHWA. (2021). *Construction.* U.S. Department of Transportation/Federal Highway Administration

Graybeal, B. A. (2009). *Structural behavior of a prototype ultra-high performance concrete pi-girder* (No. FHWA-HRT-10-027). United States. Federal Highway Administration. Office of Infrastructure Research and Development.

Graybeal, B. A., Yuan, J. (2014). *Bond behavior of reinforcing steel in ultra-high performance concrete* (No. FHWA-HRT-14-090). United States. Federal Highway Administration. Office of Infrastructure Research and Development.

Graybeal, B.A. (2014). *Splice Length of Prestressing Strand in Field-Cast Ultra-High Performance Concrete Connections*, FHWA-HRT-14-041, Federal Highway Administration, Department of Transportation, McLean, VA

Looney, T., McDaniel, A., Volz, J., & Floyd, R. (2019). *Development and characterization of ultra-high performance concrete with slag cement for use as bridge joint material*. British Journal of Civil and Architecture Engineering, Vol. 1, No. 2.

Mesigh, Michael. (2021). *Evaluation of Specialized Concretes for the Repair of Damaged Continuity Joints in Prestressed Girder Bridges.* Master's Thesis, Civil Engineering and Environmental Science, University of Oklahoma, Norman, OK: University of Oklahoma.

Miller, R., United States. Federal Highway Administration, & National Cooperative Highway Research Program. (2004). *Connection of simple-span precast concrete girders for continuity* (Report (National Cooperative Highway Research Program); 519). Washington, D.C.: Transportation Research Board.

Noppakunwijai, P., N. Jongpitakseel, Z. Ma, S. A. Yehia, and M. K. Tadros. (2002). *Pullout Capacity of Non-Prestressed Bent Strands for Prestressed Concrete Girders*, PCI Journal. Prestressed Concrete Institute, Chicago, IL, Vol. 47, No. 4.

Saadeghvaziri, M., Spillers, W., and Yin, L. (2004). *Improvement of Continuity Connection over* Fixed Piers, FHWA-NJ-2004-017, Federal Highway Administration, Department of Transportation, Newark, NJ.

Salmons, J. R. (1980). *Behavior of Untensioned-Bonded Prestressing Strand*. Final Report 77-1, Missouri Cooperative Highway Research Program , Missouri State Highway Department, Jefferson City, MO